

Purification of CO₂ for AMS ¹⁴C analysis:
Method development and application to permafrost deposits

INAUGURAL - DISSERTATION

zur

Erlangung des Doktorgrades
der Mathematisch-Naturwissenschaftlichen Fakultät
der Universität zu Köln

vorgelegt von

Anja Wotte, geb. Cording
aus Ostercappeln

2018

Gutachter: Prof. Dr. Janet Rethemeyer

Prof. Dr. Martin Melles

Tag der mündlichen Prüfung: 13. Juni 2018

“Science is built up of facts, as a house is built of stones;
but an accumulation of facts is no more a science than a heap of stones is a house.”

Henri Poincaré, French mathematician & physicist (1854-1912)
(Poincaré, 1905, p. 141)

Abstract

The Arctic is most sensitive to climate change and global warming. Just recently (winter 2017/2018), this region experienced its warmest winter on record. The rising temperatures have dramatic effects on the normally frozen ground – permafrost – which underlies twenty-four percent of the land area in the northern hemisphere. The permafrost thaws much deeper and rapid erosion of deep, ice-rich permafrost will increase. The Pleistocene deep permafrost (Yedoma) deposits are particularly prone to rapid degradation due to the loss of their high ice-contents upon thaw. Through this degradation, large amounts of previously stored frozen organic carbon will be exposed to microbial decomposition, resulting in the release of the greenhouse gases carbon dioxide (CO₂) and methane (CH₄) to the atmosphere. This emission in turn acts as a positive feedback to the climate system. So far, it is difficult to predict the rates of greenhouse gas emission because information on the decomposability of the organic matter is limited. As the organic matter is stored for millennia in the deep permafrost deposits, the radiocarbon (¹⁴C) analysis on CO₂ can be used to trace the decomposition of ancient (permafrost derived) vs. recent organic matter sources.

The collection and processing of the respired CO₂ for accelerator mass spectrometry (AMS) ¹⁴C analysis, however, is challenging and prone to contamination. Thus, during the progress of this thesis, we constructed a robust stainless-steel sampling device and refined a method for the collection of even small amounts (50 µg C) of CO₂. This method is based on a CO₂ sampling technique using a molecular sieve, which acts as an adsorbent. It has the advantage over other approaches (such as sampling in glass flasks) that CO₂ can be concentrated from large air volumes.

The reliability of the ¹⁴CO₂ results obtained with this molecular sieve cartridge (MSC) was evaluated in detailed tests of different procedures to clean the molecular sieve (zeolite type 13X) and for the adsorption and desorption of CO₂ from the zeolite using a vacuum rig. Under laboratory conditions, the contamination of exogenous carbon was determined to be less than 2.0 µg C from fossil and around 3.0 µg C from modern sources. In addition, we evaluated the direct CO₂ transfer from the MSC into the automatic graphitization equipment, AGE, with the subsequent ¹⁴C AMS analysis as graphite. This semi-automatic approach is promising as it resulted in a lower modern carbon contamination of only 1.5 µg C. In addition, this analyzing procedure can be performed autonomously. To collect CO₂ released from soils or sediments, additional sampling equipment, such as respiration chambers or depth samples, connected to the MSC is needed. Including the sampling equipment, a modern contamination of 3.0–4.5 µg C was obtained. Overall, these results show that the contamination becomes insignificant for large sample sizes (>500 µg C) and should be considered for smaller amounts.

With this successfully tested MSC, it became possible to investigate the decomposition of the organic matter in thawing Pleistocene Yedoma deposits. On a Yedoma outcrop in the Lena River Delta, Northeast Siberia, we measured CO₂ fluxes and their ¹⁴C signature to assess whether ancient (Yedoma derived) or younger C sources are preferentially respired. The CO₂ released from the

different sites is generally younger (2600–6500 yrs BP) than the bulk sediment (4000–31,000 yrs BP). Using isotopic mass balance calculations, we determined that up to 70% of the respired CO₂ originates from ancient OM. These data show that thawing Yedoma organic matter can be rapidly decomposed, which introduces the ancient carbon into the active carbon cycle and thus increases the permafrost carbon feedback.

Zusammenfassung

In der Arktis war der letzte Winter (2017/2018) der Wärmste seit Beginn der Wetteraufzeichnungen. Dieser Rekord verdeutlicht die Sensibilität der Arktis gegenüber dem Klimawandel und der globalen Erwärmung. Die steigenden Temperaturen haben dramatische Auswirkungen auf den normalerweise gefrorenen Boden – den Permafrost – der vierundzwanzig Prozent der Landfläche auf der Nordhalbkugel ausmacht. Mit steigenden Temperaturen erhöht sich die Auftautiefe des Permafrosts und die rasche Erosion von tiefem, eis- und organikreichem Permafrost (Yedoma) nimmt zu. Die hohen Eisgehalte des pleistozänen Permafrosts machen diese Ablagerungen besonders anfällig für Erosionsprozesse. Durch das Auftauen der Yedoma-Ablagerungen können große Mengen von zuvor gefrorenem organischem Kohlenstoff mikrobiell abgebaut werden. Dies führt zur Freisetzung der Treibhausgase Kohlenstoffdioxid (CO₂) und Methan (CH₄) in die Atmosphäre. Diese Emission verstärkt wiederum den Treibhauseffekt, was zu einer positiven Rückkopplung führen kann. Bisher ist es schwierig, die Emissionsraten von Treibhausgas aus tauendem Permafrost vorherzusagen, da die Information über die Zersetzbarkeit des organischen Materials begrenzt ist. Doch da die organische Substanz seit Jahrtausenden in den tiefen Permafrostablagerungen gespeichert ist, kann die Radiokohlenstoffanalyse (¹⁴C-Methode) angewandt werden, um den Abbau von alten (aus dem Permafrost stammenden) und neueren Quellen organischer Substanz zu verifizieren.

Die Probenahme des respirierten CO₂ und dessen Weiterverarbeitung für die ¹⁴C-Analyse mittels Beschleuniger-Massenspektrometrie (AMS) ist jedoch nicht trivial und anfällig für Kontaminationen. Im Rahmen dieser Arbeit wurde für die Beprobung von CO₂ eine robuste Probenahmeeinheit aus Edelstahl entwickelt, die selbst für die Entnahme kleiner Mengen CO₂ (50 µg C) geeignet ist. Die angewandte CO₂-Probenahmetechnik basiert auf der Verwendung von Molekularsieben, die als Adsorptionsmittel fungieren. Gegenüber anderen Verfahrensweisen (z.B. der Probenahme in Glasflaschen) hat diese Methodik den Vorteil, dass CO₂ aus großen Luftmengen in einer kleinen Edelstahlkartusche konzentriert werden kann. Die Korrektheit der mit dieser sogenannten Molekularsiebkartusche (MSC) erhaltenen ¹⁴CO₂-Ergebnisse wurde durch detaillierte Tests verschiedener Verfahren zur Reinigung des Molekularsiebs (Zeolith Typ 13X) und zur Adsorption und Desorption von CO₂ aus dem Zeolith unter Verwendung einer Vakuumlinie bewertet. Unter Laborbedingungen wurde eine Kontamination mit weniger als 2,0 µg C aus fossilen Quellen und etwa 3,0 µg C aus modernen Quellen bestimmt. Darüber hinaus haben wir den direkten CO₂-Transfer von der MSC in die automatische Graphitisierungseinheit AGE mit der anschließenden ¹⁴C-AMS-Analyse als Graphit getestet und bewertet. Dieser halbautomatische Ansatz ist sehr vielversprechend, da er in Zukunft vollständig automatisiert werden kann. Zudem konnte bei dieser Analysemethode eine deutlich geringere Kontamination mit modernem Kohlenstoff (1,5 µg C) nachgewiesen werden. Zur Beprobung von aus Böden oder Sedimenten freigesetztem CO₂ werden der MSC zusätzliche Probenahmegeräte (z.B. Respirationshauben oder Tiefenprobenehmer) vorgeschaltet. Bei der Probenahme mit dieser

Peripherie konnte eine Kontamination mit 3,0 bis 4,5 μg modernem Kohlenstoff nachgewiesen werden. Diese Werte zeigen, dass die Kontamination für große Probengrößen ($>500 \mu\text{g C}$) vernachlässigbar ist, doch für kleinere Probenmengen in Betracht gezogen werden sollte.

Mit den unter Laborbedingungen erfolgreich getesteten MSCs konnten wir den Abbau der organischen Substanz in tauenden pleistozänen Yedoma-Ablagerungen untersuchen. In einem Yedoma-Aufschluss im Lenadelta Nordostsibiriens wurden CO_2 -Flüsse und ihre ^{14}C -Signaturen gemessen, um festzustellen, ob bevorzugt alte (von den Yedoma-Ablagerungen stammende) oder jüngere Kohlenstoffquellen respiriert werden. Das von den verschiedenen Standorten freigesetzte CO_2 ist in der Regel jünger (2600-6500 Jahre BP) als das organische Material in den Sedimenten (4000-31.000 Jahre BP). Unter Verwendung von Isotopenmassenbilanzen konnte quantifiziert werden, dass bis zu 70% des respirierten CO_2 von alter organischer Substanz stammt. Diese Daten zeigen, dass das auftauende organische Material schnell zersetzt werden kann, was den fossilen Kohlenstoff in den aktiven Kohlenstoffkreislauf einträgt und somit die Permafrost-Kohlenstoff-Rückkopplung erhöht.

Contents

Abstract.....	iv
Zusammenfassung.....	vi
Contents	viii
Abbreviations.....	x
Introduction.....	11
The permafrost carbon feedback.....	11
Permafrost degradation	12
Decomposability of OM in Yedoma deposits.....	13
Molecular sieve cartridges – a tool to collect CO ₂ for ¹⁴ C analysis	14
Objective and outline of this thesis.....	15
Study area	16
Methodological background information.....	18
CO ₂ sample processing using MSCs	18
Radiocarbon	20
¹⁴ C measurement	20
Reporting of ¹⁴ C data.....	21
Paper I.....	23
¹⁴ CO ₂ processing using an improved and robust molecular sieve cartridge.....	23
Paper II.....	33
¹⁴ CO ₂ analysis of soil gas: Evaluation of sample size limits and sampling devices.....	33
Paper III	40
Radiocarbon analyses of respired CO ₂ reveal the release of large amounts of ancient carbon from thawing deep permafrost deposits	40
Discussion.....	62
Method development and improvement.....	62
Amount of zeolite	63
Cleaning of the zeolite.....	63
CO ₂ adsorption and desorption.....	64
Evaluation of sample size limits of the MSC	65
Coupling of the MSC with the AGE.....	66
Evaluation of the field equipment.....	67
Decomposability of Yedoma determined by ¹⁴ CO ₂ analysis.....	68
Composition of OM in thawing Yedoma deposits	68
Degradability of OM in thawing Yedoma deposits	69

Summary	72
Method development and improvement	72
Decomposability of Yedomas deposits	73
References	74
Acknowledgements	I
Contribution to Papers	III
Erklärung	IV

Abbreviations

^{14}C	radiocarbon
AGE	automatic graphitization equipment – used for ^{14}C analysis
AMS	accelerator mass spectrometry
C	carbon
C/N	total organic carbon to total nitrogen ratio
CH_4	methane
CO_2	carbon dioxide
EA	elemental analyzer
ETM+	enhanced thematic mapper plus – earth observing sensor on Landsat 7
GC	gas chromatography
GHG	greenhouse gases
He	helium
HVEE	High Voltage Engineering Europa
IRMS	isotope ratio mass spectrometry
m a.r.l.	meter above river level
m a.s.l.	meter above sea level
MICADAS	mini carbon dating system – small AMS
MSC	molecular sieve cartridge
N	nitrogen
NBS	National Bureau of Standards
OC	organic carbon
OM	organic matter
Ox-I	oxalic acid standard
PCF	permafrost carbon feedback
PMC	percent modern carbon
TC	total carbon
TIC	total inorganic carbon
TOC	total organic carbon
VPDB	Vienna Pee Dee Belemnite ($\delta^{13}\text{C}$ standard)
yrs BP	years before present – 1950 is the origin (present) of the time scale used in radiocarbon dating
$\delta^{13}\text{C}$	stable carbon isotopic ratio

Introduction

The permafrost carbon feedback

Permafrost is defined as ground that remains at or below 0°C for at least two consecutive years and is characteristic of the unglaciated northern circumpolar region (Muller, 1947, Washburn, 1980). It underlies twenty-four percent of the land surface in the northern hemisphere (around 23 million km²; *Figure 1a*; Zhang *et al.*, 2008). This permafrost region stores huge quantities (1100–1800 Pg) of organic carbon (OC) (*Figure 1b*; Hugelius *et al.*, 2014, Schuur *et al.*, 2015), about twice as much carbon (C) as that in our current atmosphere (829 Pg C; Ciais *et al.*, 2013). The permafrost C pool accumulated organic matter (OM) from vegetation and plant litter over thousands of years and acted as a substantial sink for atmospheric C during the late Quaternary. This accumulation became possible as the decomposition of OM was limited by short growing seasons, water saturated conditions, and freezing temperatures (Harden *et al.*, 1992, Smith *et al.*, 2004, Zimov *et al.*, 2006, McGuire *et al.*, 2009, Grosse *et al.*, 2011a).

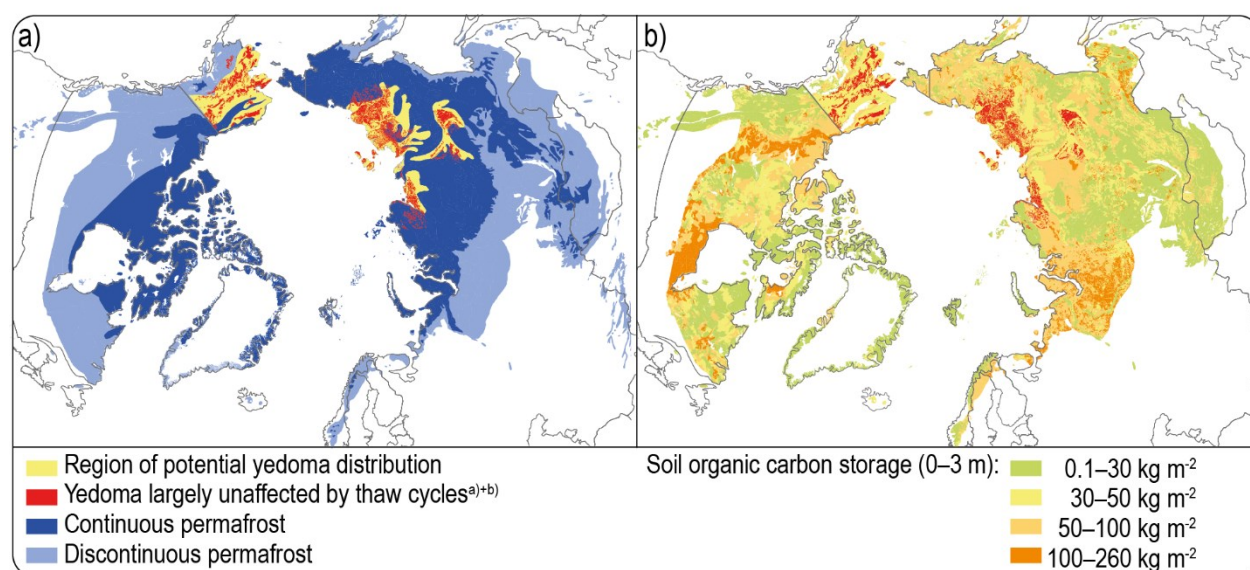


Figure 1. a) Distribution of permafrost in the northern circumpolar region, including the extent of deep permafrost deposits (Yedoma). In the continuous permafrost region, permafrost occurs everywhere (>90%), whereas in the discontinuous zone, permafrost only lies beneath some locations (<90%). Data based on Romanovsky (1993), Brown *et al.* (2002), Grosse *et al.* (2013). b) Soil organic carbon (OC) map showing the OC content of the top 0–3 m in the circumpolar region (Hugelius *et al.*, 2014). Modified from Schuur *et al.* (2015).

Currently, as an effect of global warming, the temperature is rising more than twice as fast in the Arctic compared to the temperature in lower latitudes (Overland *et al.*, 2017). This phenomenon is called polar amplification (Serreze & Barry, 2011) and is accelerating the thawing and loss of permafrost at higher latitudes. Once thawed, previously frozen OM becomes available for microbial decomposition, leading to the release of the greenhouse gases carbon dioxide (CO₂) and methane (CH₄) to the atmosphere (Elberling *et al.*, 2013, Voigt *et al.*, 2016). The release of this

old C can potentially further contribute to the global warming that is already anticipated from anthropogenic greenhouse gas emission alone. This amplification is known as the permafrost C feedback (Figure 2; Ciais *et al.*, 2013, Schuur *et al.*, 2015, Zimov *et al.*, 2006). Despite the remoteness of the permafrost region, its large C pool in combination with the polar amplification potentially make the permafrost C feedback to one of the globally most important carbon-climate feedbacks (Schuur *et al.*, 2008).

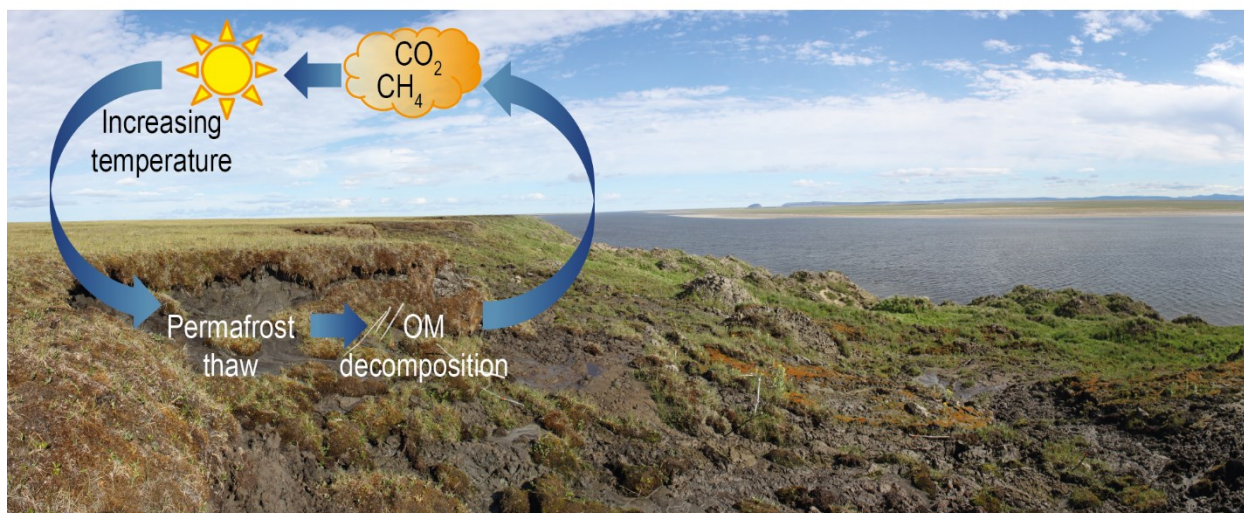


Figure 2. The permafrost C feedback illustrated at the riverine erosion site on Kurungnakh Island, Lena Delta, Siberia.

Permafrost degradation

Permafrost degrades not only through deeper (seasonal) thawing of the surface layer, the active layer that thaws in summer, but also through rapid erosional processes (Schuur *et al.*, 2008, Grosse *et al.*, 2011a, Grosse *et al.*, 2011b, Morgenstern *et al.*, 2013). High ice contents can exceed the sediment pore volume in permafrost deposits and can lead to abrupt permafrost degradation. This degradation is caused by the ice melting and the remaining ground collapsing into the ensuing voids (Jorgenson *et al.*, 2006, Kokelj *et al.*, 2013, Schuur *et al.*, 2015). This process and the resulting landscape are called thermokarst (French, 2017). Additionally, enhanced thermoerosion can take place at coastal or river shorelines (Günther *et al.*, 2013, Kanevskiy *et al.*, 2016).

In contrast to top-down thaw, which only affects the surface layer, the rapid degradation processes of thermokarst and thermoerosion result in the thaw of much deeper and thus older permafrost deposits and are likely to increase with future warming (Jorgenson *et al.*, 2006, Kokelj *et al.*, 2013). Accordingly, deep (>3 m) permafrost (Yedoma) deposits are particularly prone to degradation, as these deposits contain massive syngenetic ice wedges (Schirrmeister *et al.*, 2002, Kanevskiy *et al.*, 2011, Schirrmeister *et al.*, 2013). The term Yedoma originally describes the elevated areas of erosional remnants of a former accumulation plain, but it is now widely used as a stratigraphic term for the fine-grained, organic- and ice-rich permafrost deposits of Pleistocene age (Schirrmeister *et al.*, 2013). Synonymously to Yedoma the term Ice Complex is often used. Degrading Yedoma deposits can also feedback to the C cycle because they store a substantial part (>25%) of the perennially frozen permafrost OC (213 to 456 Pg C; Strauss *et al.*, 2013, Hugelius *et al.*, 2014, Walter Anthony *et al.*, 2014).

In response to ongoing global warming, the increase in ground temperatures and the subsequent decrease in the thickness and spatial extent of permafrost have already been observed in different Arctic regions (Romanovsky *et al.*, 2010, Smith *et al.*, 2010). Different model projections agree that further degradation will also occur, releasing greenhouse gases and thus affecting the global climate cycle significantly (see Schaefer *et al.*, 2014 for a discussion). However, the timing and magnitude of the permafrost response to changes in climate are still uncertain (Ciais *et al.*, 2013, Schaefer *et al.*, 2014, Koven *et al.*, 2015). This uncertainty is illustrated by the large variability in the modelled C losses ranging between 40 and 350 Pg C (by 2100) for thawing permafrost (Schaefer *et al.*, 2014). Besides high variabilities, these current global-scale models are limited since they do not consider the contribution of C released by rapid thaw of Yedoma deposits (Schneider von Deimling *et al.*, 2015, Strauss *et al.*, 2015). Even if these rapid degradation processes occur locally, the phenomenon is widespread and could substantially impact the emission of C to the atmosphere (Grosse *et al.*, 2011a). To improve model simulations of greenhouse gas fluxes from degrading permafrost, it is necessary to enhance our knowledge of the total amount of OM stored in permafrost deposits and its microbial decomposability. In addition, Yedoma deposits and abrupt thaw processes occurring in Yedoma deposits should be included in the next generation of global climate models (Grosse *et al.*, 2011a, Schuur *et al.*, 2013, Schneider von Deimling *et al.*, 2015).

Decomposability of OM in Yedoma deposits

Previous studies suggest that the OM in Pleistocene Yedoma deposits arises from relatively little decomposed plant material, which became quickly locked in perennially frozen sediments (Dutta *et al.*, 2006, Zimov *et al.*, 2006, Lee *et al.*, 2012, Knoblauch *et al.*, 2013, Strauss *et al.*, 2015, Stapel *et al.*, 2016, Weiss *et al.*, 2016, Strauss *et al.*, 2017). As a result, it can be easily degraded once thawed and thus lead to increased respiration rates. While there is growing effort to assess the quality of OM in Yedoma (Lee *et al.*, 2012, Knoblauch *et al.*, 2013, Strauss *et al.*, 2015, Stapel *et al.*, 2016, Weiss *et al.*, 2016), information on rates of C release from thawing Yedoma deposits is scarce and the topic needs further investigation (Dutta *et al.*, 2006, Lee *et al.*, 2012, Knoblauch *et al.*, 2013). Most previous studies were performed using laboratory (incubation) experiments, thus excluding the in-situ conditions of the natural ecosystem (Dutta *et al.*, 2006, Lee *et al.*, 2012, Knoblauch *et al.*, 2013). To consider the environmental conditions, field studies investigating in-situ greenhouse gas emissions from Yedoma deposits are needed. Moreover, flux measurements alone do not give any information on the organic substrates degraded, i.e. fresh OM components being part of the active C cycle vs. ancient sources being stored for millennia. The radiocarbon (^{14}C) signature of respired CO_2 makes it possible identify contributions of ancient, Yedoma derived C to the overall CO_2 flux (Trumbore, 2000).

So far, no field study evaluated the decomposition of OM in Pleistocene Yedoma deposits using ^{14}C analysis of respired CO_2 . Only CO_2 emissions from the active layer of the Holocene tundra have been investigated, showing increasing amounts of old C released during longer warming and thawing periods (Schuur *et al.*, 2009, Nowinski *et al.*, 2010, Natali *et al.*, 2011, Hicks Pries *et al.*, 2013, Lupascu *et al.*, 2014). This significant loss of old C potentially make thawing permafrost to a large C source (Schuur *et al.*, 2009). As deep Yedoma deposits also store large amounts of OM,

it is important to understand to what extent this old OM is decomposable and potentially releases C to the atmosphere.

Molecular sieve cartridges – a tool to collect CO₂ for ¹⁴C analysis

The sampling of respired CO₂ for accelerator mass spectrometry (AMS) ¹⁴C analysis is not yet a routine method because it is not easy to sample gas volumes large enough to obtain sufficient amounts of C for ¹⁴C analysis. To extract CO₂ from air and concentrate it in a small volume, a sampling device filled with molecular sieve was developed, the molecular sieve cartridge (MSC; Hardie *et al.*, 2005, Garnett & Murray, 2013). This technique is advantageous compared to earlier methods since there is no need for cryogenic treatment, caustic sodium hydroxide, and it does not need large amounts of evacuated flasks to collect the CO₂.

Molecular sieves are solid materials (e.g. zeolites) with a porous structure. They adsorb molecules with diameters less than the pore size, while molecules that are larger pass the sieve (Flanigen, 1991). Moreover, the sorption process is reversible so that they can be reused. During first attempts to implement the ¹⁴CO₂ sampling and analysis at the CologneAMS ¹⁴C laboratory, a MSC design was adapted from (Bol & Harkness, 1995, Hardie *et al.*, 2005). This sampling device was applied in the Siberian Arctic to collect CO₂ respired from permafrost. As the device was composed of quartz glass tubing and plastic auto-shutoff couplings, it was very fragile. Some of the MSCs were broken during shipping. Additionally, we determined severe contamination issues by contributions of atmospheric CO₂, which indicated leaking couplings during the long transport and storage time of several months after the CO₂ collection. Therefore, there is the need for a new MSC, which is robust and leak tight over several months and thus particularly suitable for extreme conditions on expeditions. Detailed tests of the new MSC as well as their handling procedures will be mandatory to obtain reliable ¹⁴CO₂ results (Hardie *et al.*, 2005, Palonen & Oinonen, 2013).

Objective and outline of this thesis

The ongoing global warming is most pronounced in the polar regions. The rapid warming is causing the normally continuously frozen ground, permafrost, to thaw, leading to the decomposition of huge amounts of organic matter (OM) stored in permafrost. This decomposition releases CO₂ and CH₄ to the atmosphere and can provide a positive feedback to climate change. To understand the impact of permafrost OM decomposition on climate change, and vice versa, requires identifying the carbon (C) sources currently sustaining CO₂ emissions from permafrost soils. Whether the CO₂ emitted from thawing deep permafrost (Yedoma) originates from young or ancient OM, can be evaluated by the ¹⁴C analysis of the released CO₂. So far, no ¹⁴CO₂ analyses have been performed on Yedoma deposits, primarily caused by the lack of an adequate CO₂ sampling technique and a challenging measurement process. Against this background, the primary objectives of the thesis are:

- i The development and improvement of a robust sampling device (MSC) and method to collect CO₂ for subsequent ¹⁴C analysis.
- ii The application of the MSC involving the sampling for ¹⁴CO₂ analyses to trace the degradation of ancient vs. young organic matter sources in deep permafrost Yedoma deposits.

To collect respired CO₂ for subsequent ¹⁴C analysis, a robust sampling device (MSC) was developed for field application under extreme conditions in remote areas. This MSC is entirely made of stainless steel. During its development, different laboratory procedures were rigorously tested to evaluate the reliability of the ¹⁴CO₂ results. Recommendations are given for an optimized cleaning procedure of the molecular sieve, as well as for adsorbing and desorbing the CO₂ for subsequent ¹⁴C analysis (**Paper I**).

In a next step, we evaluated the sample size limit of the MSC and tested its connectivity with the field equipment like respiration chambers and depth samplers. These first tests in the field in addition with further improved laboratory procedures helped to determine any contamination of the whole sampling and analyzing process (**Paper II**).

Finally, our successfully evaluated sampling device was ready for the application in the Siberian permafrost landscape in order to determine the decomposability of Pleistocene Yedoma deposits directly in the field (**Paper III**).

Data obtained by this novel approach, the ¹⁴C analysis of respired CO₂, will help improve predictions of C releases from thawing permafrost to the atmosphere.

Study area

The decomposability of Pleistocene Yedoma deposits was investigated on Kurungnakh Island, one of more than 1500 islands in the Lena River Delta in northeast Siberia (Figure 3). The Lena River Delta is the largest river delta in the Arctic with an area of about 32,000 km² (Antonov, 1967, Walker, 1998). This region lies in the subarctic tundra and continuous permafrost zone with permafrost extending down to a depth of about 600 m and low mean annual permafrost temperatures of -8.6°C at 10.7 m depth (Grigoriev, 1960, Boike *et al.*, 2013).

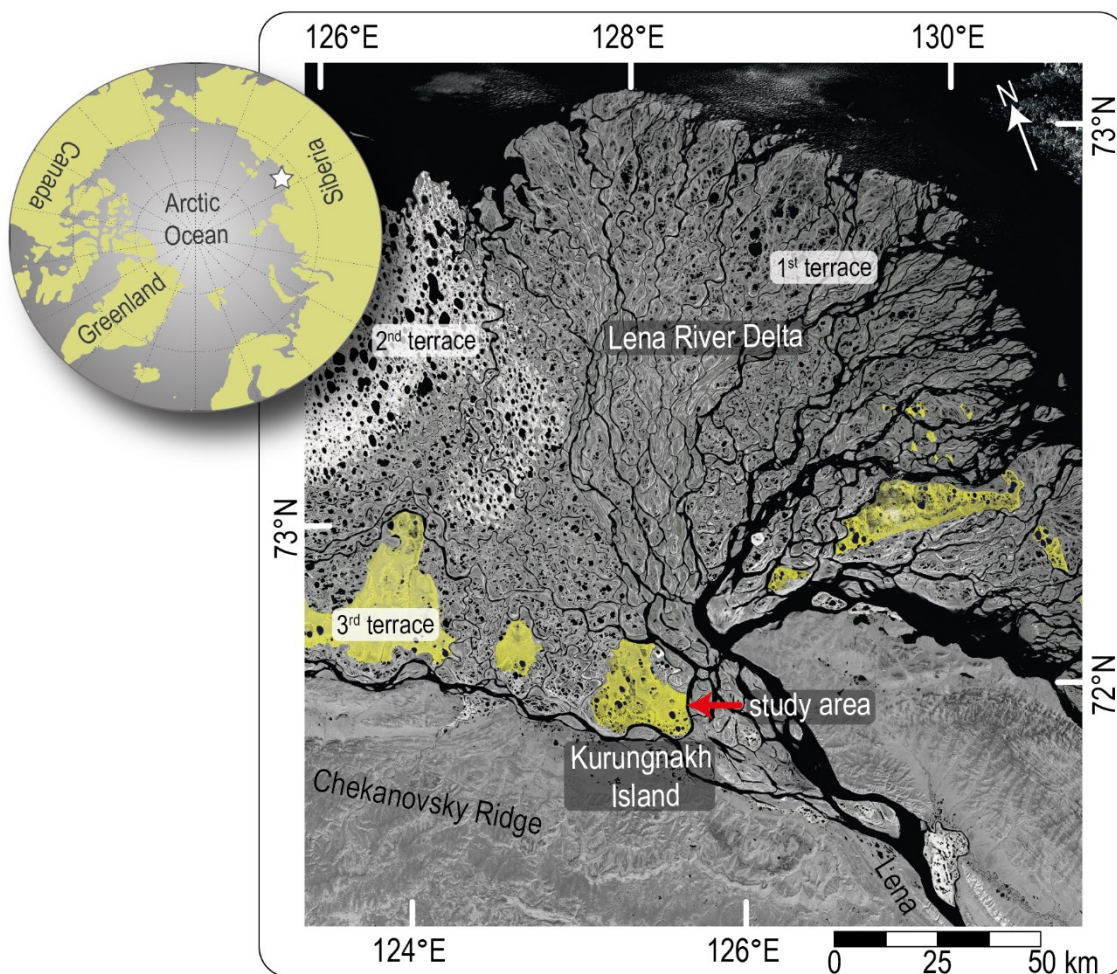


Figure 3. Position of the study area in northeast Siberia in the southern part of the Lena River Delta on Kurungnakh Island. Remnants of the third geomorphologic terrace and thus Yedoma deposits are highlighted in yellow. The red arrow points to the investigated Yedoma outcrop at the east coast of Kurungnakh Island. The light-gray area in the northwest of the map represent the second geomorphologic terrace, whereas the remaining dark-gray area represent the first terrace. (Landsat-7 ETM+, GeoCover 2000 © NASA)

The Lena River Delta can be divided into three geomorphological terraces (Figure 3; Grigoriev, 1993). The first, youngest terrace (1–12 m a.s.l.; middle Holocene) is characterized by an ice-wedge polygonal tundra and is mainly located in the central and eastern delta. The second terrace

(20–30 m a.s.l.; Late Pleistocene to early Holocene), which is formed of sandy sediments with low ice contents, occupies ~23% of the delta mainly in the northwestern part (Schwamborn *et al.*, 2002). The third, non deltaic terrace (30–60 m a.s.l.) is an erosional remnant of a Late Pleistocene accumulation plain located in the southern part of the Lena River Delta, north of the Chekanovsky ridge (Schwamborn *et al.*, 2002). This terrace is composed of three units: a lower sand unit, the Yedoma deposits, and Holocene polygonal tundra at the surface. Characteristic for the Yedoma deposits is the high ice content developed as syngenetic ice wedges of several meters height and width. These large ice-wedges were formed during a strongly continental climate, which prevailed over several thousand years, in a non-glaciated polygonal tundra environment (Schirrneister *et al.*, 2011). During these climate conditions up to 50 m thick organic-rich Yedoma sediments were accumulated, because organic-rich sediments of the active layer were incorporated quickly into the permafrost (Schirrneister *et al.*, 2002, Kanevskiy *et al.*, 2011, Schirrneister *et al.*, 2013).

Kurungnakh Island is part of the third terrace. Along the river bank at the eastern side of the island the Yedoma deposits are exposed in a bluff of up to 40 m a.s.l. (*Figure 4*; Morgenstern *et al.*, 2013). The terrace surface at the outcrop is retreating rapidly with up to 6.9 m of annual cliff-top erosion and thus exposing large, steep ice walls and the remaining frozen sediment cores of thawed Pleistocene polygonal centers, which form conical shaped mounds (*Figure 4*; Stettner *et al.*, 2018). These so-called thermokarst mounds are typical features of the thermokarst landscape and are composed of the organic-rich Yedoma sediments. Thus, the outcrop on Kurungnakh Island is an ideal site to study the degradability of the thawing Yedoma deposits.



Figure 4. Outcrop of Pleistocene Yedoma deposits along the river bank of Kurungnakh Island. The gray steep walls in the background are massive ice wedges. In the foreground conical shaped thermokarst mounds can be seen.

Methodological background information

CO₂ sample processing using MSCs

The new MSC design is described in detail in Paper I. Briefly, the molecular sieve (zeolite type 13X) is centered in a stainless steel tube and held in place by quartz wool. Both endings of the tube are closed with stainless steel quick couplings (*Figure 5*). Generally, the sampling of CO₂ with a MSC involves three steps: (1) the cleaning of the MSC prior to usage, which is necessary to ensure that the zeolite is free of contamination, (2) the actual sampling, i.e. adsorption, of CO₂ onto the zeolite, and (3) the release of the CO₂ from the zeolite and transfer to a glass ampoule for the subsequent ¹⁴C analysis (*Figure 6*).

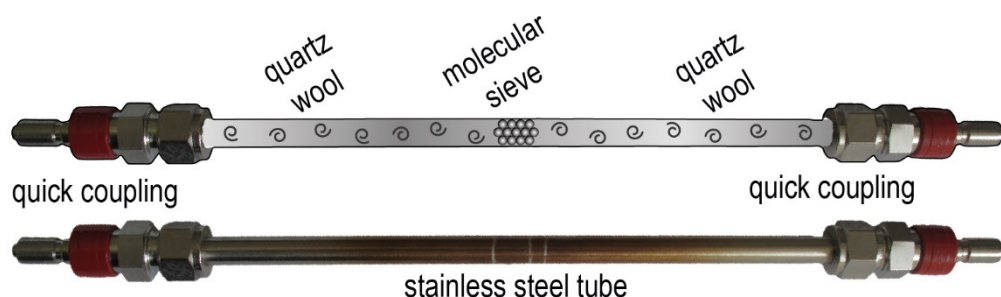


Figure 5. New MSC design: The molecular sieve is placed in the center of a stainless steel tube and closed at both ends with quick couplings.

For the cleaning process, the MSC is heated to ~500°C and simultaneously evacuated (passive cleaning) or flushed with a purge gas (e.g. helium; active cleaning; *Figure 6*). Afterwards, the regenerated MSC is ready for sampling. In the field, the CO₂ emissions can be collected, e.g. with respiration chambers or depth samplers (*Figure 6*), by transferring the respired CO₂ either passively by gas diffusion (Garnett *et al.*, 2009) or actively by circulation of the gas from the chamber through the MSC using a pump-based system (Hardie *et al.*, 2005, Biasi *et al.*, 2014). In the laboratory the adsorbed CO₂ can be released by heating the MSC while it is connected to a vacuum rig (*Figure 6*). The CO₂ is transferred to the vacuum rig, where it is purified and split into aliquots for ¹⁴C- and δ¹³C analysis, if required. Another option is the direct release of CO₂ from the MSC to the automatic graphitization equipment (AGE; Ionplus AG, Switzerland; *Figure 6*) for graphitization. In the AGE the CO₂ is automatically transferred to one of the seven reactors, where it is reduced to graphite with H₂ over iron as catalyst (Wacker *et al.*, 2010). After CO₂ release, the MSC can be cleaned again and reused for further sampling campaigns. Finally, either the glass ampoule containing the sampled CO₂ or the graphite target can be sent for AMS analysis (*Figure 6*).

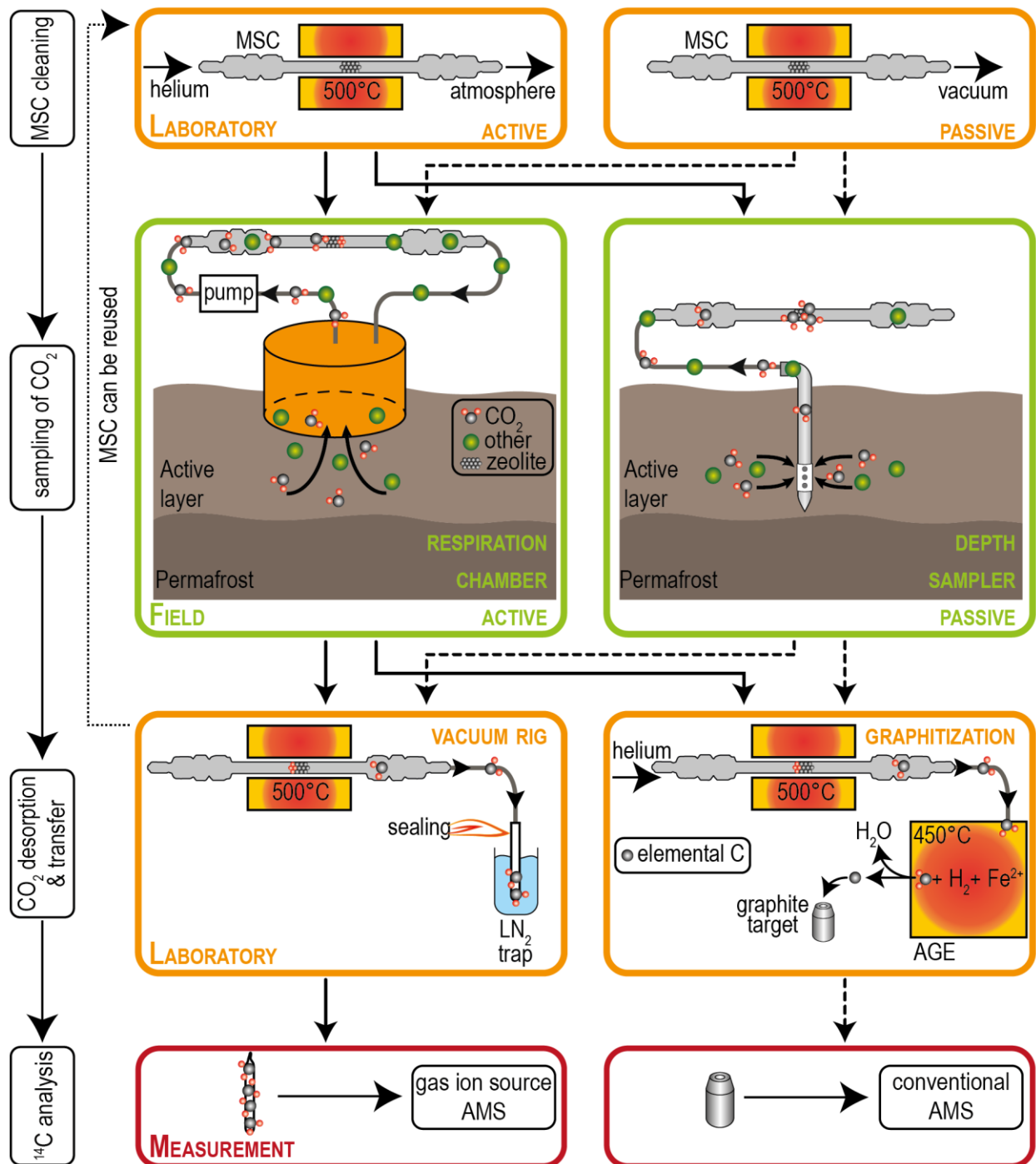


Figure 6. Illustration of the sampling workflow using the molecular sieve cartridge (MSC). Prior usage, the MSC has to be cleaned in the laboratory (actively or passively). In the field, the respired CO₂ can be collected using a respiration chamber or a depth sampler. After the expedition, the adsorbed CO₂ will be released from the MSC via heating and transferred to a vacuum rig using a liquid nitrogen (LN₂) trap. The purified CO₂ will be sealed in a glass ampoule. Another option is the direct release of CO₂ to an automatic graphitization equipment (AGE) for graphitization. Finally, the glass ampoule containing the CO₂ gas or the graphite target are ready for measurement with the accelerator mass spectrometer (AMS).

Radiocarbon

^{14}C is a naturally occurring radioactive isotope, which is produced by the interaction of cosmic rays with Earth's atmosphere (Libby, 1946). The ^{14}C concentration in the atmosphere is determined by its production, radioactive decay and exchange with the ocean and global biomass. Carbon enters the global biomass via photosynthesis. Therefore, living biomass has the same ^{14}C signature as the atmosphere at the time of C fixation. After death, the exchange of C between organism and atmosphere stops and the ^{14}C concentration in the dead OM decreases according to the radioactive decay of ^{14}C with a half-life of 5730 years (Godwin, 1962). Consequently, the ^{14}C signature of different C pools varies dependent on their residence time within the ecosystem (Trumbore, 2000, Schuur & Trumbore, 2006). During respiration of recent photosynthetic products and living plants, CO_2 will be released with a ^{14}C signature similar to that of the atmosphere, whereas respiration of OM hundreds to thousands of years old will release CO_2 depleted in ^{14}C . Consequently, the ^{14}C signature of respired CO_2 offers the potential to evaluate contributions of different C pools to the overall CO_2 flux.

Large differences in ^{14}C concentration exist especially between the active layer and the underlying permafrost with depth, because the OM stored in permafrost deposits was locked frozen for several thousand years (Harden *et al.*, 1992, Schirrmeister *et al.*, 2002, Zimov *et al.*, 2006). Thus, this stored C pool is depleted in ^{14}C and the ^{14}C signature of the respired CO_2 can be used as a fingerprint to identify the microbial decomposition of ancient C stored in the permafrost. The decomposition and influence of ancient C on the respiration of CO_2 can be evaluated with a simple mass balance calculation using the ^{14}C signature of the underlying ancient permafrost C ($F^{14}\text{C}_{\text{OM}}$), of the respired CO_2 ($F^{14}\text{C}_{\text{CO}_2}$) and that of the recent biomass ($F^{14}\text{C}_{\text{Y-OM}}$; Trumbore, 2000, Schuur & Trumbore, 2006):

$$F^{14}\text{C}_{\text{CO}_2} = f_{\text{OM}} \times F^{14}\text{C}_{\text{OM}} + f_{\text{Y-OM}} \times F^{14}\text{C}_{\text{Y-OM}}$$

$$f_{\text{OM}} + f_{\text{Y-OM}} = 1$$

The unknowns are the fraction (f) of each source on the respired CO_2 . Thus, the fraction of ancient, permafrost derived C (f_{OM}) in the respired CO_2 can be calculated. In combination with CO_2 flux measurements, also the amount of ancient C released from permafrost can be determined. As the decomposition of ancient permafrost C would have large effects on the atmospheric CO_2 concentration, the ^{14}C analysis of respired CO_2 is an ideal tool to investigate the permafrost C feedback (Schuur *et al.*, 2009).

^{14}C measurement

Today, the technique to measure the ^{14}C ratio is the AMS technology, which separates isotopes of the same element based on their different masses. The combination of mass spectrometry with an accelerator allows to directly measure the low isotopic $^{14}\text{C}/^{12}\text{C}$ ratios. In modern natural samples the $^{14}\text{C}/^{12}\text{C}$ ratio lies around 10^{-12} . Usually, 500 to 1000 μg of C are prepared as graphite targets for ^{14}C analysis. However, due to the increasing demand for analyses of smaller sample sizes, micro-graphitization systems (Santos *et al.*, 2007, Liebl *et al.*, 2010) and gas ion sources (Ruff *et*

al., 2007, Fahrni *et al.*, 2013) have been developed. These microscale AMS ^{14}C analyses allow the measurement of sample sizes of less than $10\ \mu\text{g C}$. AMS ^{14}C analysis of samples converted to graphite produce much higher negative ion currents, thus resulting in a higher precision compared to the direct analysis of CO_2 samples (Fahrni *et al.*, 2013, McIntyre *et al.*, 2013). This allows the dating of older samples up to 50,000 yrs BP. Nevertheless, the use of a gas ion source has the great advantage that the CO_2 sample can be measured directly and does not need to be graphitized prior analysis, which reduces the risk of contamination and sample loss.

In this dissertation, the AMS ^{14}C analyses were primarily performed directly as gaseous CO_2 ($\sim 50\ \mu\text{g C}$) with the gas ion source of the mini carbon dating system (MICADAS, Ionplus AG, Switzerland) at the Laboratory of Ion Beam Physics of the ETH Zurich (Switzerland; Ruff *et al.*, 2007, Synal *et al.*, 2007). Additionally, the direct CO_2 transfer from the developed sampling device to an AGE system (Wacker *et al.*, 2010) was tested. ^{14}C analyses of the CO_2 converted to graphite ($700\text{--}1000\ \mu\text{g C}$) were performed at the CologneAMS facility (Germany) with a 6 MV Tandatron AMS (HVEE, The Netherlands; Dewald *et al.*, 2013).

Reporting of ^{14}C data

The measurement of absolute isotope concentrations is difficult. Therefore, their relative isotope abundance is analyzed. The relative isotope abundance (R) is always expressed as the ratio between the rare isotope in comparison to the abundant isotope:

$$R = \frac{\text{rare}}{\text{abundant}} = \frac{^{14}\text{C}}{^{12}\text{C}}$$

As the differences between isotopic ratios of different samples in nature is rather small, it is common to express them in relation to a standard material and give them as a relative deviation. For ^{14}C , the data is reported relative to 95% of the ratio of the NBS (National Bureau of Standards) oxalic acid I standard (Ox-I) measured in parallel (Stuiver & Polach, 1977). The resulting value is expressed as fraction modern C ($F^{14}\text{C}$), which is also sometimes reported in percent modern C ($\text{PMC} = 100 \times F^{14}\text{C}$; Reimer *et al.*, 2004, Stuiver & Polach, 1977):

$$F^{14}\text{C} = \frac{R_{\text{sample}}}{0.95 \times R_{\text{Ox-I}}} = \frac{\frac{^{14}\text{C}}{^{12}\text{C}}_{\text{sample}}}{0.95 \times \frac{^{14}\text{C}}{^{12}\text{C}}_{\text{Ox-I}}}$$

Within this calculation, the used ratios of the standard and samples are corrected for mass dependent isotope fractionation. By convention, the Ox-I standard is normalized to its actual $\delta^{13}\text{C}$ value of -19‰ and the samples are normalized to -25‰ (Stuiver & Polach, 1977).

In addition to $F^{14}\text{C}$, the ^{14}C age is used in this dissertation. This age assumes that the radiocarbon concentration in the atmosphere is constant and is based on the Libby half-life (5568 yr; Libby, 1952). It is defined as the age (t) of a sample before 1950 (present) and therefore reported in years before present (yrs BP):

$$t = -8033 \times \ln(F^{14}C)$$

The ^{14}C age can be converted to an actual calendar age by applying a calibration curve (e.g. IntCal13; Reimer *et al.*, 2013), which accounts for natural ^{14}C abundance variations occurring in the atmosphere.

Paper I

$^{14}\text{CO}_2$ processing using an improved and robust molecular sieve cartridge

Anja Wotte, Patrick Wordell-Dietrich, Lukas Wacker, Axel Don, Janet Rethemeyer

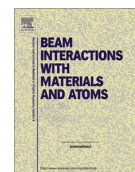
Nuclear Inst. and Methods in Physics Research B 400, 65-73, 2017



ELSEVIER

Contents lists available at ScienceDirect

Nuclear Instruments and Methods in Physics Research B

journal homepage: www.elsevier.com/locate/nimb $^{14}\text{CO}_2$ processing using an improved and robust molecular sieve cartridgeAnja Wotte^{a,*}, Patrick Wordell-Dietrich^{b,1}, Lukas Wacker^c, Axel Don^b, Janet Rethemeyer^a^a Institute of Geology and Mineralogy, University of Cologne, Cologne, Germany^b Thünen Institute of Climate-Smart Agriculture, Braunschweig, Germany^c Ion Beam Physics, ETH Zurich, Zurich, Switzerland

ARTICLE INFO

Article history:

Received 12 January 2017

Received in revised form 14 March 2017

Accepted 5 April 2017

Keywords:

Radiocarbon

 CO_2

Molecular sieve

Zeolite

13X

Respiration

ABSTRACT

Radiocarbon (^{14}C) analysis on CO_2 can provide valuable information on the carbon cycle as different carbon pools differ in their ^{14}C signature. While fresh, biogenic carbon shows atmospheric ^{14}C concentrations, fossil carbon is ^{14}C free. As shown in previous studies, CO_2 can be collected for ^{14}C analysis using molecular sieve cartridges (MSC). These devices have previously been made of plastic and glass, which can easily be damaged during transport. We thus constructed a robust MSC suitable for field application under tough conditions or in remote areas, which is entirely made of stainless steel. The new MSC should also be tight over several months to allow long sampling campaigns and transport times, which was proven by a one year storage test. The reliability of the $^{14}\text{CO}_2$ results obtained with the MSC was evaluated by detailed tests of different procedures to clean the molecular sieve (zeolite type 13X) and for the adsorption and desorption of CO_2 from the zeolite using a vacuum rig. We show that the $^{14}\text{CO}_2$ results are not affected by any contamination of modern or fossil origin, cross contamination from previous samples, and by carbon isotopic fractionation. In addition, we evaluated the direct CO_2 transfer from the MSC into the automatic graphitization equipment AGE with the subsequent ^{14}C AMS analysis as graphite. This semi-automatic approach can be fully automated in the future, which would allow a high sample throughput. We obtained very promising, low blank values between 0.0018 and 0.0028 F^{14}C (equivalent to 50,800 and 47,200 yrs BP), which are within the analytical background and lower than results obtained in previous studies.

© 2017 Elsevier B.V. All rights reserved.

1. Introduction

The ^{14}C analysis of CO_2 is a valuable method to identify different carbon sources, i.e. carbon of different age and origin. This analytical technique was used in previous studies to investigate anthropogenic influences as well as natural processes in the carbon cycle. For example $^{14}\text{CO}_2$ analysis of atmospheric samples is used to identify and quantify natural and urban (petroleum derived) emissions in urban environments [1–3]. More frequently, $^{14}\text{CO}_2$ analyses are performed to investigate soil and sedimentary organic matter turnover and to determine sources of microbial respired CO_2 released from temperate soils and peatlands [4–7], from permafrost soils [8–10] as well as from aquatic environments to understand the CO_2 transport processes therein [11–14].

A promising approach to collect and concentrate CO_2 samples for ^{14}C analysis is the use of molecular sieves [3,15–17]. This approach has the advantage that low concentrations of CO_2 can be collected in a small volume without the need of cryogenic methods or caustic NaOH for the trapping of CO_2 . This makes molecular sieves very useful in field studies particularly in remote areas [e.g. 15–17]. Molecular sieves are porous, solid materials that act as sieves on molecular dimensions, i.e. molecules smaller than the pore size are adsorbed while larger molecules pass the sieve [18]. The most suitable molecular sieve for trapping CO_2 is the zeolite type 13X, which is a low silica sodium aluminosilicate, also known as FAU type (faujasite topology; after the IZA Atlas of zeolite structures [19]), used in several applications to (pre-)concentrate CO_2 for ^{14}C as well as for ^{13}C analysis [3,15–17,20–22]. 13X has higher adsorption capacities for CO_2 compared to other zeolites like type 4A and 5A [23–25] and compared to other gases like N_2 , CH_4 , H_2 , and He [25,26]. The adsorbed CO_2 can be released by heating the zeolite, whereby it is regenerated and can be reused.

* Corresponding author.

E-mail address: Anja.Wotte@uni-koeln.de (A. Wotte).¹ Present address: Institute of Soil Science and Site Ecology, TU Dresden, Dresden, Germany.

Several of the mentioned studies did not validate their CO_2 sampling and desorption procedures and the cleaning of the zeolite or did not report the results of such analyses [e.g. 6, 8–10, 27–29]. However, this is of great importance to obtain reliable results [16,17]. For example, insufficient cleaning of the zeolite can lead to memory effects, while incomplete sample ad- and desorption, e.g. caused by H_2O adsorption, can cause isotopic fractionation [17]. So far, there is no consensus about the optimal procedure for cleaning the molecular sieve and for adsorbing and desorbing the CO_2 . Most previous studies use a passive cleaning and desorption procedure under vacuum with different heating times and temperatures (5–150 min; 240–500 °C) [16,17,21]. Other studies use an active procedure, i.e. an inert purge gas during cleaning of the zeolite and during CO_2 desorption [15,22]. Recently Walker et al. [3] combined both methods including the active cleaning of the zeolite under a purge gas stream and the passive release of sampled CO_2 under vacuum.

For the implementation of $^{14}\text{CO}_2$ analysis at the CologneAMS ^{14}C laboratory we assembled in a pilot study a MSC using quartz glass tubes, Tygon® tubing (Carl Roth GmbH & Co. KG, Germany) and plastic quick couplings (Colder Products Company, USA) based on published methods [16,21]. During the application of this MSC in the Siberian Arctic, we had severe contamination issues by large contributions of atmospheric CO_2 because the MSC obviously was not tight during the long transport and storage time of several months after the CO_2 collection. Moreover, some of the glass tubes were broken during transport. Consequently, we constructed a new MSC, which is entirely made of stainless steel, and thus more resistant against damages. Another important property of a MSC suitable for field applications in remote areas is that no atmospheric CO_2 is leaking into the MSC during storage of the CO_2 loaded onto the MSC, which has never been evaluated before. We thus, determined the contribution of atmospheric CO_2 to a ^{14}C free CO_2 sample in a MSC, which was stored one year. We evaluated different zeolite cleaning and CO_2 desorption procedures to identify the most suitable method yielding the lowest contamination from exogenous sources or from samples previously loaded onto the molecular sieve and producing no isotopic fractionation. In addition, we tested the use of smaller amounts of zeolite (300–3000 mg) to minimize possible contaminations and the adsorption of water molecules. To enable the automated processing of larger sets of CO_2 samples, we evaluated for the first time the connection of the MSC to the automated graphitization equipment AGE [22].

2. Material and methods

2.1. Design of the MSC

The new MSC constructed and evaluated in this study is based on the design by Bol and Harkness [21]. In contrast to devices made of quartz tubes and plastic fittings used in previous studies [3,15,16,21,30] we built a MSC, which is entirely made of stainless steel. It consists of a stainless steel tube (10 mm or 3/8" OD, ~24 cm length) in which zeolite type 13X (40/60 mesh, Charge 5634, IVA Analysentechnik GmbH & Co. KG, Germany) is placed in the central part and held in place by quartz wool (Fig. 1). The tube is closed on both ends with stainless steel quick couplings (Q2DSH, Hy-Lok D Vertriebs GmbH, Germany). Thereby the number of fittings is reduced, which lowers the risk of leaks.

For cleaning the zeolite as well as for CO_2 adsorption to and desorption from the molecular sieve the MSC was attached to a vacuum rig shown in Fig. 2 using quick couplings (Q2BH-6T, Hy-Lok D Vertriebs GmbH, Germany).

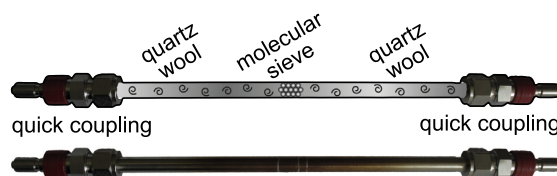


Fig. 1. Image of the new MSC consisting of a stainless steel tube and two quick couplings. The upper MSC illustrates the filling of the stainless steel tube. Note that the stainless steel tube is completely filled with quartz wool and so the molecular sieve in the center cannot move.

2.2. Amount of zeolite and MSC storage

Zeolite type 13X is not only effectively trapping CO_2 but also water that can even displace CO_2 . This is particularly a problem in wet environments (e.g. peatlands, permafrost soils, aquatic environments) and was a problem in our pilot field study applying the glass/plastic MSCs in Siberia. Using respiration chambers and the desiccant Drierite (10–20 mesh, Stock No. 24001, W. A. Hammond Drierite Company, USA) installed in front of the MSC, we trapped little CO_2 but large amounts of water, which complicated the CO_2 purification for AMS ^{14}C analysis. We thus tested if the use of different amounts of zeolite (300, 1000, and 3000 mg) influences the trapping of unwanted water and other molecules using a ^{14}C free CO_2 standard.

Exogenous carbon, particularly atmospheric CO_2 may enter the MSC through leaking couplings and this is expected to depend on the duration of the MSC storage. For field studies in remote areas it is particularly important that the CO_2 loaded onto the MSC can be stored weeks to several month without any significant atmospheric CO_2 contribution entering the MSC because of long sampling campaigns and transport times. To test if the new MSC can store the CO_2 free of contamination over long periods, we filled two MSCs with ^{14}C free CO_2 (~1300 $\mu\text{g C}$) and stored them for one year prior to CO_2 desorption (cf. 2.3 for standard preparation).

2.3. Sample processing with MSCs

For testing our new MSC and different CO_2 processing procedures (Table 1) we used CO_2 standards of different carbon isotopic compositions (^{14}C and ^{13}C) including ^{14}C free CO_2 from a gas bottle (Quellkohlen säure 3.5, Westfalen AG, Germany) and CO_2 derived from solid IAEA standards C1 ($0.0000 \pm 0.0002 \text{ F}^{14}\text{C}$, $2.42 \pm 0.11\text{‰}$ VPDB), IAEA C3 ($1.2941 \pm 0.0006 \text{ F}^{14}\text{C}$, $-24.91 \pm 0.16\text{‰}$ VPDB), and IAEA C7 ($0.4953 \pm 0.0012 \text{ F}^{14}\text{C}$, $-14.48 \pm 0.21\text{‰}$ VPDB; [31,32]). The standards were either combusted (organic standards: IAEA C3 and C7) at 900 °C for 4 h in quartz tubes together with copper oxide (150 mg) and silver wool (50 mg) or hydrolyzed (inorganic standard: IAEA C1) with 99% H_3PO_4 (1.5 ml) in borosilicate tubes heated at 75 °C for ~12 h. The CO_2 evolved was purified cryogenically, quantified, and splits were transferred into glass tubes for the cross contamination and storage tests of the MSC (~1300 $\mu\text{g C}$). The standard size of 1300 $\mu\text{g C}$ was chosen as a realistic amount of C that can be sampled according to published field studies [1,5,6].

2.3.1. Cleaning of the zeolite

Prior to sampling, the zeolite in the MSC has to be cleaned to remove any contaminants from exogenous sources or CO_2 of previous loaded samples to prevent memory effects. Therefore, the MSC was attached to the vacuum rig and its central part containing the zeolite was heated (500 °C) using a self-made tube furnace (Ceramic Fiber Heaters, VS402A06S with controller EZ-Zone® PM

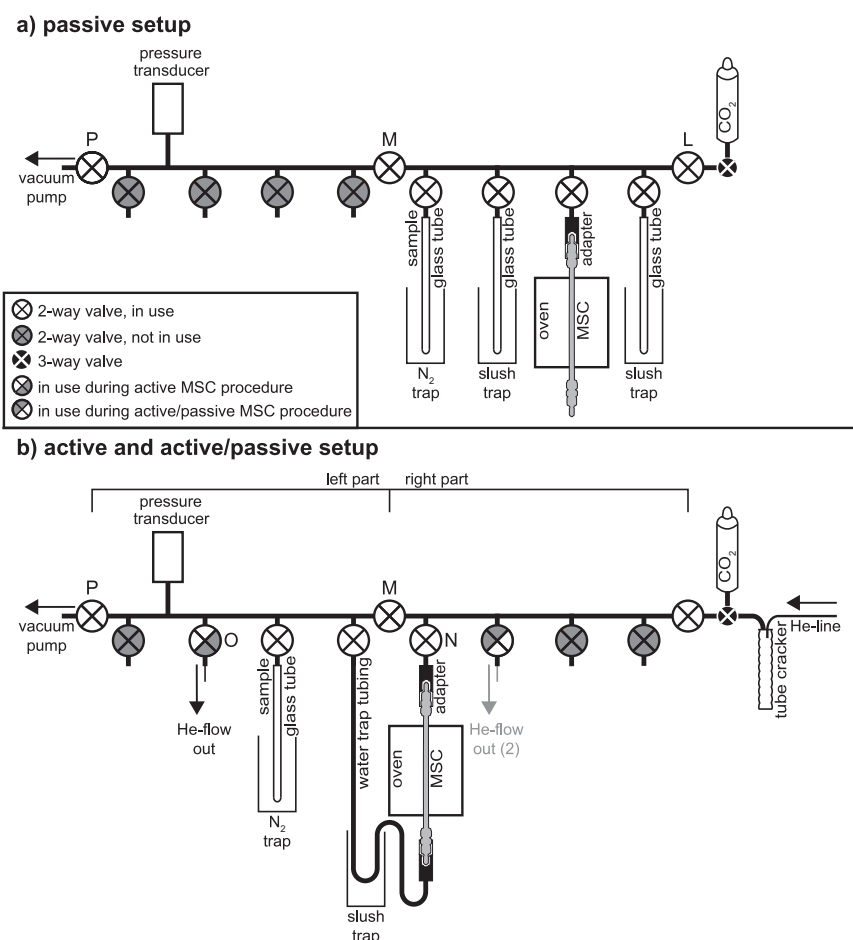


Fig. 2. Schematic illustration of the vacuum rig used to process the MSC. The CO₂ standards were transferred onto the MSC either directly from the gas bottle or by releasing CO₂ standards from glass ampoules using a tube cracker. The desorbed CO₂ was collected in a glass tube placed in liquid N₂ after water was removed by the slush traps (dry ice ethanol slurry). Fig. a) shows the arrangement during the passive procedure, and in Fig. b) the setup for both, the active and for the combined active/passive procedure using He as purge gas is displayed. The CO₂ quantification was performed on a separate vacuum rig.

Table 1

Passive (under vacuum) and active procedures (with helium flow) tested for cleaning the zeolite as well as for CO₂ adsorption to and desorption from the zeolite. Parameters tested include: (1) vacuum or helium flow, (2) duration and temperature of heating (the heating time does not include the preheating time to 500 °C of 15 min), (3) way of CO₂ transfer, and (4) CO₂ adsorption time.

		MSC procedures		
		Passive	Active	Combined active/passive
Zeolite cleaning	(1)	$p < 10^{-3}$ mbar	He flow ~ 120 ml min ⁻¹	He flow ~ 40 ml min ⁻¹
	(2)	15–120 min, 500 °C	45 min, 500 °C	20 min, 150 °C + 25 min, 500 °C
CO ₂ adsorption	(3)	Gas expansion	He flow ~ 100 ml min ⁻¹	He flow ~ 40 ml min ⁻¹
	(4)	10 min	10 min	30 min
CO ₂ desorption	(3)	Under vacuum	(a) He flow ~ 100 ml min ⁻¹	Under vacuum
	(2)	20 min, 150 °C + 15 min, 500 °C sampling during 500 °C heating only	20 min, 150 °C + 15 min, 500 °C	(b) He flow ~ 100 ml min ⁻¹ 60 min, 150 °C 20 min 150 °C + 25 min 500 °C

1/16 DIN, both Watlow, USA). During passive cleaning of the zeolite the rig was held under vacuum ($p < 10^{-3}$ mbar; Fig. 2a) while active cleaning was performed by flushing with He (40/120 ml min⁻¹, 45 min; Fig. 2b) similar to Garnett and Murray [15] and Wacker et al. [22]. In addition, we tested different heating times for the passive cleaning ranging from 15 to 165 min (plus a preheating time of 15 min). All cleaning procedures investigated

are summarized in Table 1. When not in use, the MSC was filled with pure He (grade 4.6) slightly above atmospheric pressure similar to Hardie et al. [16].

2.3.2. CO₂ adsorption and desorption

We transferred the CO₂ standards of different isotopic compositions onto the zeolite using passive and active methods (Table 1,

Fig. 2). The CO₂ standards made from IAEA standards were released from the glass tubes using a tube cracker, while the ¹⁴C free CO₂ from a gas bottle was transferred over the vacuum rig to the zeolite of the MSC (Fig. 2).

To identify the optimal procedure for CO₂ desorption from the zeolite we compared four different procedures including one passive, two active, and a combined approach listed in Table 1. In all cases the vacuum rig to which the sample glass tube was attached (Fig. 2) was evacuated in advance to approximately 10⁻⁴ mbar.

The passive CO₂ desorption from the zeolite was done under vacuum while heating the MSC for 20 min at 150 °C (valve L was closed) followed by heating within 15 min to 500 °C (valve M was closed), which was held for another 15 min (Table 1, Fig. 2a). H₂O evolved during the desorption process was removed with two slush traps (dry ice-ethanol slurry) attached at two glass tubes, whereas the CO₂ released from the MSC was collected in a glass tube placed in liquid nitrogen (Fig. 2a). The latter was used only during the last five minutes of heating in order to allow sufficient time for the trapping of water.

The active CO₂ desorption was performed using a He stream while heating the zeolite (Table 1, Fig. 2b). The MSC was quickly attached to the vacuum line, while the whole system was flushed with He (~120 ml min⁻¹, <5 min; valves M and P were closed). Then, the MSC was heated to release the CO₂, which was transferred with the He stream (100 ml min⁻¹) via the water trap into the sample glass tube, placed in liquid nitrogen. In method (a) the same heating program was applied as for the passive method (20 min at 150 °C, heating within 15 min to 500 °C held for another 15 min), while method (b) is using a longer desorption time of 60 min and a constant and lower temperature of 150 °C.

The active/passive (adsorption/desorption) method combines the three methods described previously (Table 1). First, the right section of the vacuum rig including the MSC adapter (Fig. 2b) was flushed with He (~120 ml min⁻¹). Then the MSC was connected to the vacuum line and the left section including the MSC

was evacuated quickly (<5 min, p < 5 × 10⁻³ mbar) to pump away any potentially introduced atmospheric CO₂, which may contaminate the sample. The CO₂ was then desorbed passively (by expansion) from the zeolite and released into a closed volume (valves M, N, O and P were closed; Fig. 2b) by stepwise heating the MSC (20 min at 150 °C, heating within 15 min to 500 °C, held for another 25 min).

The desorbed CO₂ was flame sealed in the glass tube after non-condensable gases were pumped away (p < 10⁻⁴ mbar). CO₂ quantification was done on a separate vacuum line involving an additional cryogenic purification step. After quantification, the CO₂ was portioned in pre-combusted (450 °C, 4 h) glass tubes for gas ion source AMS ¹⁴C analysis (~50 µg C) and ¹³C analysis (300–730 µg C). The split for ¹³C analysis was taken only during cross-contamination tests.

2.3.3. Cross-contamination and isotopic fractionation

To evaluate potential cross-contamination effects derived from samples previously trapped on the MSC, we loaded three IAEA standards (~1300 µg C, each) of different carbon isotopic compositions consecutively onto one MSC (filled with 500 mg zeolite) and desorbed these subsequently. For this, the combined active/passive MSC procedure was used (Table 1). Two different sequences using two MSCs were tested including 1) IAEA C1, C1, C3, and C7 and 2) IAEA C3, C1, C7, and C7 (Table 2). In addition to ¹⁴C, we analyzed the δ¹³C concentration of both untreated and loaded/desorbed standards. Differences in the stable carbon composition will indicate isotopic fractionation. These tests described above were also applied to evaluate the MSC-AGE coupling (see Section 2.3.4).

2.3.4. Coupling of the MSC with the AGE

AMS ¹⁴C analysis of samples converted to graphite still produce much higher negative ion currents thus resulting in a higher precision compared to the direct analysis of CO₂ samples [33,34]. This also allows the dating of older samples (40,000–50,000 yrs).

Table 2

δ¹³C and F¹⁴C results of the test to identify cross-contamination and isotopic fractionation. Different IAEA standards were consecutively adsorbed and recovered from four different MSCs (labeled 1–4) and analyzed with an AMS either as CO₂ or as graphite. Reported δ¹³C values are measured with an IRMS. F¹⁴C is also reported for two IAEA C1 standards stored for >1 year on a MSC. Consensus values for standards are reported by a = [31] b = [32].

	MSC Run order	Source of CO ₂	Labcode (¹³ C)	Labcode (¹⁴ C)	δ ¹³ C (‰VPDB)	F ¹⁴ C (±1σ)	
AMS CO ₂ analysis	Previous	Atmosphere					
	1-1	IAEA C1	COL1100.1.0.3f	COL1100.1.0.3g	2.06 ± 0.1	0.0086 ± 0.0009 ^a	
	1-2	IAEA C1	COL1100.1.0.2f	COL1100.1.0.2g	2.12 ± 0.1	0.0130 ± 0.0011 ^a	
	1-3	IAEA C3	COL1003.1.0.1i	COL1003.1.0.1j	-24.79 ± 0.1	1.2792 ± 0.0135	
	1-4	IAEA C7	COL1007.1.0.1k	COL1007.1.0.1l	-14.44 ± 0.1	0.4876 ± 0.0077	
	Previous	IAEA C3					
	2-1	IAEA C3	COL1003.1.0.1n	COL1003.1.0.1l	-25.4 ± 0.1	1.2755 ± 0.0136	
	2-2	IAEA C1	COL1100.1.0.2i	COL1100.1.0.2j	2.02 ± 0.1	0.0101 ± 0.0010 ^a	
	2-3	IAEA C7	COL1007.1.0.1p	COL1007.1.0.1q	-14.66 ± 0.1	0.5172 ± 0.0083	
	2-4	IAEA C7	COL1007.1.0.1u	COL1007.1.0.1t	-14.85 ± 0.1	0.4808 ± 0.0074	
	Storage-test	IAEA C1	-	COL1100.1b.0.4a	-	0.0088 ± 0.0008	
	Storage-test	IAEA C1	-	COL1100.1b.0.4b	-	0.0144 ± 0.0010	
	AMS graphite analysis	Previous	Atmosphere				
		3-1	IAEA C3	-	COL1003.1.1.1p	-	1.2906 ± 0.0059
3-2		IAEA C1	-	COL1100.1.1.1b	-	0.0028 ± 0.0002	
3-3		IAEA C7	-	COL1007.1.1.2c	-	0.4955 ± 0.0029	
3-4		IAEA C7	-	COL1007.1.2.2d	-	0.4961 ± 0.0030	
Previous		Atmosphere					
4-1		IAEA C1	-	COL1100.1.3.5a	-	0.0023 ± 0.0002 ^a	
4-2		IAEA C1	-	COL1100.1.4.5b	-	0.0018 ± 0.0002 ^a	
4-3		IAEA C3	-	COL1003.1.2.1o	-	1.3003 ± 0.0062	
4-4		IAEA C7	-	COL1007.1.4.1d	-	0.4980 ± 0.0034	
Consensus values		IAEA C1			2.42 ± 0.11	0.0000 ± 0.0002 ^a	
		IAEA C3			-24.91 ± 0.16	1.2941 ± 0.0006 ^a	
		IAEA C7			-14.48 ± 0.21	0.4953 ± 0.0012 ^b	

^a No blank correction.

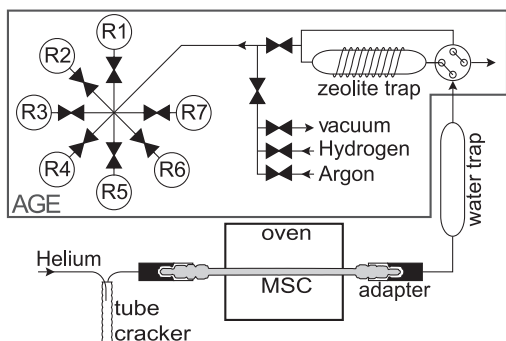


Fig. 3. Schematic illustration of the MSC connected to the AGE system with its zeolite trap and seven reactors (R1–R7; modified figure from [22]). For our tests, the CO_2 standards were released from the glass tubes using a tube cracker and flushed onto the MSC with He. The CO_2 is desorbed by heating the MSC and flushed with He over a water trap to the zeolite trap of the AGE.

Moreover, when using an automated graphitization system, e.g. AGE [22], no cryogenic gas purification is needed and the CO_2 processing can be fully automated allowing a high sample throughput. We tested the coupling of our MSC with the AGE to release the CO_2 directly onto the zeolite trap of the graphitization system (Fig. 3), using stainless-steel quick couplings (Q2BH, Hy-Lok D Vertriebs GmbH, Germany). The CO_2 standards were released from the glass tubes using a tube cracker mounted in front of the MSC and transferred in a He flow (40 ml/min) onto the zeolite of the cleaned MSC (Fig. 3). The MSC was prepared in a similar way as described above. In order to increase the sample throughput, the cleaning time was reduced to 30 min (at 500 °C, $\sim 40 \text{ ml min}^{-1}$ He flow) and the desorption time was reduced to 22 min (7 min at 150 °C followed by heating within 10 min to 500 °C held for 5 min). These durations may still be reduced because previous studies showed that >99% of the CO_2 are released from the molecular sieve within less than 5 min of heating [15,20].

During the desorption process the released CO_2 was transferred with a He flow (40 ml/min) via a water trap (phosphorus pentoxide, Merck Sicapent[®]) to the zeolite trap of the AGE (Fig. 3). In the AGE the CO_2 is transferred automatically to one of the seven reactors where it is reduced to graphite with H_2 over iron as catalyst [22].

2.4. Carbon isotopic analyses

AMS ^{14}C analyses were performed on CO_2 converted either to graphite targets, or measured directly as CO_2 . The $^{14}\text{CO}_2$ analysis was performed with the gas ion source of the MICADAS AMS at the ETH Zurich (Switzerland, [35,36]). The graphite targets were measured at the CologneAMS facility (Germany) with a 6 MV Tandemron AMS (HVE, The Netherlands, [37]). The ^{14}C results are reported in $F^{14}\text{C}$ with 1- σ uncertainties and normalized to $\delta^{13}\text{C}$ of -25‰ following the convention by Stuiver and Polach [38] and Reimer et al. [39]. The ^{14}C concentrations of the IAEA C3 and C7 standards were blank corrected, while the ^{14}C free standards were not blank corrected.

The stable carbon isotope measurements were performed on a ThermoFinnigan Delta Plus isotope ratio mass spectrometer (IRMS) at the Institute for Geology and Paleontology, University of Münster (Germany). The cryogenically purified CO_2 standards were introduced into the mass spectrometer using a dual inlet system. The results are expressed in per mil relative to the Vienna-PDB reference standard.

3. Results and discussion

3.1. Amount of zeolite and MSC storage

In previous studies a large range of 0.25–12 g of zeolite was used for trapping CO_2 for ^{14}C analysis, [3,15–17,20,21,40]. The large amounts of >1 g zeolite type 13X used in most studies are unnecessary for adsorbing sufficient CO_2 for AMS ^{14}C analysis and may complicate the CO_2 desorption process because besides more CO_2 also more unwanted molecules such as water may be trapped. Likewise, in the AGE graphitization system a relatively small amount of 200 mg of zeolite is used, which is sufficient to trap at least 1000 $\mu\text{g C}$ [22]. We thus tested different amounts of zeolite (300, 1000, 3000 mg) that were filled in the MSC. Surprisingly we determined similar ^{14}C concentrations for ^{14}C free CO_2 using comparable cleaning, adsorption, and desorption procedures for the different amounts of zeolite (Fig. 4). In contrast, Walker et al. [3] showed decreasing contributions of exogenous carbon for smaller amounts of zeolite (0.015–0.005 $F^{14}\text{C}$ for 100–250 mg zeolite). Our result may be explained by the very effective and long cleaning procedure used in our tests, but dependent on the application a shorter (<60 min) cleaning time is necessary. Therefore, it is recommendable to use smaller amounts of zeolite, which traps sufficient CO_2 for AMS ^{14}C analysis on both, gas or graphite targets and minimizes contamination issues. We thus used a small amount of 500 mg type 13X zeolite for the cross contamination tests.

We evaluated if CO_2 can be stored in the new MSC without being contaminated by atmospheric CO_2 over periods of up to several months, which is essential if transport and storage times of the MSC are long. To test this, we stored two MSCs filled with IAEA C1 ($\sim 1300 \mu\text{g C}$) for one year and measured ^{14}C concentrations of 0.0088 ± 0.0008 and $0.0144 \pm 0.0010 F^{14}\text{C}$ (equivalent to 38,000 and 34,100 yrs BP; Table 2) using AMS gas ion source analysis. These low $F^{14}\text{C}$ values are in the range of the MSC tests, which were immediately processed (mean value: $0.0105 \pm 0.0022 F^{14}\text{C}$; cf. 3.4; Table 2). An amount of 6 $\mu\text{g C}$ of atmospheric origin would be needed to significantly (beyond 2- σ) shift the ^{14}C signature of

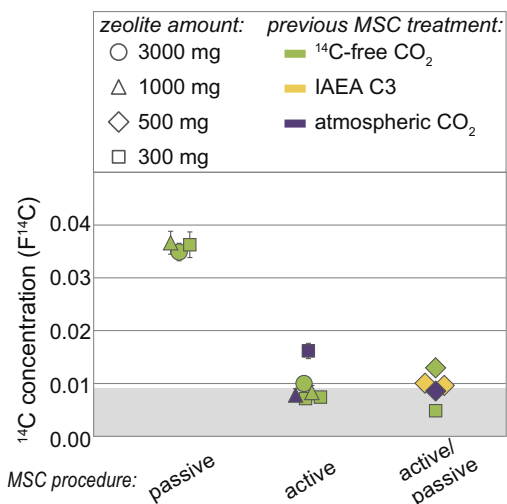


Fig. 4. ^{14}C results (AMS analysis of CO_2) of ^{14}C free CO_2 recovered from the MSC a) filled with different amounts of zeolite (300, 500, 1000, and 3000 mg) and b) using different cleaning, adsorption and desorption procedures listed in Table 1. The different colors of the symbols represent the standard loaded previously onto the sieve. The gray shaded area represents the analytical background of the AMS ^{14}C analysis of CO_2 samples. Most error bars (1- σ) are within the symbol size.

the ¹⁴C free CO₂ trapped on the MSC when using a similar sample size of 1300 μg C.

3.2. Cleaning of the zeolite

The comparison of different cleaning protocols reveals considerable differences between the active and passive methods and the duration of heating the MSC. The passive cleaning is strongly dependent on the cleaning (heating) time as indicated by decreasing F¹⁴C concentrations for ¹⁴C free CO₂ which range from 0.3045 ± 0.0071 F¹⁴C, obtained by heating 15 min, to 0.0349 ± 0.0017 F¹⁴C, for a much longer heating time of 165 min both at 500 °C (excluding preheating of 15 min, Fig. 5). The active regeneration of the zeolite accelerates the cleaning process and yields much lower ¹⁴C concentrations for ¹⁴C free CO₂ of 0.0048 ± 0.0008–0.0162 ± 0.0014 F¹⁴C when using a heating time of 60 min, whereas passive cleaning under comparable conditions yields concentrations of 0.0349 ± 0.0017–0.0366 ± 0.0022 F¹⁴C (Fig. 4). Our results underline the findings of Walker et al. [3] that sufficient cleaning is essential to entirely remove contaminations from the zeolite. Accordingly, we recommend the active cleaning of the zeolite using an inert purge gas like He. The cleaning time of 60 min might be significantly reduced to a few minutes as it is done in the AGE system [22], which uses a heating time of only two minutes to clean the zeolite trap (at 450 °C).

3.3. CO₂ adsorption and desorption

To evaluate our laboratory tests of the MSC, the CO₂ prepared from reference materials needs to be transferred onto the zeolite. This adsorption process is most effectively done by active flushing with an inert gas, as this is less time consuming than the passive transfer by gas expansion. In field applications CO₂ from ambient air or CO₂ respired from soils and sediments will be collected with MSCs by other methods, e.g. respiration chambers can be used either passively by diffusion [5,41] or actively using a pump based system [6,8,16]. The choice of active or passive adsorption will depend on the application.

The CO₂ can be desorbed from the zeolite either actively or passively. There are no significant differences between the active desorption method or the passive desorption of the combined active/passive method. For example, both methods yield ¹⁴C concentrations for ¹⁴C free CO₂ in the range of 0.0048 ± 0.0008–0.0162 ± 0.0014 F¹⁴C equivalent to 42,900–33,100 yrs BP, which is close to the analytical background of AMS ¹⁴C analyses of gas samples (determined by the ¹⁴C analysis of untreated standards; Fig. 4). The active method is certainly a bit faster, as can be seen

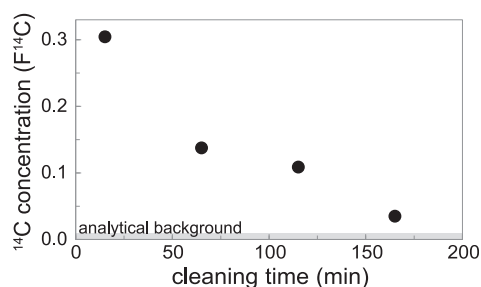


Fig. 5. ¹⁴C concentrations (not blank corrected) of ¹⁴C free CO₂ loaded on and released from the MSC passively using different cleaning times of the zeolite (preheating times of 15 min are not included). The gray bar represents the analytical background of the AMS ¹⁴C analysis of CO₂ samples. Error bars are within symbol size.

also from the cleaning procedures. This is, however, less important for the CO₂ desorption.

The cold finger (placed in liquid nitrogen) of the vacuum rig shown in Fig. 2, however, is not capable to collect the desorbed CO₂ completely, because the He flow is not forced to go through the trap, whereby a significant amount of the desorbed CO₂ is flushed out. Thus, it is essential to use a flow-through CO₂ trap when using active desorption procedures (Fig. 2b).

The reproducibility of the most favorable method – the active/passive procedure – was proven by the more detailed test of cross-contamination and isotopic fractionation shown in Table 2 and Fig. 6 and is discussed below.

3.4. Cross-contamination and isotopic fractionation

In order to determine a potential cross-contamination of CO₂ from samples previously loaded onto the MSC and a potential carbon isotopic fractionation, we performed test series in which CO₂ standards with different isotopic compositions were consecutively transferred to and removed from the MSC using the combined active cleaning and adsorption/passive desorption procedure. Two series were measured as CO₂ using AMS gas ion source analysis and splits were taken for δ¹³C analysis (Fig. 6a), while two other series were converted to graphite for AMS analysis (no δ¹³C IRMS data available; Fig. 6b). Thus, isotopic fractionation was evaluated from the sample series displayed in Fig. 6a. The δ¹³C values of the different standards all lay within two standard deviations (2-σ) of their consensus values (Table 2; Fig. 6a). This indicates that no statistically significant isotopic fractionation is occurring during the sample processing using the combined active/passive method. These results agree well with the findings of other studies, which also determined no fractionation effects using active [15] or passive [16,21] desorption procedures. During the four test series we obtained a mean recovery of 86%, which is similar to [21], but about 10% lower compared to [15–17]. The reason for the lower recoveries compared to the latter studies is not clear but we think that they do not result from incomplete CO₂ desorption, because the δ¹³C results in this study do not show any fractionation effect. Isotopic fractionation may only occur during long evacuation times of the MSC (35–75 min in our tests) at room temperature which will lead to elevated δ¹³C values (by 1.6‰ to 6.8‰ in our tests), which was already observed by Palonen and Oinonen [17]. Thus, we recommend evacuating the MSC only for few minutes (<5 min) at room temperature to avoid the preferential release of ¹²CO₂. However, the fractionation has no effect on the ¹⁴C results, because they are normalized to fixed ¹³C values.

The ¹⁴C results for the different sample series reveal no statistically significant (beyond the 2-σ range) cross-contamination derived from standards previously loaded on the MSC because they are all in agreement with their consensus values and/or similar to the untreated (non-trapped) standards (Table 2, Fig. 6a and b).

3.5. CO₂ processing with the MSC-AGE system

The coupling of the MSC with the AGE has so far not been tested but allows a faster processing of larger sample sets even under the currently semi-automatic conditions. Our tests using the ¹⁴C free IAEA C1 standard yield very low ¹⁴C concentrations of 0.0018 ± 0.0002–0.0028 ± 0.0002 F¹⁴C equivalent to 50,800 and 47,200 yrs BP (Table 2; Fig. 6b). These values are lower compared to our tests processed on the vacuum rig due to the higher precision of the AMS analysis of graphite samples compared to AMS ¹⁴CO₂ analysis (Fig. 6a and b). Likewise, the ¹⁴C concentrations for the modern (IAEA C3) and intermediate standards (IAEA C7) show an even better agreement (within 1-σ) with the standard consensus values compared to the CO₂ analyses (Fig. 6b). This data set,

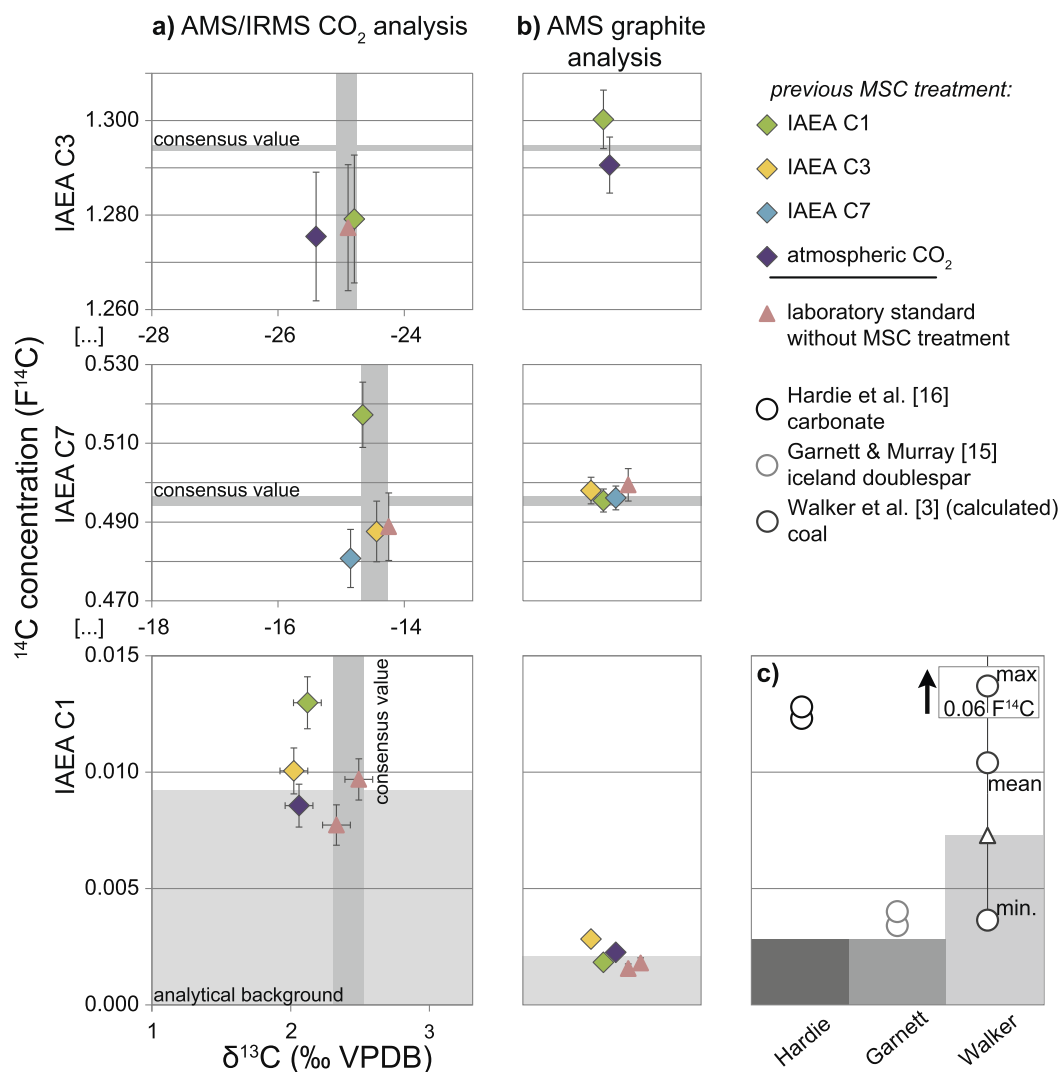


Fig. 6. ^{14}C and $\delta^{13}\text{C}$ results of tests for cross-contamination and isotopic fractionation. The results for the modern (IAEA C3), intermediate (IAEA C7), and ^{14}C free (IAEA C1) standards are shown from top to bottom. The color-coding represents the standard loaded previously onto the zeolite. Error bars display 1- σ measurement uncertainties. The gray shaded areas represent the consensus values of the respective standards with 1- σ errors or the analytical background. Fig. a) shows results of AMS ^{14}C and IRMS $\delta^{13}\text{C}$ analyses, and Fig. b) the results of AMS ^{14}C analysis of graphite (no IRMS $\delta^{13}\text{C}$ values are available for b). In Fig. c) the results of ^{14}C free standards of previous studies (AMS graphite analysis) are shown for comparison. The data by Walker et al. [3] are calculated based on their R-values with a broad range of data points. The analytical backgrounds are estimated based on information given in the publication [3,15,16].

which includes two sample series loaded consecutively onto one respective MSC, also demonstrates that we have no cross-contamination from samples processed previously in the MSC-AGE system (Table 2; Fig. 6).

The ^{14}C free standards processed in the coupled MSC-AGE system are lower compared to the results of previous studies [3,15,16] (Fig. 6c). However, Hardie et al. [16] and Garnett and Murray [15] used a field sampling system (respiration chamber) for transferring the CO₂ onto the MSC. These studies may have additional contributions to their background caused by the sampling system. Under laboratory conditions Walker et al. [3] used smaller amounts of CO₂ free standard and obtained highly variable ^{14}C concentrations with minimum values in the range of Garnett and Murray [15] and maximum values of 0.06 F¹⁴C (Fig. 6c).

4. Conclusion

We constructed a new MSC entirely made of stainless steel for the collection of CO₂ samples for AMS ^{14}C analysis, which is particularly useful for field applications because it is robust and the CO₂ collected on the zeolite in the MSC can be stored contamination-free over several months. Detailed tests confirm the reliability of the ^{14}C results obtained with the new device and the CO₂ processing methods. The tests performed include the use of different amounts of zeolite, the cleaning of the zeolite, the CO₂ transfer onto and removal from the molecular sieve using different active (with He flow) and passive (under vacuum) procedures as well as the evaluation of potential cross-contamination and isotopic fractionation effects. The results and our recommendations are given below:

- We did not observe any significant influence of the amount of zeolite (300–3000 mg) on ^{14}C blank values.
- The new stainless steel MSC can store CO_2 over more than one year without the contribution of significant amounts of atmospheric CO_2 as indicated by low blank values $<0.014 \text{ F}^{14}\text{C}$ ($>34,100$ yrs BP; AMS ^{14}C analysis using gas ion source).
- The active cleaning of the zeolite using an inert purge gas (like He) during heating of the MSC up to 500°C for 60 min is more efficient compared to cleaning under vacuum. Cleaning times might be reduced to few minutes as indicated by the results of the MSC-AGE coupling.
- Flushing the CO_2 actively onto the MSC in a He stream is more effective in laboratory applications. In field studies the choice of passive transfer by diffusion or active transfer using a pump-based system is dependent on the application.
- The CO_2 desorption can be done actively (with a He flow), or passively (under vacuum). When using active desorption, we recommend a flow-through liquid nitrogen trap for trapping the released CO_2 .
- We observed no cross-contamination and no isotopic fractionation during the passive CO_2 desorption. However, prior to the CO_2 desorption, the MSC should not be evacuated longer than 5 min at room temperature, which may cause isotopic fractionation.
- The coupling of the MSC with the automated graphitization system AGE yields very low blank values within the analytical background for AMS graphite analysis ($<0.0028 \text{ F}^{14}\text{C}$; $>47,200$ yrs BP). Here, the CO_2 was desorbed actively from the MSC and transferred to the zeolite trap of the AGE without any cross-contamination.

In conclusion, we developed a new MSC for collecting CO_2 samples for AMS ^{14}C analysis. The results of our tests demonstrate the importance of validating MSCs and CO_2 processing procedures prior field application.

Acknowledgements

This study was financially supported by the German Research Foundation (DFG) Research Unit 1806 and by the German Ministry of Science and Education (BMBF) joint project 'Carboperm'. We thank Ulrike Patt for her assistance in standard preparation and Harald Strauss and Artur Fugmann for the $\delta^{13}\text{C}$ analyses. We are grateful to Reka-Hajnalka Fülöp for giving the impulse for a new MSC construction.

References

- [1] M.H. Garnett, I.P. Hartley, A passive sampling method for radiocarbon analysis of atmospheric CO_2 using molecular sieve, *Atmos. Environ.* 44 (2010) 877–883, <http://dx.doi.org/10.1016/j.atmosenv.2009.12.005>.
- [2] M. Lopez, M. Schmidt, M. Delmotte, A. Colomb, V. Gros, C. Janssen, S.J. Lehman, D. Mondelain, O. Perrussel, M. Ramonet, I. Xueref-Remy, P. Bousquet, CO , NO_x and $^{13}\text{CO}_2$ as tracers for fossil fuel CO_2 : results from a pilot study in Paris during winter 2010, *Atmos. Chem. Phys.* 13 (2013) 7343–7358, <http://dx.doi.org/10.5194/acp-13-7343-2013>.
- [3] J.C. Walker, X. Xu, S.M. Fahrni, M. Lupascu, C.I. Czimczik, Developing a passive trap for diffusive atmospheric $^{14}\text{CO}_2$ sampling, *Nucl. Instrum. Methods Phys. Res., Sect. B* 361 (2015) 632–637, <http://dx.doi.org/10.1016/j.nimb.2015.05.030>.
- [4] M.H. Garnett, S.M.L. Hardie, Isotope (^{14}C and ^{13}C) analysis of deep peat CO_2 using a passive sampling technique, *Soil Biol. Biochem.* 41 (2009) 2477–2483, <http://dx.doi.org/10.1016/j.soilbio.2009.09.004>.
- [5] M.H. Garnett, I.P. Hartley, D.W. Hopkins, M. Sornmerkorn, P.A. Wookey, A passive sampling method for radiocarbon analysis of soil respiration using molecular sieve, *Soil Biol. Biochem.* 41 (2009) 1450–1456, <http://dx.doi.org/10.1016/j.soilbio.2009.03.024>.
- [6] J.B. Gaudinski, S.E. Trumbore, E.A. Davidson, S.H. Zheng, Soil carbon cycling in a temperate forest: radiocarbon-based estimates of residence times, sequestration rates and partitioning of fluxes, *Biogeochemistry* 51 (2000) 33–69, <http://dx.doi.org/10.1023/a:1006301010014>.
- [7] S.M.L. Hardie, M.H. Garnett, A.E. Fallick, A.P. Rowland, N.J. Ostle, T.H. Flowers, Abiotic drivers and their interactive effect on the flux and carbon isotope (^{14}C and $\delta^{13}\text{C}$) composition of peat-respired CO_2 , *Soil Biol. Biochem.* 43 (2011) 2432–2440, <http://dx.doi.org/10.1016/j.soilbio.2011.08.010>.
- [8] C. Biasi, S. Jokinen, M. Marushchak, K. Hämäläinen, T. Trubnikova, M. Oinonen, P. Martikainen, Microbial respiration in arctic upland and peat soils as a source of atmospheric carbon dioxide, *Ecosystems* 17 (2014) 112–126, <http://dx.doi.org/10.1007/s10021-013-9710-z>.
- [9] C.E. Hicks Pries, E.A.G. Schuur, S.M. Natali, K.G. Crummer, Old soil carbon losses increase with ecosystem respiration in experimentally thawed tundra, *Nat. Clim. Change* 6 (2015) 214–218, <http://dx.doi.org/10.1038/nclimate2830>.
- [10] M. Lupascu, J.M. Welker, X. Xu, C.I. Czimczik, Rates and radiocarbon content of summer ecosystem respiration in response to long-term deeper snow in the High Arctic of NW Greenland, *J. Geophys. Res.: Biogeosci.* 119 (2014) 1180–1194, <http://dx.doi.org/10.1002/2013JG002494>.
- [11] M.H. Garnett, K.J. Dinsmore, M.F. Billett, Annual variability in the radiocarbon age and source of dissolved CO_2 in a peatland stream, *Sci. Total Environ.* 427–428 (2012) 277–285, <http://dx.doi.org/10.1016/j.scitotenv.2012.03.087>.
- [12] M.H. Garnett, S.M.L. Hardie, C. Murray, M.F. Billett, Radiocarbon dating of methane and carbon dioxide evaded from a temperate peatland stream, *Biogeochemistry* 114 (2013) 213–223, <http://dx.doi.org/10.1007/s10533-012-9804-2>.
- [13] F.I. Leith, M.H. Garnett, K.J. Dinsmore, M.F. Billett, K.V. Heal, Source and age of dissolved and gaseous carbon in a peatland-riparian-stream continuum: a dual isotope (^{14}C and $\delta^{13}\text{C}$) analysis, *Biogeochemistry* 119 (2014) 415–433, <http://dx.doi.org/10.1007/s10533-014-9977-y>.
- [14] S.L. McCallister, P.A. del Giorgio, Evidence for the respiration of ancient terrestrial organic C in northern temperate lakes and streams, *Proc. Natl. Acad. Sci. U.S.A.* 109 (2012) 16963–16968, <http://dx.doi.org/10.1073/pnas.1207305109>.
- [15] M.H. Garnett, C. Murray, Processing of CO_2 samples collected using zeolite molecular sieve for ^{14}C analysis at the NERC Radiocarbon Facility (East Kilbride, UK), *Radiocarbon* 55 (2013) 410–415, http://dx.doi.org/10.2458/azu_js_rc.55.16058.
- [16] S.M.L. Hardie, M.H. Garnett, A.E. Fallick, A.P. Rowland, N.J. Ostle, Carbon dioxide capture using a zeolite molecular sieve sampling system for isotopic studies (^{14}C and ^{13}C) of respiration, *Radiocarbon* 47 (2005) 441–451, http://dx.doi.org/10.2458/azu_js_rc.47.2838.
- [17] V. Palonen, M. Oinonen, Molecular sieves in $^{14}\text{CO}_2$ sampling and handling, *Radiocarbon* 55 (2013) 416–420, http://dx.doi.org/10.2458/azu_js_rc.55.16335.
- [18] E.M. Flanigen, *Zeolites and Molecular Sieves an Historical Perspective Chapter 2*, in: E.M.F.H. van Bekkum, J.C. Jansen (Eds.), *Studies in Surface Science and Catalysis*, Elsevier, 1991, pp. 13–34.
- [19] C. Baerlocher, W.M. Meier, D. Olson, L.B. McCusker, *International Zeolite Atlas of Zeolite Framework Types*, Elsevier Science, Amsterdam, 2007.
- [20] J.E. Bauer, P.M. Williams, E.R.M. Druffel, Recovery of submilligram quantities of carbon dioxide from gas streams by molecular sieve for subsequent determination of isotopic (^{13}C and ^{14}C) natural abundances, *Anal. Chem.* 64 (1992) 824–827, <http://dx.doi.org/10.1021/ac00031a024>.
- [21] R.A. Bol, D.D. Harkness, The use of zeolite molecular sieves for trapping low concentrations of CO_2 from environmental atmospheres, *Radiocarbon* 37 (1995) 643–647, http://dx.doi.org/10.2458/azu_js_rc.37.1715.
- [22] L. Wacker, M. Nemej, J. Bourquin, A revolutionary graphitisation system: fully automated, compact and simple, *Nucl. Instrum. Methods Phys. Res., Sect. B* 268 (2010) 931–934, <http://dx.doi.org/10.1016/j.nimb.2009.10.067>.
- [23] T. Montanari, E. Finocchio, E. Salvatore, G. Garuti, A. Giordano, C. Pistarino, G. Busca, CO_2 separation and landfill biogas upgrading: a comparison of 4A and 13X zeolite adsorbents, *Energy* 36 (2011) 314–319, <http://dx.doi.org/10.1016/j.energy.2010.10.038>.
- [24] R.V. Siriwardane, M.-S. Shen, E.P. Fisher, J. Losch, Adsorption of CO_2 on zeolites at moderate temperatures, *Energy Fuels* 19 (2005) 1153–1159, <http://dx.doi.org/10.1021/ef040059h>.
- [25] R.V. Siriwardane, M.-S. Shen, E.P. Fisher, J.A. Poston, Adsorption of CO_2 on molecular sieves and activated carbon, *Energy Fuels* 15 (2001) 279–284, <http://dx.doi.org/10.1021/ef000241s>.
- [26] S. Cavenati, C.A. Grande, A.E. Rodrigues, Adsorption equilibrium of methane, carbon dioxide, and nitrogen on zeolite 13X at high pressures, *J. Chem. Eng. Data* 49 (2004) 1095–1101, <http://dx.doi.org/10.1021/je0498917>.
- [27] C.L. Phillips, K.J. McFarlane, D. Risk, A.R. Desai, Biological and physical influences on soil $^{14}\text{CO}_2$ seasonal dynamics in a temperate hardwood forest, *Biogeosciences* 10 (2013) 7999–8012, <http://dx.doi.org/10.5194/bg-10-7999-2013>.
- [28] E.A.G. Schuur, S.E. Trumbore, Partitioning sources of soil respiration in boreal black spruce forest using radiocarbon, *Glob. Change Biol.* 12 (2006) 165–176, <http://dx.doi.org/10.1111/j.1365-2486.2005.01066.x>.
- [29] C.I. Czimczik, J.M. Welker, Radiocarbon content of CO_2 respired from high Arctic Tundra in Northwest Greenland, *Arct. Antarct. Alp. Res.* 42 (2010) 342–350, <http://dx.doi.org/10.1657/1938-4246-42.3.342>.
- [30] K. Hämäläinen, H. Fritze, H. Jungner, K. Karhu, M. Oinonen, E. Sonninen, P. Spetz, M. Tuomi, P. Vanhala, J. Liski, Molecular sieve sampling of CO_2 from decomposition of soil organic matter for AMS radiocarbon measurements, *Nucl. Instrum. Method Phys. Res. Sect. B-Beam Interact. Mater. Atoms* 268 (2010) 1067–1069, <http://dx.doi.org/10.1016/j.nimb.2009.10.099>.
- [31] M. Le Ciercq, J. van der Plicht, M. Groening, New ^{14}C reference materials with activities of 15 and 50 pMC, *Radiocarbon* 40 (1998) 295–297.

- [32] K. Rozanski, W. Stichler, R. Gonfiantini, E.M. Scott, R.P. Beukens, B. Kromer, J.d. Plicht, The IAEA ^{14}C Intercomparison Exercise 1990, *Radiocarbon* 34 (1992) 506–519.
- [33] S.M. Fahrni, L. Wacker, H.A. Synal, S. Szidat, Improving a gas ion source for ^{14}C AMS, *Nucl. Instrum. Methods Phys. Res., Sect. B* 294 (2013) 320–327, <http://dx.doi.org/10.1016/j.nimb.2012.03.037>.
- [34] C.P. McIntyre, A.P. McNichol, M.L. Roberts, J.S. Seewald, K.F. von Reden, W.J. Jenkins, Improved precision of ^{14}C measurements for CH_4 and CO_2 using GC and continuous-flow AMS achieved by summation of repeated injections, *Radiocarbon* 55 (2013) 677–685, http://dx.doi.org/10.2458/azu_js_rc.55.16348.
- [35] M. Ruff, S. Szidat, H.W. Gäggeler, M. Suter, H.A. Synal, L. Wacker, Gaseous radiocarbon measurements of small samples, *Nucl. Instrum. Methods Phys. Res., Sect. B* 268 (2010) 790–794, <http://dx.doi.org/10.1016/j.nimb.2009.10.032>.
- [36] H.A. Synal, M. Stocker, M. Suter, MICADAS: a new compact radiocarbon AMS system, *Nucl. Instrum. Method Phys. Res. Sec. B-Beam Interact. Mater. Atoms* 259 (2007) 7–13, <http://dx.doi.org/10.1016/j.nimb.2007.01.138>.
- [37] A. Dewald, S. Heinze, J. Jolie, A. Zilges, T. Dunai, J. Rethemeyer, M. Melles, M. Staubwasser, B. Kuczewski, J. Richter, U. Radtke, F. von Blanckenburg, M. Klein, CologneAMS, a dedicated center for accelerator mass spectrometry in Germany, *Nucl. Instrum. Methods Phys. Res., Sect. B* 294 (2013) 18–23, <http://dx.doi.org/10.1016/j.nimb.2012.04.030>.
- [38] M. Stuiver, H.A. Polach, Reporting of ^{14}C data - discussion, *Radiocarbon* 19 (1977) 355–363.
- [39] P.J. Reimer, T.A. Brown, R.W. Reimer, Discussion: Reporting and Calibration of Post-Bomb ^{14}C Data, 2004.
- [40] T. Schulze-König, L. Wacker, H.A. Synal, Direct radiocarbon analysis of exhaled air, *J. Anal. At. Spectrom.* 26 (2011) 287–292, <http://dx.doi.org/10.1039/c0ja00039f>.
- [41] I.P. Hartley, M.H. Garnett, M. Sommerkorn, D.W. Hopkins, P.A. Wookey, The age of CO_2 released from soils in contrasting ecosystems during the arctic winter, *Soil Biol. Biochem.* 63 (2013) 1–4, <http://dx.doi.org/10.1016/j.soilbio.2013.03.011>.

Paper II

$^{14}\text{CO}_2$ analysis of soil gas: Evaluation of sample size limits and sampling devices

Anja Wotte, Philipp Wischhöfer, Lukas Wacker, Janet Rethemeyer

Nuclear Inst. and Methods in Physics Research B 413, 51-56, 2017



Contents lists available at ScienceDirect

Nuclear Inst. and Methods in Physics Research B

journal homepage: www.elsevier.com/locate/nimb ^{14}C analysis of soil gas: Evaluation of sample size limits and sampling devicesAnja Wotte^{a,*}, Philipp Wischhöfer^{a,1}, Lukas Wacker^b, Janet Rethemeyer^a^a Institute of Geology and Mineralogy, University of Cologne, Cologne, Germany^b Ion Beam Physics, ETH Zurich, Zurich, Switzerland

ARTICLE INFO

Keywords:

Radiocarbon
CO₂
Molecular sieve
Zeolite
13X
Soil respiration
 ^{14}C

ABSTRACT

Radiocarbon (^{14}C) analysis of CO₂ respired from soils or sediments is a valuable tool to identify different carbon sources. The collection and processing of the CO₂, however, is challenging and prone to contamination. We thus continuously improve our handling procedures and present a refined method for the collection of even small amounts of CO₂ in molecular sieve cartridges (MSCs) for accelerator mass spectrometry ^{14}C analysis. Using a modified vacuum rig and an improved desorption procedure, we were able to increase the CO₂ recovery from the MSC (95%) as well as the sample throughput compared to our previous study. By processing series of different sample size, we show that our MSCs can be used for CO₂ samples of as small as 50 µg C. The contamination by exogenous carbon determined in these laboratory tests, was less than 2.0 µg C from fossil and less than 3.0 µg C from modern sources. Additionally, we tested two sampling devices for the collection of CO₂ samples released from soils or sediments, including a respiration chamber and a depth sampler, which are connected to the MSC. We obtained a very promising, low process blank for the entire CO₂ sampling and purification procedure of $\sim 0.004 \text{ F}^{14}\text{C}$ (equal to 44,000 yrs BP) and $\sim 0.003 \text{ F}^{14}\text{C}$ (equal to 47,000 yrs BP). In contrast to previous studies, we observed no isotopic fractionation towards lighter $\delta^{13}\text{C}$ values during the passive sampling with the depth samplers.

1. Introduction

The response of the global carbon cycle to the present global warming is a crucial question in climate research. Terrestrial ecosystems are an important component of the carbon cycle because they store about four times more carbon (C) than presently in the atmosphere (830 Gt) [1]. Most of this C is stored in soils (2050 Gt, excluding the Arctic and boreal regions) [2] and in permafrost (1300–1600 Gt) [3,4]. The emission of C from soils to the atmosphere is a major C flux in the global carbon cycle [5,6], which may considerably increase in response to rising temperatures [1,7,8]. The increase in soil respiration rates induced by global warming has already been documented in several studies [9,10].

To improve model predictions of future climate change it is necessary to identify major sources of CO₂, which are released from soils or permafrost deposits. ^{14}C analysis of soil CO₂ makes it possible to differentiate these sources and thus helps to understand whether changes in soil respiration are driven by higher inputs of recently fixed C into the soil or by the mobilization of older C, stored for hundreds or thousands of years [11,12].

The collection of CO₂ for subsequent accelerator mass spectrometry (AMS) ^{14}C analysis is often performed using molecular sieves [12–15], which have the advantage that relatively large amounts of CO₂ can be concentrated in a small volume of the adsorbent. This method is based on the selectivity for CO₂ over other gases and on a high adsorption capacity of CO₂ on specific molecular sieves (e.g. zeolite type 13X) [16–18]. Different studies showed that molecular sieve cartridges (MSCs) as well as the respective sampling equipment and handling procedures need to be tested prior to their application in order to avoid the trapping of unwanted CO₂ and to obtain reliable ^{14}C results [19–21]. CO₂ emissions from soils can be collected using respiration chambers [e.g. 14,22] or sampling devices enabling the collection of CO₂ from deeper soil layers [23]. The CO₂ is then transferred from the sampling system onto the zeolite in the MSC either by active sampling, i.e. using a pump-based system to circulate the gas through the MSC [19,24], or passively by gas diffusion only [14,23,25]. Active CO₂ sampling has the advantage that the CO₂ can be collected relatively quickly (~ 1 h), while passive sampling may take several days [14] or even more than a month [23,26], depending on the CO₂ concentration and sampling equipment. Thus, passive sampling integrates longer

* Corresponding author.

E-mail address: Anja.Wotte@uni-koeln.de (A. Wotte).¹ These authors contributed equally to this work.<http://dx.doi.org/10.1016/j.nimb.2017.10.009>Received 8 July 2017; Received in revised form 7 October 2017; Accepted 12 October 2017
0168-583X/© 2017 Elsevier B.V. All rights reserved.

A. Wotte et al.

Nuclear Inst. and Methods in Physics Research B 413 (2017) 51–56

sampling periods, because it takes time to adsorb the necessary amount of > 1000 µg C, which is used in MSC studies [19,20,27]. Microscale ¹⁴C AMS analysis of sample sizes of less than 10 µg C is already established [28–30], which makes it possible to reduce CO₂ amounts for AMS ¹⁴C analysis. If less CO₂ needs to be collected on the MSC, the sampling time can be significantly reduced, which minimizes the risk of collecting unwanted CO₂, e.g. from the atmosphere or the surrounding soil. Additionally, when using respiration chambers, long sampling times disturb natural conditions, CO₂ fluxes, and natural CO₂ concentration gradients [31,32], which can be reduced if smaller amounts of CO₂ are collected for microscale ¹⁴C analysis. Small mass MSC sampling would also allow the collection of sufficient CO₂ using passive adsorption in environments with low CO₂ concentrations, like from the atmosphere during field campaigns shorter than one month.

The lower limit of CO₂ processing using MSCs has not been assessed yet. We thus evaluate a) the minimum amount of C that can be processed in the laboratory with our recently developed stainless steel MSC [21] yielding reliable ¹⁴C results and b) the process blank (contamination with exogenous C) of the entire CO₂ sampling and purification procedure using two different sampling devices for the CO₂ collection in the field. Besides a pump-based respiration chamber, we tested a passive CO₂ sampler, which can be inserted into deeper soil layers [23]. The field tests were performed at a location where ¹⁴C free CO₂ of volcanic origin is emitted.

2. Methods

2.1. CO₂ processing using the MSC

The design of the MSC has previously been described by Wotte et al. [21]. Briefly, 500 mg of zeolite type 13X (40/60 mesh, IVA Analysetechnik GmbH & Co. KG, Germany) are centered in a stainless steel tube (3/8" OD, ~24 cm length) and held in place by quartz wool. Both ends of the tube are closed with quick connector stems (Q2DSH-6T, Hy-Lok D Vertriebs GmbH, Germany).

The vacuum rig used for processing the MSCs (Fig. 1) is a modification compared to our previous study [21]. It comprises a He inlet, which is controlled by a needle valve and a flow meter (M-Series, Cole-Parmer, USA), a tube cracker, a split tube furnace (Ceramic Fiber Heaters VS402A06S, controller EZ-Zone® PM 1/16 DIN, Watlow, USA), a 0.5 µm in-line filter (F series, Swagelok, USA), two U-traps and a multipurpose vacuum rig. The latter is otherwise used for sample quantification, via two calibrated volumes connected to a pressure transducer, and partitioning. For cleaning of the zeolite as well as for CO₂ desorption, the MSCs are placed in the furnace and attached to the vacuum rig via quick connector bodies (Q2BH-6T, Hy-Lok D Vertriebs GmbH Germany). The rig is height adjustable thus allowing the MSC to be connected to an atmospheric outlet instead of the vacuum line (Fig. 1). When not in use, an empty stainless steel cartridge is connected

to the upstream quick connector to seal the left part of the rig while the right part is kept evacuated (< 5 × 10⁻⁴ mbar).

For daily setup, the empty cartridge is connected to the atmospheric outlet and the left part of the rig is flushed with He (99.996 vol% purity, ~120 ml min⁻¹) for at least half an hour. During the flushing period, a standard (cf. 2.2) can be mounted inside the tube cracker. To adsorb the standard onto a MSC, the empty cartridge is substituted with a clean MSC, the He stream is reduced to 40 ml min⁻¹ and the glass tube inside the tube cracker is broken. Purging for at least 30 min, similar to Wotte et al. [21], guarantees that the sample is adsorbed completely. When handling a previously loaded MSC, this substitutes the empty cartridge after the flushing period. In either case, the connection to the vacuum rig and the desorption follow the same protocol.

According to the results of Wotte et al. [21] we used an active desorption procedure, which was improved by a) performing all handling steps on a single vacuum rig and b) by decreasing the heating time, thus saving time. The modified procedure starts with closing the valves towards the calibrated volumes and towards the glass tubes in which the samples are finally collected. Then, the MSC is connected to the vacuum rig. Flow and pressure, respectively, are adjusted with the needle valve and the valves towards the vacuum pump to about 40 ml min⁻¹ He and 300 mbar. A slurry made of dry ice and ethanol and a liquid nitrogen (LN₂) trap are added to the left and right U-trap (Fig. 1). CO₂ is removed from the MSC by heating stepwise to 500 °C for 15 min. Afterwards the valve between slurry and LN₂ trap is closed. The vacuum line is evacuated to < 5 × 10⁻⁴ mbar. The gas is further dried by substituting the LN₂ trap with a second slurry. CO₂ is frozen out within one of the calibrated volumes and incondensable gases are pumped away. Finally, the amount of CO₂ is quantified and the gas is split into aliquots for ¹⁴C and for ¹³C analysis (provided that there is sufficient C for the latter).

While processing the gas in the right part of the rig, the MSC can already be cleaned. The downstream end is connected to the atmospheric outlet and the MSC is cleaned as described in Wotte et al. [21], i.e. the MSC is baked for 60 min at 150/500 °C with a carrier gas flow of 40 ml min⁻¹. Simultaneous sample splitting and MSC cleaning have improved our sample through-put significantly compared to the methods described in Wotte et al. [21].

2.2. Evaluation of sample size limits of the MSC

In order to determine the minimum amount of CO₂ which can be processed on the MSC with regard to accurate ¹⁴C measurements, we prepared a suite of CO₂ aliquots (25–300 mg C) from IAEA standards C1 (0.000 F¹⁴C) and C3 (1.2941 F¹⁴C) according to the CologneAMS CO₂ standard procedure [21]. To our knowledge, no ¹⁴C data of molecular sieve treated samples or standards of less than 100 µg C have been reported so far [e.g. 25,33]. The aliquots of the two standards were processed consecutively on two MSCs according to the procedure

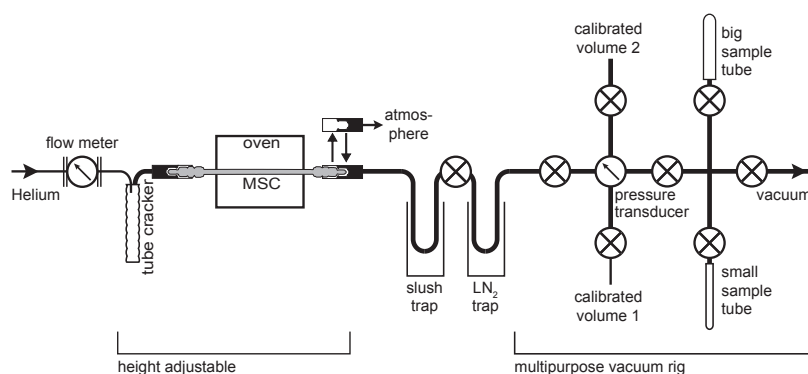


Fig. 1. Schematic of the vacuum line used for the MSC processing. The outlet allows for cleaning the molecular sieve while quantifying and splitting the previous sample in the right part of the line.



Fig. 2. Setup for the sampling of soil emissions close to Laacher See. CO_2 emissions of dry mofettes (^{14}C free) were trapped to evaluate if the sampling system is leak tight.

explained in Section 2.1. IAEA C1 and C3 standards were alternated pairwise (C1 – C1 – C3 – C3 – C1–...) to reveal possible memory effects. Recoveries were estimated as the ratio of the pressure readout after desorption from the MSC to the pressure readout during preparation of the aliquots.

2.3. CO_2 field sampling systems

We tested two different soil CO_2 sampling systems, which are based on designs by Hardie et al. [19] and Garnett and Hardie [23] (Fig. 2). Our closed respiration chamber was constructed of 25 cm OD PVC pipe. A plain piece of pipe acts as a collar to which a pipe socket is joined in the field with Apiezon grease (type M, M & I Materials Limited, UK). The socket is sealed on top by an opaque disc of acrylic glass with two 1/2" tubing connectors. Further parts are a custom build tunable diaphragm pump, glass cartridges filled with a desiccant (Merck Sicapent®) and the previously described MSCs (Fig. 2). All parts are joined by TYGON® tubing (Saint Gobain, France) and three way valves (Bürkle GmbH, Germany).

For construction of the passive depth sampler, a 6 mm OD stainless steel pipe was cut to lengths of 70 cm. One end was formed to a tip and welded. 10 cm above the tapered end, six holes of 2 mm in diameter were drilled and covered by a hydrophobic membrane (Accurel® PP V8/2 HF, 3M, Germany). Both ends of the membrane were sealed with heat shrink tubing and liquid rubber spray (mibenco GmbH, Germany). The upper 5 cm of the steel tubes were bend 90° and fitted with quick connector bodies (Q2BH, Hy-Lok D Vertriebs GmbH, Germany) via Swagelok tube adapters.

2.4. Process blank of the entire CO_2 sampling and purification procedure

We tested our sampling equipment at a CO_2 vent on the Northeastern shore of Laacher See, a caldera lake in the East Eifel Volcanic Field, Germany (N50°25'03" and E7°17'07"). These vents are found within and around the lake [e.g. 34,35] and emit gases, mainly CO_2 , of upper mantle origin [36,37]. As the mantle CO_2 is ^{14}C free, any

atmospheric contamination introduced during sampling or during processing of the MSC in the laboratory is revealed by ^{14}C concentrations higher than the analytical background. The vent, we chose for our experiment, was previously described in Pfanz [38] ("U1") and Stoiber-Lipp et al. [35] ("TM1"). Soil gas at the location contains more than 90% CO_2 .

Within a radius of 10 m we installed two respiration chambers and three depth samplers. The depth samplers were pushed into the relatively soft ground (~45 cm) and pumped about half a minute to remove initial atmospheric CO_2 . Afterwards, the MSCs were connected to collect soil gas passively for 4 h. Before installing the chambers, the plant litter was removed from the respective spots. The collars were carefully inserted to a depth of about 5 cm into the soil. Then, the chamber was closed with the upper part resulting in a total volume of ~8 L. At the beginning, the chamber was pumped for five minutes to remove atmospheric CO_2 . Subsequently, the outlet to the atmosphere was closed and the pump was switched off for ~8 min to allow for the accumulation of the CO_2 from the ground. After four cycles of pumping and pressure equilibration, the MSC was attached and CO_2 was trapped by circulating the chamber air for five minutes. At the two sites, we collected three, respectively four replicates.

The CO_2 collected was desorbed from the MSCs, purified and quantified in the laboratory within three weeks after sampling. The CO_2 sampled with the depth samplers as well as one sample of each respiration chamber were desorbed from the MSCs as described above including aliquots for ^{13}C analysis. The remaining replicate samples were processed with the automatic graphitization equipment (AGE; IonPlus, Switzerland) and converted to graphite targets [21].

2.5. ^{13}C and ^{14}C analysis of CO_2

Stable carbon isotopes were measured with the ThermoFinnigan isotope ratio mass spectrometer (IRMS) at the Institute of Geology and Paleontology, University of Münster (Germany). Results are reported as $\delta^{13}\text{C}$ values, i. e. the $^{13}\text{C}/^{12}\text{C}$ ratio relative to the standard Vienna Pee Dee Belemnite (VPDB) in per mil. If not stated otherwise, 1- σ is within the instrumental error of $\pm 0.1\text{‰}$.

The ^{14}C concentration of gaseous samples was determined using two Mini Carbon Dating Systems (MICADAS, Ionplus, Switzerland) [28] at the Laboratory of Ion Beam Physics at the ETH Zurich (Switzerland). Standards processed for evaluating the sample size limits and samples from the field were measured during different sequences and are thus compared with their respective analytical background, which can vary between different runs. Graphitized samples were measured at the HVE Tandem AMS at the CologneAMS facility (Germany) [39] with a higher precision and a lower analytical background. The results are expressed as $F^{14}\text{C}$ [40] or as conventional ^{14}C ages in years before present (yrs BP) [41] both normalized to $\delta^{13}\text{C}$ of -25‰ and given with 1- σ uncertainties. Blank corrections were only applied for IAEA C3 standards.

3. Results and discussion

3.1. Evaluation of sample size limits of the MSC

In order to determine the minimum amount of C, which can be processed on the MSC and still gives reliable ^{14}C results, it is essential to assess the contribution of exogenous C, either from modern or fossil (^{14}C free) sources. To evaluate this, we performed tests to quantify the amount of exogenous fossil and modern C, which is trapped on the zeolite in the MSC during CO_2 adsorption and desorption depending on sample sizes. We processed a size series (25–300 μg C) of fossil (IAEA C1; Fig. 3a) and modern (IAEA C3; Fig. 3b) carbon standards, which were consecutively loaded onto and desorbed from the zeolite. The results reveal a small C contribution from both, fossil and modern sources. The effect of these contaminations on the ^{14}C concentration of

A. Wotte et al.

Nuclear Inst. and Methods in Physics Research B 413 (2017) 51–56

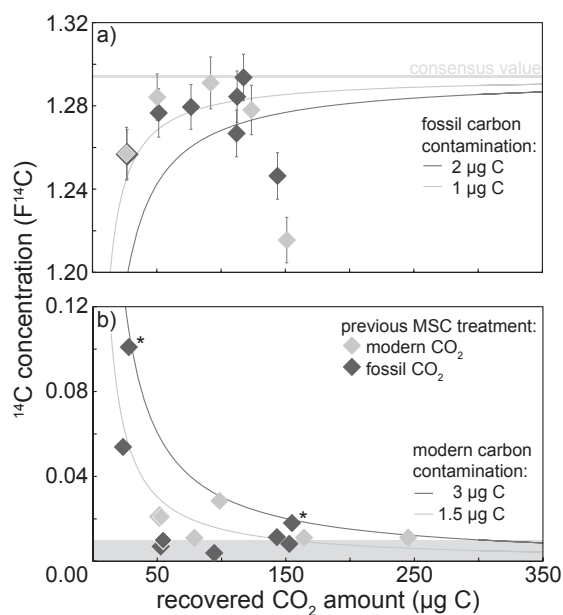


Fig. 3. ^{14}C concentrations ($F^{14}\text{C}$) of IAEA C3 (a; modern) and C1 (b; fossil) standards of different sizes processed with the MSCs and using the vacuum line illustrated in Fig. 1. The previous MSC treatment is reflected by the color of the symbols. The gray shaded area in (b) represents the analytical background. The asterisks mark the two CO_2 samples, which were processed two months after cleaning the MSC. The curves were calculated with the model of constant contamination and illustrate the exogenous C contamination by fossil (a) and modern (b) C sources. $1\text{-}\sigma$ uncertainties are shown and within symbol size for the C1 standard.

the modern and fossil standard increases relatively towards lower amounts of C (Fig. 3a + b). We quantified the contamination by modern C (e.g. atmospheric sources: $1.01 F^{14}\text{C}$, High Altitude Research Station Jungfrauojoch, Swiss Alps, in December 2015; [42]) and fossil C ($0.00 F^{14}\text{C}$) to be less than $3 \mu\text{g C}$ and $2 \mu\text{g C}$ (Fig. 3b + a) using a simple model assuming a constant contamination [43]. This contamination includes potential contributions introduced during the CO_2 processing on the MSC as well as exogenous C inputs from the preparation of the IAEA standards used for the tests, and the AMS measurement. The latter two contributions are of minor importance, because we regularly evaluate the input obtained during standard preparation, which is similar to the blank of $0.06 \mu\text{g C}$ ($0.5 F^{14}\text{C}$) of the AMS analysis [28].

Two of the ^{14}C free standards were processed on MSCs, which had been cleaned two months prior sampling. The CO_2 recovered shows slightly higher ^{14}C values (equivalent to a modern contamination by $\sim 3 \mu\text{g C}$) compared to other IAEA C1 standards ($< 1.5 \mu\text{g C}$; Fig. 3b), which were processed within 24 h subsequent to MSC cleaning. These slightly elevated ^{14}C values are not caused by a memory effect, because the CO_2 loaded onto the MSC previously also was ^{14}C free. Thus, during MSC storage under He at least some CO_2 with an elevated ^{14}C signature (potentially atmospheric) may enter the MSCs. However, larger sample sizes above $1000 \mu\text{g C}$ can be stored on the MSC for at least one year without any significant contribution of modern C [21]. To minimize the contamination, we suggest to process CO_2 samples as quickly as possible if less than $250 \mu\text{g C}$ are trapped on the MSC.

In order to determine a potential cross-contamination of CO_2 from samples previously loaded onto the MSC, the isotopically distinct CO_2 produced from the IAEA standards C1 und C3 was consecutively transferred to and removed from the MSC. A small memory effect is only visible for the low sample sizes ($50\text{--}100 \mu\text{g C}$) of the ^{14}C free standard (IAEA C1) (Fig. 3b). The ^{14}C concentrations of these small standards processed on the MSC after a modern (IAEA C3) standard are

slightly enriched ($0.020 F^{14}\text{C}$ equal to 31,000 yrs BP) compared to the standards processed after a fossil standard ($0.007 F^{14}\text{C}$ equal to 40,000 yrs BP). In contrast, the modern CO_2 standards of different sample size that were trapped after a ^{14}C free standard do not differ from other modern standards (Fig. 3a). The results of the ad- and desorbed modern standards include two outliers (1.246 ± 0.011 and $1.216 \pm 0.011 F^{14}\text{C}$; Fig. 3a) with a fossil contamination of more than $2 \mu\text{g C}$. This contamination cannot be explained by any laboratory anomalies and therefore these standards have been repeated giving ^{14}C concentrations (1.278 ± 0.012 and $1.284 \pm 0.012 F^{14}\text{C}$; Fig. 3a), which are equal within $2\text{-}\sigma$ to the consensus value.

Our improved MSC procedure using a modified vacuum rig increased the CO_2 recovery from on average 86% [21] to about 95%, which is now well in the range of other studies [19,20,27]. Our size test shows that CO_2 samples as small as $50 \mu\text{g C}$ can be processed reliably with our MSC in the laboratory (Fig. 3).

3.2. Evaluation of the sampling devices

In order to evaluate the analytical background of our CO_2 sampling devices including the respiration chamber and depth sampler, we collected ^{14}C free CO_2 with both devices at a gas vent in the Eifel Volcanic Field. Any deviation from the analytical background during ^{14}C analysis will therefore determine our process blank, i.e. the contamination introduced during sampling, transport of the MSCs and desorption in the laboratory.

3.2.1. Process blank of the respiration chamber

We collected a total of seven samples by circulating the air from one of two respiration chambers onto the MSCs. In order to compare the contribution to the process blank of different desorption and ^{14}C measurement procedures, two samples were processed on the vacuum rig with subsequent ^{14}C AMS analysis using the gas ion source, whereas the other samples were transferred to the AGE system and graphitized for AMS analysis of solid (graphite) targets. We recovered more than $8400 \mu\text{g C}$ from the MSCs that were processed on the vacuum rig. A quantification of the replicates released to the AGE system was not possible, because our trapped CO_2 amounts exceeded the capacity of the AGE system, which is designed for amounts of $\sim 1000 \mu\text{g C}$.

The ^{14}C concentration of the two CO_2 samples ($0.0027 \pm 0.0004 F^{14}\text{C}$ and $0.0040 \pm 0.0013 F^{14}\text{C}$) processed on the vacuum line equals the analytical background within $1\text{-}\sigma$ uncertainty (Fig. 4a). Samples reduced to elemental C using the AGE and measured as graphite cathodes show similar ^{14}C concentrations ($0.0043 \pm 0.0011 F^{14}\text{C}$) but differ from our laboratory blanks (Fig. 4b). The desorption of the CO_2 from the MSC connected to the AGE has previously shown to introduce very little contamination ($0.0023 \pm 0.0004 F^{14}\text{C}$) [21]. In that experiment, standards were processed with a MSC, which had already been connected to the AGE system. Thus, the slightly elevated ^{14}C concentration of our samples from the field may originate from contamination introduced during the coupling of the MSC and therefore may represent the limit of this MSC procedure.

The average process blank of the respiration chamber calculated from all seven samples is $0.0040 F^{14}\text{C}$ (equal to 44,000 yrs BP). Bearing in mind the initial volume of air within the chamber (8L à $\sim 400 \text{ppm CO}_2$ corresponding to $\sim 1200 \mu\text{g C}_{\text{modern}}$), this value indicates effective cleaning and low contamination during the sample processing.

3.2.2. Process blank of the depth sampler

The depth samplers have the advantage that CO_2 can be collected from specific depths, whereas the respiration chamber reflects a depth-integrated signal of the bulk soil below the chamber. Thus, we tested our depth samplers by collecting three samples passively on the MSCs. The amount of CO_2 desorbed from the respective MSCs was in the range of $5000\text{--}7000 \mu\text{g C}$. The mean ^{14}C concentration of these ^{14}C free CO_2

A. Wotte et al.

Nuclear Inst. and Methods in Physics Research B 413 (2017) 51–56

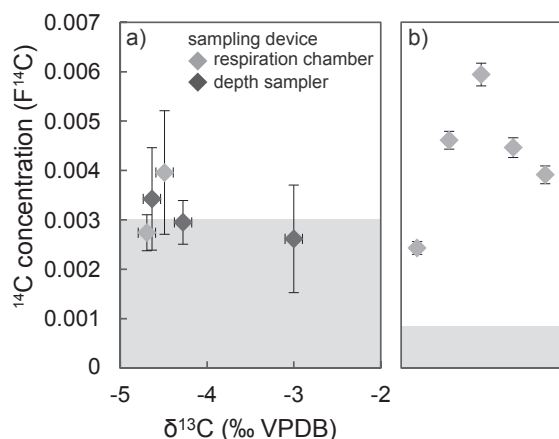


Fig. 4. ¹⁴C concentrations (F¹⁴C) and δ¹³C of CO₂ collected with the respiration chambers (active sampling) and the depth samplers (passive sampling) at Laacher See. All results are shown without blank correction. ¹⁴C concentrations in a) were measured with the gas ion source of the MICADAS, whereas ¹⁴C concentrations in b) were measured in graphite targets at CologneAMS. The gray shaded areas represent the analytical background. 1-σ uncertainties are shown.

samples is 0.0030 F¹⁴C (equal to 47,000 yrs BP). All samples were equal to the AMS background within 1-σ uncertainty (Fig. 4a). Not removing the atmospheric CO₂ from the depth samplers prior to sampling (0.009 L à ~400 ppm CO₂ corresponding to ~2 μg C_{modern}) would have changed the F¹⁴C by less than 1-σ. The amount of C, which was recovered from the MSCs connected to the depth samplers, is too high to be explained by Fick's law and the dimension of the sampler [44], even when assuming that the gas entering the sampler was 100% CO₂. We thus attribute the high recovery to the short pumping period prior to the connection of the MSC.

3.2.3. Evaluation of isotopic fractionation

Previous studies showed that the δ¹³C of passively collected CO₂ becomes isotopically lighter [14,45], which is not a problem for ¹⁴C results as they are corrected for fractionation [41]. However, the δ¹³C of the CO₂ can contain important information on the source of the respired C. To account for any fractionation during sampling and CO₂ processing, we measured the δ¹³C values of samples collected actively using the respiration chamber and passively with the depth sampler. The results are shown in Fig. 4 with an average δ¹³C of -4.22‰. One of the samples collected passively using a depth sampler appears to be an outlier with -3.00‰. This may indicate a fractionation towards heavier δ¹³C values, which occurred during processing of the MSC. Nevertheless, all values are within the range of previous δ¹³CO₂ measurements of the area [37,46,47], suggesting the origin from the upper mantle [36]. As we do not observe a general trend to heavier or lighter δ¹³C values for the samples collected passively, no further correction was applied.

4. Conclusion

In this study we evaluated a) the sample size limits of our stainless steel molecular sieve cartridge (MSC) for the collection of CO₂ for the subsequent AMS ¹⁴C analysis in the laboratory as well as b) the process blank of two different sampling devices for collecting gases released from soils or sediments. The CO₂ samples were processed using a modified vacuum rig and an improved desorption procedure of the CO₂ from the MSC, which resulted in an increase of both, the CO₂ recovery up to 95% as well as the sample throughput. The saving in time is caused by an accelerated desorption procedure and the fact that the cleaning of the MSC can now run at the same time as the desorbed CO₂

is being processed. For a) we demonstrated that it is possible to process CO₂ samples using our MSC of as small as 50 μg C, which still give process blank values for the adsorption and desorption procedure of about 0.015 F¹⁴C equivalent to 34,000 yrs BP using AMS ¹⁴C gas ion source analysis. The contamination by exogenous C from modern and fossil sources is less than 2.0 and 3.0 μg C, respectively. For small samples (< 250 μg C) the contamination by modern C can be probably reduced to 1.5 μg C by cleaning of the zeolite in the MSC and desorption of the CO₂ from the device within less than two months. For b) we revealed very promising, low process blank values for the entire CO₂ sampling procedure in the field using the (active) respiration chamber as well as by passive sampling with depth samplers and including the CO₂ desorption from the MSCs of 0.004 F¹⁴C (equal to 44,000 yrs BP) and 0.003 F¹⁴C (equal to 47,000 yrs BP), respectively. These results demonstrate that no significant atmospheric contamination is introduced during the entire sampling procedure. In contrast to previous studies [14,45], we observed no isotopic fractionation during passive sampling in the field. This study forms a reliable basis for environmental sampling of CO₂ for ¹⁴C analysis, which will help to understand the changes in soil respiration caused by the present global warming.

Acknowledgements

This study was funded by the German Research Foundation (DFG) Research Unit 1806 and by the German Ministry of Science and Education (BMBWF) within the joint project 'CarboPerm'. We thank Harald Strauss and Artur Fugmann for the δ¹³C analyses. Ulrike Patt is acknowledged for her assistance in standard preparation. Stefan Heinze performed the AMS analysis at CologneAMS.

References

- [1] P. Ciais, C. Sabine, G. Bala, L. Bopp, V. Brovkin, J. Canadell, A. Chhabra, R. DeFries, J. Galloway, M. Heimann, C. Jones, C. Le Quéré, R.B. Myneni, S. Piao, P. Thornton, Carbon and other biogeochemical cycles, in: T.F. Stocker, D. Qin, G.-K. Plattner, M. Tignor, S.K. Allen, J. Boschung, A. Nauels, Y. Xia, V. Bex, P.M. Midgley (Eds.), Climate Change 2013: The Physical Science Basis. Contribution of Working Group I to the Fifth Assessment Report of the Intergovernmental Panel on Climate Change, Cambridge University Press, Cambridge, UK and New York, USA, 2013, p. 465.
- [2] E.G. Jobbágy, R.B. Jackson, The vertical distribution of soil organic carbon and its relation to climate and vegetation, Ecol. Appl. 10 (2000) 423–436.
- [3] G. Hugelius, J. Strauss, S. Zubrzycki, J.W. Harden, E.A.G. Schuur, C.L. Ping, L. Schirmer, G. Grosse, G.J. Michaelson, C.D. Koven, J.A. O'Donnell, B. Elberling, U. Mishra, P. Camill, Z. Yu, J. Palmtag, P. Kuhry, Estimated stocks of circumpolar permafrost carbon with quantified uncertainty ranges and identified data gaps, Biogeosciences 11 (2014) 6573–6593.
- [4] E.A.G. Schuur, A.D. McGuire, C. Schadel, G. Grosse, J.W. Harden, D.J. Hayes, G. Hugelius, C.D. Koven, P. Kuhry, D.M. Lawrence, S.M. Natali, D. Olefeldt, V.E. Romanovsky, K. Schaefer, M.R. Turetsky, C.C. Treat, J.E. Vonk, Climate change and the permafrost carbon feedback, Nature 520 (2015) 171–179.
- [5] J.W. Raich, C.S. Potter, Global patterns of carbon dioxide emissions from soils, Global Biogeochem. Cycles 9 (1995) 23–36.
- [6] J.W. Raich, W.H. Schlesinger, The global carbon dioxide flux in soil respiration and its relationship to vegetation and climate, Tellus B 44 (1992) 81–99.
- [7] E.A. Davidson, I.A. Janssens, Temperature sensitivity of soil carbon decomposition and feedbacks to climate change, Nature 440 (2006) 165–173.
- [8] M.U.F. Kirschbaum, Soil respiration under prolonged soil warming: are rate reductions caused by acclimation or substrate loss? Glob. Change Biol. 10 (2004) 1870–1877.
- [9] B. Bond-Lamberty, A. Thomson, Temperature-associated increases in the global soil respiration record, Nature 464 (2010) 579–582.
- [10] C.E. Hicks Pries, C. Castanha, R.C. Porras, M.S. Torn, The whole-soil carbon flux in response to warming, Science 355 (2017) 1420–1423.
- [11] S. Trumbore, Carbon respired by terrestrial ecosystems – recent progress and challenges, Glob. Change Biol. 12 (2006) 141–153.
- [12] C.E. Hicks Pries, E.A.G. Schuur, S.M. Natali, K.G. Crummer, Old soil carbon losses increase with ecosystem respiration in experimentally thawed tundra, Nat. Clim. Change 6 (2015) 214–218.
- [13] E.A.G. Schuur, S.E. Trumbore, Partitioning sources of soil respiration in boreal black spruce forest using radiocarbon, Glob. Change Biol. 12 (2006) 165–176.
- [14] M.H. Garnett, I.P. Hartley, D.W. Hopkins, M. Sommerkorn, P.A. Wookey, A passive sampling method for radiocarbon analysis of soil respiration using molecular sieve, Soil Biol. Biochem. 41 (2009) 1450–1456.
- [15] I.P. Hartley, M.H. Garnett, M. Sommerkorn, D.W. Hopkins, P.A. Wookey, The age of CO₂ released from soils in contrasting ecosystems during the arctic winter, Soil Biol. Biochem. 63 (2013) 1–4.

A. Wotte et al.

Nuclear Inst. and Methods in Physics Research B 413 (2017) 51–56

- [16] S. Cavenati, C.A. Grande, A.E. Rodrigues, Adsorption equilibrium of methane, carbon dioxide, and nitrogen on zeolite 13X at high pressures, *J. Chem. Eng. Data* 49 (2004) 1095–1101.
- [17] T. Montanari, E. Finocchio, E. Salvatore, G. Garuti, A. Giordano, C. Pitarino, G. Busca, CO_2 separation and landfill biogas upgrading: a comparison of 4A and 13X zeolite adsorbents, *Energy* 36 (2011) 314–319.
- [18] R.V. Siritwardane, M.-S. Shen, E.P. Fisher, J. Losch, Adsorption of CO_2 on zeolites at moderate temperatures, *Energy Fuels* 19 (2005) 1153–1159.
- [19] S.M.L. Hardie, M.H. Garnett, A.E. Fallick, A.P. Rowland, N.J. Ostle, Carbon dioxide capture using a zeolite molecular sieve sampling system for isotopic studies (^{13}C and ^{14}C) of respiration, *Radiocarbon* 47 (2005) 441–451.
- [20] V. Palonen, M. Oinonen, Molecular sieves in $^{14}\text{CO}_2$ sampling and handling, *Radiocarbon* 55 (2013) 416–420.
- [21] A. Wotte, P. Wordell-Dietrich, L. Wacker, A. Don, J. Rethemeyer, $^{14}\text{CO}_2$ processing using an improved and robust molecular sieve cartridge, *Nucl. Instr. Meth. B* 400 (2017) 65–73.
- [22] J.B. Gaudinski, S.E. Trumbore, E.A. Davidson, S.H. Zheng, Soil carbon cycling in a temperate forest: radiocarbon-based estimates of residence times, sequestration rates and partitioning of fluxes, *Biogeochemistry* 51 (2000) 33–69.
- [23] M.H. Garnett, S.M.L. Hardie, Isotope (^{14}C and ^{13}C) analysis of deep peat CO_2 using a passive sampling technique, *Soil Biol. Biochem.* 41 (2009) 2477–2483.
- [24] C. Biasi, S. Jokinen, M. Marushchak, K. Hämäläinen, T. Trubnikova, M. Oinonen, P. Martikainen, Microbial respiration in arctic upland and peat soils as a source of atmospheric carbon dioxide, *Ecosystems* 17 (2014) 112–126.
- [25] J.C. Walker, X. Xu, S.M. Fahrni, M. Lupascu, C.I. Czimczik, Developing a passive trap for diffusive atmospheric $^{14}\text{CO}_2$ sampling, *Nucl. Instr. Meth. B* 361 (2015) 632–637.
- [26] M.H. Garnett, I.P. Hartley, A passive sampling method for radiocarbon analysis of atmospheric CO_2 using molecular sieve, *Atmos. Environ.* 44 (2010) 877–883.
- [27] M.H. Garnett, C. Murray, Processing of CO_2 samples collected using zeolite molecular sieve for ^{14}C analysis at the NERC radiocarbon facility (East Kilbride, UK), *Radiocarbon* 55 (2013) 410–415.
- [28] M. Ruff, S. Szidat, H.W. Gäggeler, M. Suter, H.A. Synal, L. Wacker, Gaseous radiocarbon measurements of small samples, *Nucl. Instr. Meth. B* 268 (2010) 790–794.
- [29] G.M. Santos, J.R. Southon, S. Griffin, S.R. Beaupre, E.R.M. Druffel, Ultra small-mass AMS ^{14}C sample preparation and analyses at KCCAMS/UCI Facility, *Nucl. Instr. Meth. B* 259 (2007) 293–302.
- [30] R. Drosch, W. Kutschera, K. Scholz, P. Steier, D. Wagenbach, E.M. Wild, Treatment of small samples of particulate organic carbon (POC) for radiocarbon dating of ice, *Nucl. Instr. Meth. B* 259 (2007) 340–344.
- [31] F. Conen, K.A. Smith, An explanation of linear increases in gas concentration under closed chambers used to measure gas exchange between soil and the atmosphere, *Eur. J. Soil Sci.* 51 (2000) 111–117.
- [32] R.W. Healy, R.G. Striegl, T.F. Russell, G.L. Hutchinson, G.P. Livingston, Numerical evaluation of static-chamber measurements of soil—atmosphere gas exchange: identification of physical processes, *Soil Sci. Soc. Am. J.* 60 (1996) 740–747.
- [33] J.E. Bauer, P.M. Williams, E.R.M. Druffel, Recovery of submilligram quantities of carbon dioxide from gas streams by molecular sieve for subsequent determination of isotopic (^{13}C and ^{14}C) natural abundances, *Anal. Chem.* 64 (1992) 824–827.
- [34] A. Goepel, M. Lonschinski, L. Viereck, G. Büchel, N. Kukowski, Volcano-tectonic structures and CO_2 -degassing patterns in the Laacher See basin, Germany, *Int. J. Earth Sci.* 104 (2015) 1483–1495.
- [35] J. Stoiber-Lipp, S. Wirth, J. Tischer, S. Gärtner, G. Büchel, L. Viereck, Kartierung von Trockenmoften im Laacher See Becken., in: *Ein-Blicke, Sonderband Deutsche Vulkanologische Gesellschaft e.V., Mendig*, 2012, pp. 101–110.
- [36] W. Aeschbach-Hertig, R. Kipfer, M. Hofer, D.M. Imboden, R. Wieler, P. Signer, Quantification of gas fluxes from the subcontinental mantle: the example of Laacher See, a maar lake in Germany, *Geochim. Cosmochim. Acta* 60 (1996) 31–41.
- [37] W.F. Giggenbach, Y. Sano, H.U. Schmincke, CO_2 -rich gases from Lakes Nyos and Monoun, Cameroon; Laacher See, Germany; Dieng, Indonesia, and Mt. Gambier, Australia—variations on a common theme, *J. Volcanol. Geoth. Res.* 45 (1991) 311–323.
- [38] H. Pfanz, Mofetten: Kalter Atem schlafender Vulkane, *Rheinischer Ver. f. Denkmalpflege u. Landschaftsschutz*, 2008.
- [39] A. Dewald, S. Heinze, J. Jolie, A. Zilges, T. Dunai, J. Rethemeyer, M. Melles, M. Staubwasser, B. Kuczewski, J. Richter, U. Radtke, F. von Blanckenburg, M. Klein, CologneAMS, a dedicated center for accelerator mass spectrometry in Germany, *Nucl. Instr. Meth. B* 294 (2013) 18–23.
- [40] P.J. Reimer, T.A. Brown, R.W. Reimer, Discussion: Reporting and Calibration of Post-Bomb ^{14}C Data, 2004.
- [41] M. Stuiver, H.A. Polach, Reporting of ^{14}C data – discussion, *Radiocarbon* 19 (1977) 355–363.
- [42] S. Hammer, I. Levin, Monthly mean atmospheric $\Delta^{14}\text{CO}_2$ at Jungfrauoch and Schauinsland from 1986 to 2016, *heidata Dataverse*, 2017.
- [43] G.M. Santos, J.R. Southon, N.J. Drenzek, L.A. Ziolkowski, E. Druffel, X.M. Xu, D.C. Zhang, S. Trumbore, T.I. Eglinton, K.A. Huguen, Blank assessment for ultra-small radiocarbon samples: chemical extraction and separation versus AMS, *Radiocarbon* 52 (2010) 1322–1335.
- [44] G. Bertoni, C. Ciuchini, R. Tappa, Measurement of long-term average carbon dioxide concentrations using passive diffusion sampling, *Atmos. Environ.* 38 (2004) 1625–1630.
- [45] G.R. Davidson, The stable isotopic composition and measurement of carbon in soil CO_2 , *Geochim. Cosmochim. Acta* 59 (1995) 2485–2489.
- [46] M. Krüger, D. Jones, J. Frerichs, B.I. Oppermann, J. West, P. Coombs, K. Green, T. Barlow, R. Lister, R. Shaw, M. Strutt, I. Möller, Effects of elevated CO_2 concentrations on the vegetation and microbial populations at a terrestrial CO_2 vent at Laacher See, Germany, *Int. J. Greenhouse Gas Control* 5 (2011) 1093–1098.
- [47] H.P. Taylor, J. Frechen, E.T. Degens, Oxygen and carbon isotope studies of carbonates from the Laacher See District, West Germany and the Alnö District, Sweden, *Geochim. Cosmochim. Acta* 31 (1967) 407–430.

Paper III

Radiocarbon analyses of respired CO₂ reveal the release of large amounts of ancient carbon from thawing deep permafrost deposits

Anja Wotte, Janet Rethemeyer, Philipp Wischhöfer, Andrea Jaeschke, Christian Knoblauch

Submitted to Global Change Biology

Radiocarbon analyses of respired CO₂ reveal the release of large amounts of ancient carbon from thawing deep permafrost deposits

Anja Wotte^{1*}; Janet Rethemeyer¹; Philipp Wischhöfer¹; Andrea Jaeschke¹; Christian Knoblauch²

¹ Institute of Geology and Mineralogy, University of Cologne, Cologne, Germany

² Institute of Soil Science, University of Hamburg, Hamburg, Germany

Abstract

Deep permafrost in northern high latitudes stores a substantial part (>25%) of the perennially frozen carbon, while covering a small area in the circumarctic permafrost region (8%). As a response to global warming, this carbon reservoir will gradually thaw and become exposed to microbial decomposition, which results in the release of the greenhouse gases CO₂ and CH₄ to the atmosphere. Predicting greenhouse gas emission rates is difficult because they are strongly controlled by the degradability of the organic matter (OM), which is not yet well constrained. The ice- and organic-rich Yedoma deposits in northeastern Siberia, which developed in unglaciated areas during the Pleistocene, contain OM assumed to be little decomposed and thus particularly prone to rapid microbial breakdown upon thaw. Presently, information on OM degradability is largely based on incubation experiments that do not consider the complexity of natural conditions. We thus designed a field study on a Yedoma outcrop in the Lena River Delta (Northeast Siberia) considering different characteristics of thawing permafrost. We measured CO₂ fluxes and their radiocarbon signature at three selected sites on the outcrop to assess if ancient or younger carbon sources are preferentially respired. The CO₂ released from the different sites is younger (2600–6500 yrs BP) than the bulk sediment (4000–31,000 yrs BP). Using isotopic mass balance calculations, we quantified that up to 70% of respired CO₂ originates from ancient OM. Our data suggest that the admixture of poorly decomposed, carbon-rich OM from the Holocene active layer may stimulate the degradation of ancient OM more strongly compared to the input of root-derived organic carbon. The results reveal the complexity of (priming) effects that may take place during thawing of deep permafrost deposits as well as the rapid in situ decomposition of thawing Pleistocene permafrost organic matter, which is increasing the permafrost carbon feedback.

Introduction

The terrestrial northern circumpolar permafrost region contains, with a total of 1300 to 1600 Pg, large amounts of organic carbon (OC) of which about 800 Pg are permanently frozen in permafrost (Hugelius *et al.*, 2014; Schuur *et al.*, 2015). This pool of OC makes permafrost important to the global climate system because of its potential to thaw with ongoing global warming. Rising

temperatures, particularly at high northern latitudes (IPCC, 2013), will cause the perennial frozen ground to thaw deeper whereby the frozen organic matter (OM) in permafrost will be exposed to microbial decomposition. Elevated soil temperatures accelerate decomposition rates (e.g. Davidson & Janssens, 2006; Bond-Lamberty & Thomson, 2010) and thereby amplify the release of the greenhouse gases (GHG) carbon dioxide (CO₂) and methane (CH₄) to the atmosphere (Elberling *et al.*, 2013; Voigt *et al.*, 2016). These GHG emissions will potentially provide a large positive feedback in the climate-carbon system known as the permafrost carbon feedback (PCF), which is still not well quantified (Ciais *et al.*, 2013; Schaefer *et al.*, 2014; Schuur *et al.*, 2015).

Uncertainties in GHG emission rates and, in consequence, the PCF extent arise from the amount of OC stored in the permafrost region and its microbial degradability in particular in deep permafrost deposits (Grosse *et al.*, 2011; Strauss *et al.*, 2017). Such deposits are particularly found in the so-called Yedoma region where ice- and organic-rich silty to sandy deposits (also named ice complex deposits) accumulated in unglaciated lowlands of the northern circumpolar region during the Pleistocene. They build up to 50 m thick sediments that hold massive syngenetic ice wedges (Schirrmeister *et al.*, 2002; Kanevskiy *et al.*, 2011; Schirrmeister *et al.*, 2013). The average OC content of these deposits is about 3 wt%, but individual layers are strongly variable and include very C-rich (up to 30 wt% OC) layers such as fossil cryosols and concentrated lenses of organic remnants (Zimov *et al.*, 2006; Schirrmeister *et al.*, 2011b; Strauss *et al.*, 2013). The Yedoma region stores a substantial portion (>25%) of the perennially frozen OC of 213 to 456 Pg, while covering only 8% (1.4 x 10⁶ km²) of the total permafrost region (17.8 x 10⁶ km²; Strauss *et al.*, 2013; Hugelius *et al.*, 2014; Walter Anthony *et al.*, 2014). The main OC source in Yedoma deposits is the late Pleistocene vegetation that accumulated at relatively fast rates (Kuhry *et al.*, 2009; Schirrmeister *et al.*, 2011b; Strauss *et al.*, 2017), whereby the OM became quickly buried in perennially frozen sediments (permafrost). Thus, the well-preserved OM is suspected to be quickly decomposable by microorganisms upon thaw because it has not undergone alteration processes during the Holocene (Strauss *et al.*, 2017).

With sustained warming, these ancient deep permafrost deposits may degrade relatively rapidly caused by the thawing of the ice wedges and associated thermokarst processes that may take place on decadal time scales (Jorgenson *et al.*, 2006; Sannel & Kuhry, 2011; Kokelj *et al.*, 2013; Raynolds *et al.*, 2014). As a consequence, the OM stored in these sediments since millennia will be exposed to microbial degradation and thus become part of the active carbon (C) cycle, i.e. increasing the PCF (Schuur *et al.*, 2009). The prediction of GHG fluxes from thawing permafrost OM is complicated because information on its microbial decomposability is limited (Kuhry *et al.*, 2013). Most information presently derives from laboratory incubation experiments (Dutta *et al.*, 2006; Zimov *et al.*, 2006; Lee *et al.*, 2012; Knoblauch *et al.*, 2013; Weiss *et al.*, 2016), which do not adequately mirror the complexity of natural conditions. Moreover, CO₂ flux measurements alone give no information on the organic substrates degraded, and a differentiation between fresh OM components that are part of the active C cycle and ancient C pools stabilized in the soil is not possible. The radiocarbon (¹⁴C) signature of the respired CO₂, however, makes it possible to identify and quantify the proportion of ancient OC that was stored in the permafrost for millennia and is now being decomposed upon thawing (Trumbore, 2000).

To improve the predictions of GHG emissions from thawing Yedoma deposits in response to global warming, we evaluated the degradability of ancient OM directly in the field. We chose an outcrop of Pleistocene Yedoma located on Kurungnakh Island along the banks of the Lena River

in Northeast Siberia. Our study area represents different characteristics of thawing Yedoma including sites where Pleistocene sediments are mixed with the overlying Holocene active layer including the tundra vegetation cover by thermoerosion, as well as sites where new vegetation grows on the exposed sediments. We selected three sites on the outcrop differing in their depositional age and the admixture of younger OM to study OM degradability and its stimulation by the incorporation of more easily degradable substrates (known as priming effect; Bingeman *et al.*, 1953; Fontaine *et al.*, 2003; Kuzyakov & Bol, 2006). Besides measuring CO₂ fluxes to quantify the total release of CO₂, we performed ¹⁴C analysis of directly in the field respired CO₂ to trace the degradation of ancient vs. young OM sources. This has not been done so far on deep permafrost deposits because such measurements were very challenging in remote locations until the development (Hardie *et al.*, 2005; Garnett & Murray, 2013) and improvement of CO₂ sampling techniques using molecular sieves (Wotte *et al.*, 2017a). Furthermore, δ¹³C and lipid biomarker analyses were used to better characterize the OM and identify substrates that are most vulnerable to microbial decomposition upon permafrost thaw.

Material and methods

Study area

Our study site is located on Kurungnakh Island (72°20'21''N; 126°17'33''E) in the northeast Siberian Lena River Delta (Fig. 1) in the zone of continuous permafrost and arctic tundra. Kurungnakh Island consists of two main sedimentary formations deposited during the late Pleistocene, which are covered by Holocene sediments (Schwamborn *et al.*, 2002; Wetterich *et al.*, 2008; Schirrmeister *et al.*, 2011a). The oldest, lowest Pleistocene formation comprises fluvial sandy deposits (88,000–43,000 yrs BP; Schwamborn *et al.*, 2002), which are overlain by the ice-rich (38–133 wt%), silty to sandy sediments of the Yedoma suite (Schirrmeister *et al.*, 2011b). The Yedoma deposit includes peat horizons, single peat lenses, and large ice wedges (Wetterich *et al.*, 2008). It can be subdivided into two units: the lower unit (42,000–32,000 yrs BP), which developed under a relatively warm and wet climate, and the upper unit (14,000–29,000 yrs BP) deposited under cold and dry climatic conditions (Wetterich *et al.*, 2008; Knoblauch *et al.*, 2013). The lower unit is characterized by a higher total OC (TOC; 2–7%) and a lower stable C isotopic composition (δ¹³C; ~-27‰ VPDB) compared to the upper unit (1.7–2% TOC; ~ -25.5‰ VPDB; unit III and unit IV, respectively, in Wetterich *et al.*, 2008). The TOC to nitrogen (N) ratio (C/N) in both units is highly variable (9–23). The Holocene deposit that covers the Yedoma consists of cryoturbated silty sands with peat inclusions having much higher TOC contents (3–12%) and C/N ratios (15–20), but lower δ¹³C values (~-29‰; Wetterich *et al.*, 2008). The surface is characterized by polygonal tundra with a moss-, sedge-, and dwarf shrub-dominated vegetation. We chose three different sites on an outcrop along the riverbank of the Olenyeksaya Channel all located in a radius of 30 m at an altitude of 20 to 30 m above sea level (m a.s.l.; Fig. 2). The Yedoma outcrop is strongly affected by thermal erosion with up to 7 m of annual cliff-top erosion (Stettner *et al.*, 2018).

All sites chosen differ in bulk OC ages and in the influences of thermoerosional processes. K4 is located at an altitude of 29 m a.s.l. between thermokarst mounds on redistributed Pleistocene and Holocene material (Fig. 2). The two other sites, K7 (22 m a.s.l.) and KX (30 m a.s.l.), are

located on conical thermokarst mounds (called baydzherakhs in Russian language) that formed due to the thawing of the surrounding large syngenetic ice wedges. The thermokarst mounds derive from different parts of the Yedoma deposit, which were identified using the ^{14}C ages of the OM (Fig. 3; S1). Both sites K7 and KX contain no visible input of Holocene material. K7 has a sparse vegetation cover that recently started growing on the bare sediment, while KX is covered only by very few fresh grasses and mosses (Fig. 2b, c).

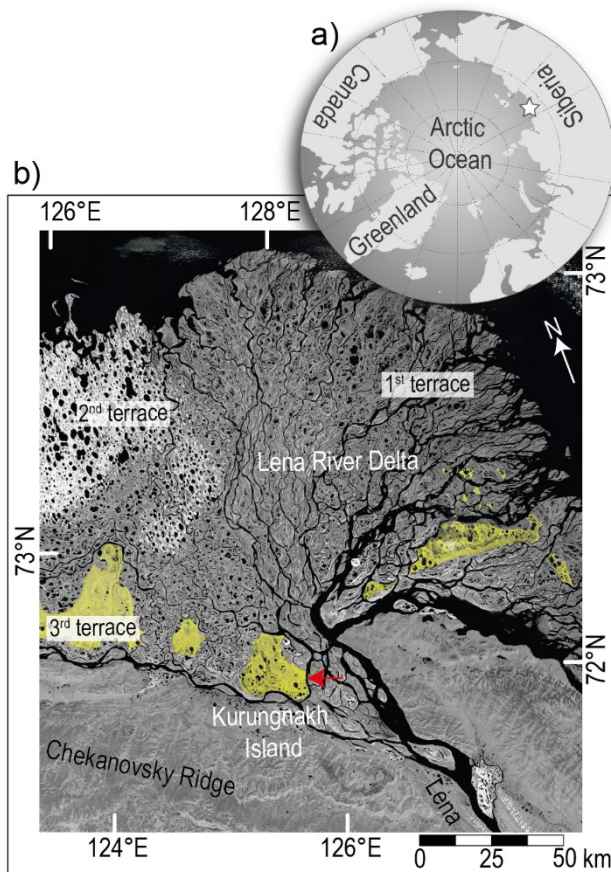


Fig. 1: Location of the study area a) in Northeast Siberia. b) Overview of the Lena River Delta showing the location of outcrop on Kurungnakh Island on the third geomorphological terrace, built up of Yedoma deposits (in yellow; Landsat-7 ETM+, GeoCover 2000 © NASA).

Sediment and CO_2 sampling

Our sampling campaign was performed during August 2016. We first collected CO_2 using opaque closed dynamic respiration chambers. After removing the chambers, sediment samples were taken from different depth intervals of the thawed surface sediment at the three sites. We assume that CO_2 is mainly respired from the thawed surface sediment. All sediment samples were stored and transported frozen until analysis.

For the collection of respired CO_2 and the measurement of CO_2 fluxes, we carefully installed PVC collars (~25 cm OD, ~24 cm height) into the sediment down to a depth of at least 12 cm. We placed the lid on these collars resulting in a total chamber volume of ~7 L as illustrated in Wotte *et al.* (2017b). At the beginning and after CO_2 collection, the increase in CO_2 concentration within the respiration chamber was measured over a ten-minute interval with an infrared gas analyzer (IRGA; LI-840A, LI-COR Biosciences GmbH, Germany). The CO_2 flux was calculated from the linear increase of the CO_2 concentration over two minutes within the measuring interval.

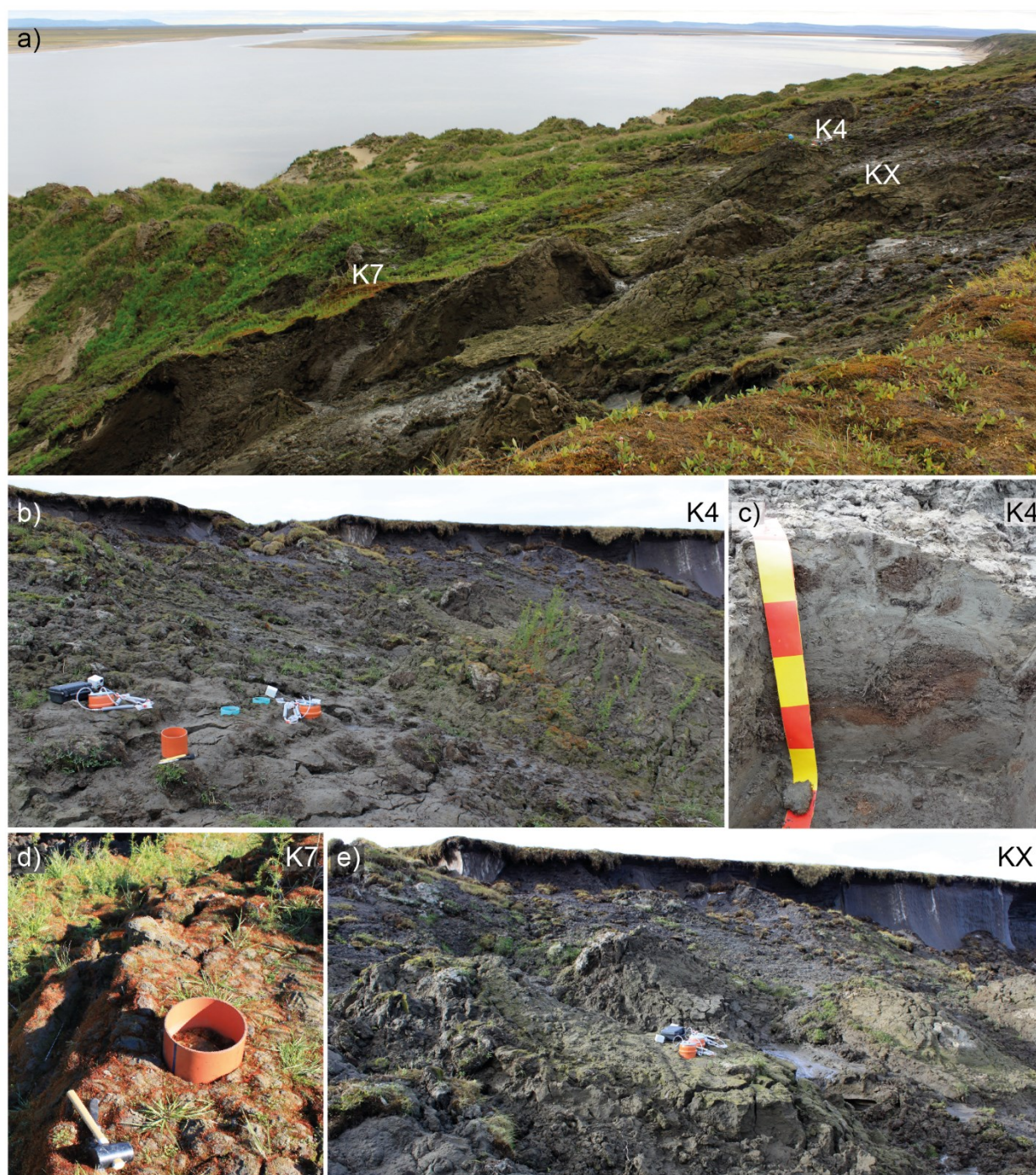


Fig. 2: a) The Yedoma outcrop along the Olenyetskaya Channel on Kurungnakh Island (viewing direction to the south) with the locations of the three study sites: b) site K4 with the highest admixture of Holocene OM, including c) lenses of fresh organic material from the surface, and the thermokarst mounds d) K7, and e) KX.

Before CO₂ sampling, the atmospheric CO₂ was removed by circulating the air of the chamber via a CO₂ trap (soda lime) until at least two chamber volumes passed the trap. Then, the chamber was coupled with a molecular sieve cartridge (MSC) containing zeolite type 13X for CO₂ adsorption described in detail in Wotte *et al.* (2017a). The CO₂ was quantitatively trapped on the zeolite by circulating the chamber air through a water trap (Merck Sicapent®) and the MSC for at least 15 min depending on the CO₂ concentration until an amount of about 1 mg C was reached. Sampling took place between 1 and 6 PM using two replicate chambers at each site.

Elemental analysis

Prior to elemental analyses all samples were freeze-dried and ground. For total OC analysis, inorganic C was removed by treatment with hydrochloric acid (0.5%; 60°C, 4 h). Total C, TOC, and total N contents were determined using an elemental analyzer (Vario MICRO cube, Elementar, Germany) and inorganic C (TIC) was calculated based on the difference between TOC and total C.

Lipid analysis

Freeze-dried and homogenized sediment (1–5 g depending on TOC content) was extracted using accelerated solvent extraction (Dionex ASE 350, USA; 75 bar, 120°C, 20 min) with a mixture of dichloromethane and methanol (DCM:MeOH 9:1, v:v). The bulk of the solvent was removed by rotary evaporation under vacuum. The resulting total lipid extract was saponified with methanolic KOH (0.5 M) for 2 h at 80°C. Non-saponifiable lipids (neutral lipids) were extracted out of the basic solution using *n*-hexane. Fatty acids were obtained by acidifying the residue to pH 1 and subsequent extraction with DCM. The neutral fractions were further separated by column chromatography using silica gel (1% deactivated; mesh size 60). Hydrocarbons were eluted with *n*-hexane, followed by DCM:*n*-hexane (2:1 v:v) for ketones, and MeOH for polar compounds including alcohols. The fatty acids were derivatized using MeOH:HCl_{conc} (95:5 v:v) for 10 h at 50°C. The resulting fatty acid methyl esters (FAMES) were further separated and purified over a SiO₂–Na₂SO₄ column by eluting with DCM:*n*-hexane (2:1 v:v). Lipids were quantified with a gas chromatograph (GC) with a flame ionization detector (7890, Agilent Technologies, USA) and helium as carrier gas. Chromatographic separation of compounds was achieved using an Agilent DB-5 MS capillary column (50 m length, 0.2 mm diameter, 0.33 μm film thickness). The oven temperature was programmed to be held at 40°C for 2 min, then increased at 10°C min⁻¹ to 140°C, followed by 3°C min⁻¹ until 320°C, and held for 38 min. Identification and quantification of individual compounds was done using external standard mixtures. All lipid concentrations were normalized to TOC (wt%).

The total amount of plant-derived long-chain *n*-fatty acids (C₂₀ to C₃₂) increases with depth at all sites (S1) characteristic for contributions of this compound class from other sources explained below. We thus did not use *n*-fatty acids as indicators for OM composition and stage of degradation as they might provide misleading information. Instead, we used proxies based on *n*-alkanes including relative proportions of dominant long-chain *n*-alkanes derived from plant cuticular waxes (Eglinton & Hamilton, 1967) as well as the average chain length (ACL; Eq. 1; Poynter, 1989) both indicating the dominant type of vegetation. In addition, the C preference index (CPI; Eq. 2; Marzi *et al.*, 1993) representing the relative distribution of odd and even C numbers in a sample was used as OM degradation and alteration proxy.

Average chain length (ACL):

$$ACL_{25-33} = \frac{25 \times C_{25} + 27 \times C_{27} + 29 \times C_{29} + 31 \times C_{31} + 33 \times C_{33}}{C_{25} + C_{27} + C_{29} + C_{31} + C_{33}} \quad (\text{Eq. 1})$$

Carbon Preference Index (CPI):

$$CPI = \frac{\sum(C_{23}, C_{25}, C_{27}) + \sum(C_{25}, C_{27}, C_{29})}{2 * \sum(C_{24}, C_{26}, C_{28})} \quad (\text{Eq. 2})$$

Carbon isotopic analysis of sedimentary organic matter

An aliquot of the ground sediment was treated with 0.5% HCl (at 60°C for 4 h) to remove inorganic C. $\delta^{13}\text{C}$ analysis was performed using an isotope-ratio mass spectrometer (IRMS; Delta V, Thermo Scientific, Germany) coupled to an elemental analyzer (Flash 2000, Thermo Scientific, Germany). The $\delta^{13}\text{C}$ values of three replicate measurements are expressed in per mille relative to Vienna Pee Dee Belemnite (VPDB).

^{14}C analyses of bulk sediments were performed on decarbonized samples (0.5% HCl at 60°C for 4 h), which were converted to elemental C using the automated graphitization equipment (AGE; Ionplus AG, Switzerland; Wacker *et al.*, 2010; Rethemeyer *et al.*, 2013), at the Cologne AMS facility (HVVE, The Netherlands; Dewald *et al.*, 2013). The results are reported in fraction modern C ($F^{14}\text{C}$) and as conventional radiocarbon ages (in years before present, yrs BP) with 1- σ uncertainties (Stuiver & Polach, 1977; Reimer *et al.*, 2004).

Carbon isotopic analysis of respired CO_2

The CO_2 collected on the MSCs was desorbed from the zeolite by heating the MSC (5 min at 150°C, 10 min at 500°C) under a purge gas (helium, 40 ml min⁻¹; Wotte *et al.*, 2017a). The CO_2 released was quantified and split into aliquots for ^{14}C and $\delta^{13}\text{C}$ analysis using a vacuum line (cryogenic distillation system; Wotte *et al.*, 2017b) and an improved cleaning procedure. Prior to connecting the MSC with the vacuum line an overpressure was created with helium (about 1,400 mbar). This avoids the penetration of atmospheric CO_2 into the vacuum system during the connection of the MSC.

^{14}C analyses of CO_2 samples were performed with the gas ion source of the mini C dating system (MICADAS, Ionplus AG, Switzerland) at ETH Zurich (Switzerland; Ruff *et al.*, 2007; Synal *et al.*, 2007). All ^{14}C results are reported in $F^{14}\text{C}$ with 1- σ uncertainties (Stuiver & Polach, 1977; Reimer *et al.*, 2004). Besides correcting for analytical uncertainties of the AMS analysis, all results were corrected for potential contamination with modern or ^{14}C -free C introduced during CO_2 processing with the MSCs. Therefore, ^{14}C -free and modern standards (IAEA C1 and C3) were processed similar to the samples. The results of the samples were corrected for a constant contamination of $29 \pm 12 \mu\text{g C}$ having a ^{14}C concentration of $0.97 \pm 0.10 F^{14}\text{C}$ including error propagation (Hanke *et al.*, 2017).

The stable C isotopic composition of the CO_2 samples was measured with an IRMS (Finnigan Delta Plus, Thermo Scientific, Germany) coupled to a GC (6890, Agilent Technologies, USA).

Quantification of ancient CO_2 respired

We used an isotopic mass balance calculation (Eq. 3) in order to quantify the fraction of ancient OM in the respired CO_2 at each study site using a two end-member model:

$$F^{14}\text{C}_{\text{CO}_2} = f_{\text{OM}} \times F^{14}\text{C}_{\text{OM}} + f_{\text{Y-OM}} \times F^{14}\text{C}_{\text{Y-OM}} \quad (\text{Eq. 3})$$

$$\text{and: } f_{\text{OM}} + f_{\text{Y-OM}} = 1$$

with $F^{14}\text{C}_{\text{CO}_2}$, representing the measured ^{14}C content of the emitted CO_2 , and $F^{14}\text{C}_{\text{OM}}$ and $F^{14}\text{C}_{\text{Y-OM}}$ the ancient OM in the thawed surface, and the ^{14}C content of the young OM inputs at each site,

respectively. We calculated average ^{14}C contents for the ancient endmember, $F^{14}\text{C}_{\text{OM}}$, of 0.61 at K4, 0.18 at K7, and 0.027 at KX. We calculated the fraction of old OM (f_{OM}) assuming that the admixed young OM ($f_{\text{Y-OM}}$) originates either from the active layer of the Holocene sediment (at K4 and KX) or from recent roots and their exudates (at K7). Both sources have very similar $F^{14}\text{C}$ values of 0.97 (average age of the Holocene active layer; S1) and 1.00 (measured atmospheric ^{14}C content in August 2016), respectively. We thus chose the rounded ^{14}C content of $F^{14}\text{C}_{\text{Y-OM}} = 1.0$ as minimal endmember and the resulting fraction of ancient OM in consequence is the maximum proportion of ancient OM in the respired CO_2 .

The results of this calculation will reveal if younger or ancient substrates are preferentially respired and if the degradation of ancient permafrost OM may be stimulated by the admixture of C-rich and more easily degradable organic substrates.

Results

Sediment age/origin

The study sites on the thawing Yedoma outcrop are characterized by differences in the depositional age of the OM. We used the ^{14}C ages of the OM to reconstruct from which sedimentary unit the studied materials originate and to correlate our study sites with published information on the Yedoma deposits of Kurungnakh Island (Fig. 3; S1; Wetterich *et al.*, 2008).

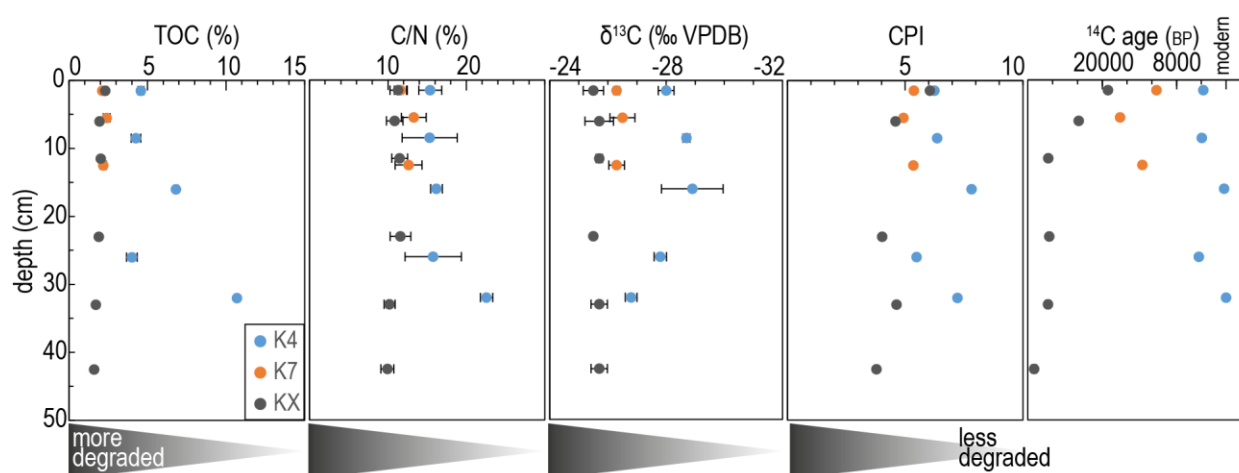


Fig. 3: Distribution of organic matter (OM) decomposition parameters and ^{14}C age in the thawed surface sediment of the three different sites K4 (blue), K7 (orange), and KX (grey) located on a thawing and eroding outcrop of the Yedoma deposit on Kurungnakh Island. Each graph is showing more degraded OM on the left and less degraded OM on the right side. The standard deviation is shown for TOC, C/N and $\delta^{13}\text{C}$ and the 1- σ measurement uncertainty for the ^{14}C ages is within symbol size.

The sediment at K4 (0–34 cm), the youngest location on the outcrop, contains two visible, 300 yrs BP and >modern (>1950) old peat lenses at 14–18 and 30–34 cm depth (Fig. 3, S1). These reduce the age of the sedimentary OM to an average age of 2200 yrs BP. The average OM age excluding these younger admixtures is 4000 yrs BP thus belonging to the middle to late Holocene deposit on top of the Pleistocene Yedoma (Unit V in Wetterich *et al.*, 2008) but containing most probably also inputs of Yedoma-derived OM from the adjacent thermokarst mounds. The sediments of the two thermokarst mounds, sites K7 and KX, have average ages of 13,600 yrs BP and 26,300 yrs BP, respectively, thus originating from the upper Yedoma unit (Unit IV in

Wetterich *et al.*, 2008). Against our expectation, the bulk OM at K7 located at the lowest altitude (about 22 m a.s.l.) is much younger (11,200–17,100 yrs BP, 0–15 cm) than those of KX (about 30 m a.s.l.; 19,000–29,000 yrs BP, 0–13 cm; S1). The thermokarst mound on which K7 is located thus seems to be more strongly displaced, which could be due to a stronger melting of the underlying ice wedge. Unfortunately, we were not able to sample the complete thawed layer at site K7, because of difficult weather conditions and problems with the sampling equipment. At KX, the thaw layer can be subdivided into two sections: the uppermost 10 cm show a strong increase in ^{14}C age (19,000–23,800 yrs BP), indicating admixtures of younger OM, whereas the lower 10–45 cm have a considerably high and nearly constant age (28,500–31,000 yrs BP). The lower section most probably represents the depositional age of the sediment. Accordingly, KX can be correlated with the lower part of the upper Yedoma unit (Wetterich *et al.*, 2008).

Composition of organic matter

The OM composition in the thawed surface sediments of the youngest site, K4, differs considerably from those of the two thermokarst mounds, K7 and KX (Fig. 3; S1). At K4, TOC contents (4.0–10.7%) and C/N ratios (15.4–22.6) are much higher and more variable with depth having the highest values in the two peat lenses (Fig. 3; S1). These results agree well with the variable ^{14}C depth distribution at K4 given above, reflecting the mixture of primarily early and late Holocene OM and OM from the recent vegetation. In contrast, the sedimentary OM at K7 and KX is characterized by lower TOC contents and C/N ratios in the range of 1.6–2.4% and 9.9–13.3, respectively (Fig. 3; S1). The ^{14}C depth distribution at KX, which suggests contributions of younger OM to the uppermost 10 cm, is not reflected by TOC and C/N values. These values vary in a narrow range and are comparable at KX and K7 suggesting similar OM sources.

The stable C isotopic composition of the OM shows analogous differences between the investigated sites. $\delta^{13}\text{C}$ values are quite similar and less depleted at K7 and KX (mean values at K7: -26.4 ± 0.3 and KX: -25.6 ± 0.3 ‰ VPDB; Fig. 3). At K4, $\delta^{13}\text{C}$ values are more depleted and more variable with depth (-26.8 to -28.9 ‰ VPDB; Fig. 3; S1) following the depth distribution of C/N ratios both reflecting a variable composition of the OM. At all sites, the $\delta^{13}\text{C}$ signature is reflecting that C_3 plants are the dominant source of the OC. The differences in $\delta^{13}\text{C}$ between the sites indicate a different degree of OM decomposition rather than a change in vegetation because the plant remains in the Yedoma deposits represent similar grass/sedge tundra vegetation (Schirrmeister *et al.*, 2011c).

Plant-derived *n*-alkanes occur at all sites with chain lengths in the range of C_{21} to C_{33} and having a strong odd C number predominance (S2). Total *n*-alkane concentration diminishes continuously with depth in the surface sediment at K4 but stays relatively constant at K7 and KX below the uppermost few cm (S2). The *n*-alkanes are dominated by C_{27} , C_{29} , and C_{31} resulting in ACL values of 28.3 at K4 and 29.3 and 28.8 at K7 and KX, respectively. The relative proportion of the dominant *n*-alkanes reflect differences between sites with K4 being dominated by C_{27} , while K7 contains predominantly C_{31} *n*-alkanes (S2). At KX, the *n*-alkane distribution exhibits a shift from

C₂₇ in the surface sediment to predominantly C₃₁ at greater depth similar to the different ¹⁴C contents of the uppermost 10 cm and the intervals below. Both parameters indicate the input of younger, Holocene OM into the uppermost 10 cm. The compositional differences between K4 and the two older sites K7 and KX are also reflected by the CPI values. These are slightly higher and more variable with depth at K4 (5.5–7.8) compared to K7 (4.9–5.4) and KX (3.8–6.1) and show a very similar depth distribution to those of the C/N ratio at K4 (Fig. 3). The two peaty layers have typically the highest CPI values of 7.8 and 7.2, respectively (Fig. 3).

n-Fatty acids were detectable with chain lengths of C₁₄ to C₃₂ with a strong even over odd predominance dominated by C₂₂ and C₂₄ homologues (S2). The total amount of plant-derived long-chain compounds (C₂₀ to C₃₂) increases with depth in particular at sites K7 and KX having much lower concentrations than K4 (S2). This has been interpreted to reflect their production by humification of OM or microbial transformation of other lipids (Ficken *et al.*, 2000; Zhou *et al.*, 2010; Andersson & Meyers, 2012). It may also indicate the presence of roots containing long-chain (C₂₀–C₃₀) fatty acids being part of the cell wall component suberin (Bull *et al.*, 2000; Kögel-Knabner, 2002).

CO₂ fluxes and carbon isotopic composition

The CO₂ fluxes determined for the three locations on the Yedoma outcrop sorted by increasing sediment age, K4, K7, and KX, were 49 ± 21 (n=6), 127 ± 37 (n=3), and 57 ± 5 μg CO₂ m⁻² s⁻¹ (n=5), respectively (Fig. 4; S3). Against our expectations, CO₂ fluxes are lowest at K4 having the highest TOC contents and containing a considerable admixture of little decomposed, C-rich peaty material, while K7 showed more than twice as high CO₂ fluxes. At K7, the CO₂ flux may be affected by higher air

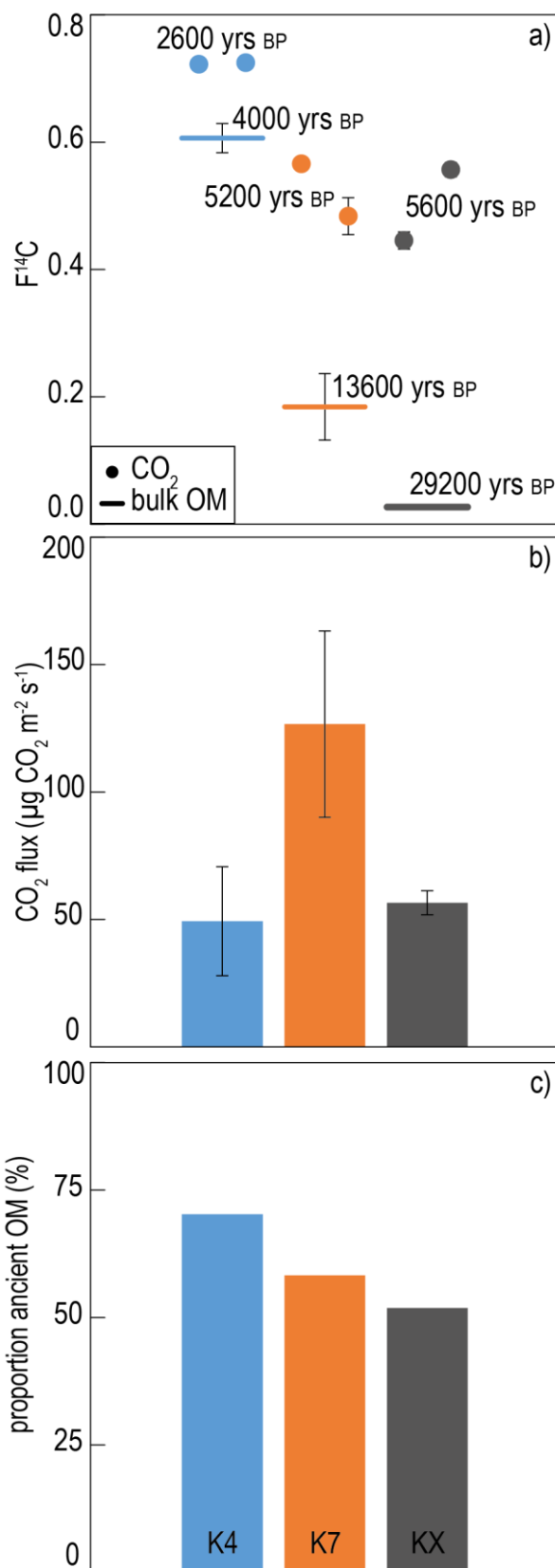


Fig. 4: a) ¹⁴C content (F¹⁴C) of the respired CO₂ in comparison to the average ¹⁴C content of the underlying bulk organic matter (OM). 1-σ uncertainty is shown for the CO₂ data and the standard deviation for the mean bulk ¹⁴C content. b) CO₂ fluxes determined in the field with standard deviation. And c) the calculated proportion of ancient OM in the respired CO₂ using isotopic mass balance calculation (Eq. 3) for each site (K4, K7, and KX).

temperatures ($\sim 12^{\circ}\text{C}$) during the day of measurement than during sampling at the two other sites ($\sim 7^{\circ}\text{C}$), which may have intensified microbial respiration (Dutta *et al.*, 2006; Schädel *et al.*, 2014; Treat *et al.*, 2015; Hicks Pries *et al.*, 2016).

The $\delta^{13}\text{C}$ values of the respired CO_2 are very similar at all sites (-19.2 to -21.1‰ VPDB) apart from one outlier at site K7 (-13.6‰ VPDB; S3). We can exclude a possible contamination with atmospheric CO_2 , because of the lower ^{14}C content of the same sample, which is even lower than the replicate sample. At all sites, the $\delta^{13}\text{C}$ values of CO_2 are more enriched in ^{13}C compared to the bulk OM, to CO_2 respired from the active layer of permafrost soils (-22.1 to -24.8‰ VPDB; Hicks Pries *et al.*, 2016), and to CO_2 respired from incubated Yedoma samples (-25.3 to -30.1‰ VPDB; Dutta *et al.*, 2006). However, our data are in good agreement with $\delta^{13}\text{C}$ results of respired CO_2 from incubated samples of the same outcrop (unpublished data), which are on average -20‰ VPDB.

The ^{14}C concentration and conventional age of the CO_2 at the three study sites is in the range of 0.45–0.72 F^{14}C , which is equivalent to 6500–2600 yrs BP (Fig. 4; S3). At all sites, the respired CO_2 is considerably younger than the respective bulk OM. The youngest CO_2 (2600 yrs BP) was released from the youngest sediment at site K4 having the largest admixture of Holocene OM. CO_2 emissions were about twice as old at K7 (5200 yrs BP), which has an average bulk OC age of about 14,000 yrs BP. The oldest CO_2 (5600 yrs BP) was released from the oldest sediment at KX (about 26,000 yrs BP).

Discussion

Composition of organic matter in thawing Yedoma deposits

Organic matter decomposition rates in permafrost depend strongly on the chemical composition of the source material, i.e. the composition of differing vegetation (Jenkins & Adams, 2010), and their stage of degradation (Schädel *et al.*, 2014; Treat *et al.*, 2014; Chen *et al.*, 2016). The faster the plant litter is incorporated into the frozen sediment, the lower is the alteration of the organic components. During thaw of deep permafrost deposits, the OM will be eroded, translocated, and thereby sediments of different OM composition (often synonymously named quality) will be mixed, which may considerably alter decomposition rates. The admixture of C-rich, well-preserved OM derived from the Holocene surface layer with ancient sediment may promote the degradation of the ancient OM components in these deposits known as priming effect (Bingeman *et al.*, 1953; Kuzyakov *et al.*, 2000).

We use different proxies to evaluate the composition of the OM in the different sites on the thawing Yedoma outcrop. TOC contents and C/N ratios of the OM are widely used for characterizing the amount and microbial availability of OM in permafrost (e.g. Schädel *et al.*, 2014; Gentsch *et al.*, 2015; Strauss *et al.*, 2015; Weiss *et al.*, 2016). C/N ratios decrease in case of stronger microbial degradation because C is released to the atmosphere and N to the soil (Melillo *et al.*, 1989; Kuhry & Vitt, 1996). Likewise, ongoing microbial decomposition preferentially releases ^{12}C and thus the OM will be enriched in ^{13}C (Nadelhoffer & Fry, 1988; Ågren *et al.*, 1996; Kuhry & Vitt, 1996). The specific distribution of long-chain *n*-alkanes expressed as CPI and ACL give further information on OM alteration and the relative freshness of the plant material.

On the Yedoma outcrop the sedimentary OM of site K4 has been strongly mixed with overlaying material during thaw and erosion. In consequence, this deposit contains considerable proportions of younger OM resulting in the depletion of the average ^{14}C age in the surficial sediment (0–34 cm). The two distinct peat lenses in the thawed surface sediment are very similar in their ^{14}C content (0.96–1.0 $F^{14}\text{C}$) to the average ^{14}C value of the active layer of the non-eroded polygonal tundra surface soil (0.95–0.98 $F^{14}\text{C}$ polygon center and rim, respectively; S1). Further evidence for the origin of the peat lenses from the active layer comes from their similar composition consisting both of less decomposed plant material having higher TOC contents and C/N ratios (S1). Besides the admixture of the peat lenses, the OM in the thawed sediment profile at K4 has an overall higher abundance of less degraded OM illustrated by depleted $\delta^{13}\text{C}$ values and higher CPI values of the plant wax-derived *n*-alkanes compared to the two other sites (Fig. 3; S1, 2).

Sites K7 and KX represent thawing Yedoma exposed as thermokarst mounds containing small admixtures of younger OM. Considerably lower TOC contents and C/N ratios, and enriched $\delta^{13}\text{C}$ values of the OM in the thawed sediments, which are comparable with previous analyses (Wetterich *et al.*, 2008), indicate its higher degree of microbial transformation compared to K4. The higher ^{14}C concentrations, i.e. younger ages, of the OM in the uppermost (0–15 cm) part of the profiles suggest that younger OC is introduced into the surface layer. Both sites are covered by some (K7) and very sparse (KX) vegetation that started growing on the bare soil, which typically happens during thawing of exposed permafrost deposits. The fresh vegetation might be responsible for relatively high concentrations of *n*-fatty acids and slightly lower $\delta^{13}\text{C}$ values in the surface sediment at K7, which is, however, not confirmed by other proxies (TOC, C/N, CPI). The higher ^{14}C concentration and different composition of the OM in the uppermost sediment layer at KX most likely characterizes the mixture of Holocene and Pleistocene sediments that have been eroded and moved within a mudflow across the top of the thermokarst mound. The very smooth surface at KX argues for this kind of sediment. Further indication is given by the *n*-alkane distribution in the surface sediments of KX (ACL~28.4), which is very similar to the sediments at site K4 (ACL~28.3; S2).

Degradability of organic matter in thawing Yedoma deposits

To evaluate the degradability of the sedimentary OM in the Yedoma outcrop, we measured CO_2 fluxes and analyzed their ^{14}C concentration at maximal summer thaw-depth. The latter was compared with the ^{14}C content of the bulk sedimentary OM and its compositional information. We quantified the fraction of ancient OM in the respired CO_2 using isotopic mass balance calculation (Eq. 3)

Generally, the CO_2 fluxes determined at the three sites (49–127 $\mu\text{g CO}_2 \text{ m}^{-2} \text{ s}^{-1}$, mean: $78 \pm 35 \mu\text{g CO}_2 \text{ m}^{-2} \text{ s}^{-1}$; Fig. 4) are at the lower limit of CO_2 fluxes measured on bare Yedoma deposit in northeastern Siberia near Cherskii (100–225 $\mu\text{g CO}_2 \text{ m}^{-2} \text{ s}^{-1}$; Zimov *et al.*, 2006). However, our results are in the same order of magnitude like measurements from Yedoma deposits just east of the Lena River Delta on Muostakh Island (1.6–220 $\mu\text{g CO}_2 \text{ m}^{-2} \text{ s}^{-1}$, mean $19 \pm 40 \mu\text{g CO}_2 \text{ m}^{-2} \text{ s}^{-1}$; Vonk *et al.*, 2012).

Several laboratory incubation experiments (summarized by Schädel *et al.*, 2014) revealed higher respiration rates for C-rich permafrost having higher C/N ratios. We thus expected the maximum CO_2 fluxes at site K4, containing the least microbially transformed OM with the highest

TOC contents and the highest proportion of fresh, plant material originating from the active layer. This material may prime the degradation of more strongly transformed OM, which has been documented for various permafrost soils in which poorly decomposed topsoil OM or plant remnants were mixed (Wild *et al.*, 2014; Wild *et al.*, 2016; Walz *et al.*, 2017). At K4, however, we measured the lowest CO₂ fluxes similar to those at KX, which contains less OC that was more strongly transformed before being freeze-locked in the permafrost. These CO₂-flux data agree well with similar total CO₂ productions derived from aerobically incubated Holocene and Pleistocene sediments from the same Yedoma outcrop by Knoblauch *et al.* (2013). The low fluxes may result from N-limitation of the microbial decomposers due to the admixture of the little decomposed OM having high C/N ratios and lacking any easily degradable or N-rich substrates. This phenomenon, which results from a less active decomposer community under cold and moist conditions, is well known for Arctic soils (e.g. Hobbie *et al.*, 2002; Gough & Hobbie, 2003; Karhu *et al.*, 2010; Sistla *et al.*, 2012). Using the isotopic mass balance (Eq. 3), we determined a maximum proportion of ancient OM of 70% in the respired CO₂ at K4 ($F^{14}C_{CO_2} = 0.72$) when using the average bulk OM age without the admixed, modern peat lenses ($F^{14}C_{OM} = 0.61$).

On the thermokarst mound at K7 we measured about two times higher CO₂ fluxes in comparison to K4 and KX. The results may be biased by the higher temperature (an about 5°C higher air temperature) during the day of measurement at K7, as higher temperatures can increase respiration rates (Dutta *et al.*, 2006; Schädel *et al.*, 2014; Treat *et al.*, 2015; Hicks Pries *et al.*, 2016; Walz *et al.*, 2017). The CO₂ released from both thermokarst mounds has nearly similar ¹⁴C concentrations in the range of 0.446–0.566 $F^{14}C$, while the average ¹⁴C content of the underlying sediment is significantly higher at K7 ($F^{14}C_{OM} = 0.184$) compared to KX ($F^{14}C_{OM} = 0.038 F^{14}C$) leading to a higher difference in the ¹⁴C content between the bulk OM and the respired CO₂ at K7. According to our mass balance calculation up to 60% ancient sedimentary OM may be respired at K7 and up to 50% at KX. The relatively low ¹⁴CO₂ concentration at K7 argues for an enhanced release of ancient C instead of contributions of root respiration. The latter would result in much higher ¹⁴CO₂ values because root respired CO₂ has an atmospheric ¹⁴C concentration (Trumbore, 2000).

The largest proportion of ancient sedimentary OM being respired at K4 demonstrates that the admixture of less decomposed, C-rich OM has the strongest priming effect. Roots and their exudates containing low molecular weight sugars and organic acids (Jones, 1998; Girkin *et al.*, 2018), which are the preferential, quickly degradable substrate for microorganisms, also strongly promote the degradation of the ancient OM in the thermokarst mounds at K7 and KX. The more intense the vegetation cover (like at K7), the larger the fraction of ancient C that is released as CO₂.

In order to assess the potential loss of C on longer time scales, we calculated annual respiration rates and the amount of ancient OC that may be released. By assuming constant CO₂ fluxes over the summer season of about four months (120 days; Boike *et al.*, 2013), we calculated annual respiration rates of 140, 360, and 160 g C m⁻² yr⁻¹ for sites K4, K7, and KX. These emission rates from Yedoma deposits are of similar magnitude as observed in the active layer of different tundra ecosystem where growing season respiration ranged from 80 to 403 g C m⁻² yr⁻¹ (Schuur *et al.*, 2009; Biasi *et al.*, 2014). The respiration rates from a peat plateau and upland mineral tundra by Biasi *et al.* (2014) are at the lower end of this range, because their calculation is based on a shorter growing season of only 78 days.

Based on the results of our isotopic mass balance, we calculated the potential release of C from the deep permafrost during one year. For K4, K7, and KX, the maximal amount may be in the order of 85, 210, and 100 g C m⁻² yr⁻¹. This loss of ancient C determined for all three sites thus is higher compared to microbial respiration rates measured directly in the field of 20–80 g old C m⁻² yr⁻¹ for the active layer obtained by Biasi *et al.* (2014) and Schuur *et al.* (2009) for Holocene Tundra landscapes. These data indicate that the permafrost organic matter in these Yedoma sediments is rapidly degradable after thaw on short time scales. However, if these relatively high decomposition rates persist over longer time scales is still uncertain, since laboratory incubations of permafrost OM indicate a substantial decline in decomposition rates after the labile OM fraction has been decomposed (Schädel *et al.*, 2014; Knoblauch *et al.*, 2018).

Overall, the results of our study show that ancient OC stored in the Pleistocene Yedoma deposits is highly vulnerable to microbial degradation. The thawing of ice-wedges in the deep permafrost, which occurs along riverbanks and coastal areas (Lantuit *et al.*, 2012; Günther *et al.*, 2013; Stettner *et al.*, 2018), results in complex changes including the mixture of fresher, C-rich substrates with freeze-locked OM in Pleistocene-age deposits and the interplay with newly grown vegetation. Thereby the degradation of ancient OC is promoted leading to the release of CO₂ consisting of up to 70% ancient OC. Priming effects, which may significantly accelerate the break-down of millennial old OM, are not reflected by CO₂ flux measurements or compositional analyses alone. Thus, total OC content as well as C/N ratio, the well-established proxies for OM degradability, do not give unambiguous information because they do not reflect processes occurring during thawing of such deposits. Under natural conditions, i.e. in the field, we could confirm the results from previous incubation studies, which showed similar or even higher mineralization rates of old (Pleistocene) Yedoma compared to young (Holocene) permafrost deposits under laboratory conditions (Knoblauch *et al.*, 2013; Weiss *et al.*, 2016). Our results underline the need for further field studies in the Yedoma region considering the heterogeneity of these deposits and the complexity of effects during thaw. They support previous studies calling for the integration of deep permafrost deposits, including their abrupt thaw processes, in model projections of GHG emissions (Schuur *et al.*, 2008; Grosse *et al.*, 2011; Kuhry *et al.*, 2013).

Acknowledgements

This work was financially supported by the German Ministry of Science and Education (BMBF) within the joint Russian-German projects 'CarboPerm' and 'KoPf'. The authors particularly thank Waldemar Schneider and Günter Stoof (Alfred Wegener Institute for Polar and Marine Research, Potsdam, Germany) for their logistic support and Svetlana Evgrafova, Oleg Novikov, Inna Alekseenko, Vyacheslav Polyakov, Natalya Alekseeva and Justine Ramage for their help in the field during the Russian-German expedition 'LENA 2016'. Thanks also to Stefan Heinze, Alfred Dewald, Svetlana John, Dorothea Klinghardt, Ulrike Patt, Lukas Wacker and especially Reaz Hossain for their help with sample preparation and AMS ¹⁴C analysis. Finally, we want to acknowledge Harald Strauss und Artur Fugmann for ¹³CO₂ analyses.

References

- Ågren GI, Bosatta E, Balesdent J (1996) Isotope discrimination during decomposition of organic matter: A theoretical analysis. *Soil Science Society of America Journal*, **60**, 1121-1126.
- Andersson RA, Meyers PA (2012) Effect of climate change on delivery and degradation of lipid biomarkers in a Holocene peat sequence in the Eastern European Russian Arctic. *Organic Geochemistry*, **53**, 63-72.
- Biasi C, Jokinen S, Marushchak M, Hämäläinen K, Trubnikova T, Oinonen M, Martikainen P (2014) Microbial respiration in arctic upland and peat soils as a source of atmospheric carbon dioxide. *Ecosystems*, **17**, 112-126.
- Bingeman CW, Varner JE, Martin WP (1953) The effect of the addition of organic materials on the decomposition of an organic soil. *Soil Science Society of America Journal*, **17**, 34-38.
- Boike J, Kattenstroth B, Abramova K *et al.* (2013) Baseline characteristics of climate, permafrost and land cover from a new permafrost observatory in the Lena River Delta, Siberia (1998-2011). *Biogeosciences*, **10**, 2105-2128.
- Bond-Lamberty B, Thomson A (2010) Temperature-associated increases in the global soil respiration record. *Nature*, **464**, 579-582.
- Bull ID, Nott CJ, Van Bergen PF, Poulton PR, Evershed RP (2000) Organic geochemical studies of soils from the Rothamsted classical experiments — VI. The occurrence and source of organic acids in an experimental grassland soil. *Soil Biology and Biochemistry*, **32**, 1367-1376.
- Chen L, Liang J, Qin S *et al.* (2016) Determinants of carbon release from the active layer and permafrost deposits on the Tibetan Plateau. *Nature Communications*, **7**, 13046.
- Ciais P, Sabine C, Bala G *et al.* (2013) Carbon and other biogeochemical cycles. In: *Climate change 2013: The physical science basis. Contribution of Working Group I to the Fifth Assessment Report of the Intergovernmental Panel on Climate Change*. (eds Stocker TF, Qin D, Plattner G-K, Tignor M, Allen SK, Boschung J, Nauels A, Xia Y, Bex V, Midgley PM) pp Page. Cambridge, UK and New York, USA, Cambridge University Press, 465-570.
- Davidson EA, Janssens IA (2006) Temperature sensitivity of soil carbon decomposition and feedbacks to climate change. *Nature*, **440**, 165-173.
- Dewald A, Heinze S, Jolie J *et al.* (2013) CologneAMS, a dedicated center for accelerator mass spectrometry in Germany. *Nuclear Instruments and Methods in Physics Research Section B: Beam Interactions with Materials and Atoms*, **294**, 18-23.
- Dutta K, Schuur EAG, Neff JC, Zimov SA (2006) Potential carbon release from permafrost soils of Northeastern Siberia. *Global Change Biology*, **12**, 2336-2351.
- Eglinton G, Hamilton RJ (1967) Leaf Epicuticular Waxes. *Science*, **156**, 1322-1335.
- Elberling B, Michelsen A, Schadel C *et al.* (2013) Long-term CO₂ production following permafrost thaw. *Nature Climate Change*, **3**, 890-894.
- Ficken KJ, Li B, Swain DL, Eglinton G (2000) An n-alkane proxy for the sedimentary input of submerged/floating freshwater aquatic macrophytes. *Organic Geochemistry*, **31**, 745-749.
- Fontaine S, Mariotti A, Abbadie L (2003) The priming effect of organic matter: a question of microbial competition? *Soil Biology and Biochemistry*, **35**, 837-843.
- Garnett MH, Murray C (2013) Processing of CO₂ samples collected using zeolite molecular sieve for ¹⁴C analysis at the NERC Radiocarbon Facility (East Kilbride, UK). *Radiocarbon*, **55**, 410-415.
- Gentsch N, Mikutta R, Alves RJE *et al.* (2015) Storage and transformation of organic matter fractions in cryoturbated permafrost soils across the Siberian Arctic. *Biogeosciences*, **12**, 4525-4542.
- Girkin NT, Turner BL, Ostle N, Craigon J, Sjögersten S (2018) Root exudate analogues accelerate CO₂ and CH₄ production in tropical peat. *Soil Biology and Biochemistry*, **117**, 48-55.
- Gough L, Hobbie SE (2003) Responses of moist non-acidic arctic tundra to altered environment: productivity, biomass, and species richness. *Oikos*, **103**, 204-216.
- Grosse G, Harden J, Turetsky M *et al.* (2011) Vulnerability of high-latitude soil organic carbon in North America to disturbance. *Journal of Geophysical Research: Biogeosciences*, **116**.
- Günther F, Overduin PP, Sandakov AV, Grosse G, Grigoriev MN (2013) Short- and long-term thermo-erosion of ice-rich permafrost coasts in the Laptev Sea region. *Biogeosciences*, **10**, 4297-4318.
- Hanke UM, Wacker L, Haghipour N, Schmidt MWI, Eglinton TI, McIntyre CP (2017) Comprehensive radiocarbon analysis of benzene polycarboxylic acids (BPCAs) derived from pyrogenic carbon in environmental samples. *Radiocarbon*, **59**, 1103-1116.

- Hardie SML, Garnett MH, Fallick AE, Rowland AP, Ostle NJ (2005) Carbon dioxide capture using a zeolite molecular sieve sampling system for isotopic studies (^{13}C and ^{14}C) of respiration. *Radiocarbon*, **47**, 441-451.
- Hicks Pries CE, Schuur EAG, Natali SM, Crummer KG (2016) Old soil carbon losses increase with ecosystem respiration in experimentally thawed tundra. *Nature Climate Change*, **6**, 214-218.
- Hobbie SE, Miley TA, Weiss MS (2002) Carbon and Nitrogen Cycling in Soils from Acidic and Nonacidic Tundra with Different Glacial Histories in Northern Alaska. *Ecosystems*, **5**, 0761-0774.
- Hugelius G, Strauss J, Zubrzycki S *et al.* (2014) Estimated stocks of circumpolar permafrost carbon with quantified uncertainty ranges and identified data gaps. *Biogeosciences*, **11**, 6573-6593.
- IPCC (2013) *Climate Change 2013: The Physical Science Basis. Contribution of Working Group I to the Fifth Assessment Report of the Intergovernmental Panel on Climate Change.* (eds Stocker TF, Qin D, Plattner G-K, Tignor M, Allen SK, Boschung J, Nauels A, Xia Y, Bex V, Midgley PM), Cambridge, United Kingdom and New York, USA, Cambridge University Press, 1308 pp.
- Jenkins M, Adams MA (2010) Vegetation type determines heterotrophic respiration in subalpine Australian ecosystems. *Global Change Biology*, **16**, 209-219.
- Jones DL (1998) Organic acids in the rhizosphere – a critical review. *Plant and Soil*, **205**, 25-44.
- Jorgenson MT, Shur YL, Pullman ER (2006) Abrupt increase in permafrost degradation in Arctic Alaska. *Geophysical Research Letters*, **33**, 4.
- Kanevskiy M, Shur Y, Fortier D, Jorgenson MT, Stephani E (2011) Cryostratigraphy of late Pleistocene syngenetic permafrost (yedoma) in northern Alaska, Itkillik River exposure. *Quaternary Research*, **75**, 584-596.
- Karhu K, Fritze H, Hämäläinen K *et al.* (2010) Temperature sensitivity of soil carbon fractions in boreal forest soil. *Ecology*, **91**, 370-376.
- Knoblauch C, Beer C, Sosnin A, Wagner D, Pfeiffer E-M (2013) Predicting long-term carbon mineralization and trace gas production from thawing permafrost of Northeast Siberia. *Global Change Biology*, **19**, 1160-1172.
- Knoblauch C, Beer C, Liebner S, Grigoriev MN, Pfeiffer E-M (2018) Methane production as key to the greenhouse gas budget of thawing permafrost. *Nature Climate Change*, **8**, 309-312.
- Kögel-Knabner I (2002) The macromolecular organic composition of plant and microbial residues as inputs to soil organic matter. *Soil Biology and Biochemistry*, **34**, 139-162.
- Kokelj SV, Lacelle D, Lantz TC, Tunnicliffe J, Malone L, Clark ID, Chin KS (2013) Thawing of massive ground ice in mega slumps drives increases in stream sediment and solute flux across a range of watershed scales. *Journal of Geophysical Research-Earth Surface*, **118**, 681-692.
- Kuhry P, Vitt DH (1996) Fossil carbon/nitrogen ratios as a measure of peat decomposition. *Ecology*, **77**, 271-275.
- Kuhry P, Ping C-L, Schuur EAG, Tarnocai C, Zimov S (2009) Report from the International Permafrost Association: carbon pools in permafrost regions. *Permafrost and Periglacial Processes*, **20**, 229-234.
- Kuhry P, Grosse G, Harden JW *et al.* (2013) Characterisation of the Permafrost Carbon Pool. *Permafrost and Periglacial Processes*, **24**, 146-155.
- Kuzyakov Y, Bol R (2006) Sources and mechanisms of priming effect induced in two grassland soils amended with slurry and sugar. *Soil Biology and Biochemistry*, **38**, 747-758.
- Kuzyakov Y, Friedel JK, Stahr K (2000) Review of mechanisms and quantification of priming effects. *Soil Biology and Biochemistry*, **32**, 1485-1498.
- Lantuit H, Overduin PP, Couture N *et al.* (2012) The Arctic Coastal Dynamics Database: A New Classification Scheme and Statistics on Arctic Permafrost Coastlines. *Estuaries and Coasts*, **35**, 383-400.
- Lee H, Schuur EAG, Inglett KS, Lavoie M, Chanton JP (2012) The rate of permafrost carbon release under aerobic and anaerobic conditions and its potential effects on climate. *Global Change Biology*, **18**, 515-527.
- Marzi R, Torkelson BE, Olson RK (1993) A revised carbon preference index. *Organic Geochemistry*, **20**, 1303-1306.
- Melillo JM, Aber JD, Linkins AE, Ricca A, Fry B, Nadelhoffer KJ (1989) Carbon and nitrogen dynamics along the decay continuum: Plant litter to soil organic matter. *Plant and Soil*, **115**, 189-198.
- Nadelhoffer KJ, Fry B (1988) Controls on natural ^{15}N and ^{13}C abundances in forest soil organic matter. *Soil Science Society of America Journal*, **52**, 1633-1640.

- Poynter J (1989) Molecular stratigraphy: The recognition of palaeoclimatic signals in organic geochemical data. PhD, School of Chemistry, University of Bristol, Bristol, 324.
- Raynolds MK, Walker DA, Ambrosius KJ *et al.* (2014) Cumulative geocological effects of 62 years of infrastructure and climate change in ice-rich permafrost landscapes, Prudhoe Bay Oilfield, Alaska. *Global Change Biology*, **20**, 1211-1224.
- Reimer PJ, Brown TA, Reimer RW (2004) Discussion: Reporting and Calibration of Post-Bomb ^{14}C Data. *Radiocarbon*, **46**, 1299-1304.
- Rethemeyer J, Fülöp RH, Höfle S *et al.* (2013) Status report on sample preparation facilities for ^{14}C analysis at the new CologneAMS center. *Nuclear Instruments and Methods in Physics Research Section B: Beam Interactions with Materials and Atoms*, **294**, 168-172.
- Ruff M, Wacker L, Gäggeler HW, Suter M, Synal H-A, Szidat S (2007) A gas ion source for radiocarbon measurements at 200 kV. *Radiocarbon*, **49**, 307-314.
- Sannel ABK, Kuhry P (2011) Warming-induced destabilization of peat plateau/thermokarst lake complexes. *Journal of Geophysical Research-Biogeosciences*, **116**, 16.
- Schädel C, Schuur EAG, Bracho R *et al.* (2014) Circumpolar assessment of permafrost C quality and its vulnerability over time using long-term incubation data. *Global Change Biology*, **20**, 641-652.
- Schaefer K, Lantuit H, Romanovsky VE, Schuur EAG, Witt R (2014) The impact of the permafrost carbon feedback on global climate. *Environmental Research Letters*, **9**, 085003.
- Schirrneister L, Siegert C, Kuznetsova T *et al.* (2002) Paleoenvironmental and paleoclimatic records from permafrost deposits in the Arctic region of Northern Siberia. *Quaternary International*, **89**, 97-118.
- Schirrneister L, Grosse G, Schnelle M *et al.* (2011a) Late Quaternary paleoenvironmental records from the western Lena Delta, Arctic Siberia. *Palaeogeography, Palaeoclimatology, Palaeoecology*, **299**, 175-196.
- Schirrneister L, Kunitsky V, Grosse G *et al.* (2011b) Sedimentary characteristics and origin of the Late Pleistocene Ice Complex on north-east Siberian Arctic coastal lowlands and islands – A review. *Quaternary International*, **241**, 3-25.
- Schirrneister L, Grosse G, Wetterich S, Overduin PP, Strauss J, Schuur EAG, Hubberten H-W (2011c) Fossil organic matter characteristics in permafrost deposits of the northeast Siberian Arctic. *Journal of Geophysical Research: Biogeosciences*, **116**, G00M02.
- Schirrneister L, Froese D, Tumskey V, Grosse G, Wetterich S (2013) Yedoma: Late Pleistocene ice-rich syngenetic permafrost of Beringia. In: *Encyclopedia of Quaternary Science. 2nd edition.* (eds Elias S, Mock C, Murton J) Amsterdam, Elsevier, 3, 542-552.
- Schuur EAG, Bockheim J, Canadell JG *et al.* (2008) Vulnerability of permafrost carbon to climate change: Implications for the global carbon cycle. *BioScience*, **58**, 701-714.
- Schuur EAG, Vogel JG, Crummer KG, Lee H, Sickman JO, Osterkamp TE (2009) The effect of permafrost thaw on old carbon release and net carbon exchange from tundra. *Nature*, **459**, 556-559.
- Schuur EAG, McGuire AD, Schadel C *et al.* (2015) Climate change and the permafrost carbon feedback. *Nature*, **520**, 171-179.
- Schwamborn G, Rachold V, Grigoriev MN (2002) Late Quaternary sedimentation history of the Lena Delta. *Quaternary International*, **89**, 119-134.
- Sistla SA, Asao S, Schimel JP (2012) Detecting microbial N-limitation in tussock tundra soil: Implications for Arctic soil organic carbon cycling. *Soil Biology and Biochemistry*, **55**, 78-84.
- Stettner S, Beamish LA, Bartsch A, Heim B, Grosse G, Roth A, Lantuit H (2018) Monitoring Inter- and Intra-Seasonal Dynamics of Rapidly Degrading Ice-Rich Permafrost Riverbanks in the Lena Delta with TerraSAR-X Time Series. *Remote Sensing*, **10**.
- Strauss J, Schirrneister L, Grosse G, Wetterich S, Ulrich M, Herzschuh U, Hubberten H-W (2013) The deep permafrost carbon pool of the Yedoma region in Siberia and Alaska. *Geophysical Research Letters*, **40**, 6165-6170.
- Strauss J, Schirrneister L, Mangelsdorf K, Eichhorn L, Wetterich S, Herzschuh U (2015) Organic-matter quality of deep permafrost carbon – a study from Arctic Siberia. *Biogeosciences*, **12**, 2227-2245.
- Strauss J, Schirrneister L, Grosse G *et al.* (2017) Deep Yedoma permafrost: A synthesis of depositional characteristics and carbon vulnerability. *Earth-Science Reviews*, **172**, 75-86.
- Stuiver M, Polach HA (1977) Reporting of ^{14}C data - discussion. *Radiocarbon*, **19**, 355-363.
- Synal HA, Stocker M, Suter M (2007) MICADAS: A new compact radiocarbon AMS system. *Nuclear Instruments and Methods in Physics Research Section B: Beam Interactions with Materials and Atoms*, **259**, 7-13.

- Treat CC, Wollheim WM, Varner RK, Grandy AS, Talbot J, Frolking S (2014) Temperature and peat type control CO₂ and CH₄ production in Alaskan permafrost peats. *Global Change Biology*, **20**, 2674-2686.
- Treat CC, Natali SM, Ernakovich J *et al.* (2015) A pan-Arctic synthesis of CH₄ and CO₂ production from anoxic soil incubations. *Global Change Biology*, **21**, 2787-2803.
- Trumbore SE (2000) Age of soil organic matter and soil respiration: Radiocarbon constraints on belowground C dynamics. *Ecological Applications*, **10**, 399-411.
- Voigt C, Lamprecht RE, Marushchak ME *et al.* (2016) Warming of subarctic tundra increases emissions of all three important greenhouse gases – carbon dioxide, methane, and nitrous oxide. *Global Change Biology*, **23**, 3121-3138.
- Vonk JE, Sanchez-Garcia L, Van Dongen BE *et al.* (2012) Activation of old carbon by erosion of coastal and subsea permafrost in Arctic Siberia. *Nature*, **489**, 137-140.
- Wacker L, Nemeč M, Bourquin J (2010) A revolutionary graphitisation system: Fully automated, compact and simple. *Nuclear Instruments and Methods in Physics Research Section B: Beam Interactions with Materials and Atoms*, **268**, 931-934.
- Walter Anthony KM, Zimov SA, Grosse G *et al.* (2014) A shift of thermokarst lakes from carbon sources to sinks during the Holocene epoch. *Nature*, **511**, 452-456.
- Walz J, Knoblauch C, Böhme L, Pfeiffer E-M (2017) Regulation of soil organic matter decomposition in permafrost-affected Siberian tundra soils - Impact of oxygen availability, freezing and thawing, temperature, and labile organic matter. *Soil Biology and Biochemistry*, **110**, 34-43.
- Weiss N, Blok D, Elberling B, Hugelius G, Jørgensen CJ, Siewert MB, Kuhry P (2016) Thermokarst dynamics and soil organic matter characteristics controlling initial carbon release from permafrost soils in the Siberian Yedoma region. *Sedimentary Geology*, **340**, 38-48.
- Wetterich S, Kuzmina S, Andreev AA *et al.* (2008) Palaeoenvironmental dynamics inferred from late Quaternary permafrost deposits on Kurungnakh Island, Lena Delta, Northeast Siberia, Russia. *Quaternary Science Reviews*, **27**, 1523-1540.
- Wild B, Schnecker J, Alves RJE *et al.* (2014) Input of easily available organic C and N stimulates microbial decomposition of soil organic matter in arctic permafrost soil. *Soil Biology and Biochemistry*, **75**, 143-151.
- Wild B, Gentsch N, Čapek P *et al.* (2016) Plant-derived compounds stimulate the decomposition of organic matter in arctic permafrost soils. *Scientific Reports*, **6**, srep25607.
- Wotte A, Wordell-Dietrich P, Wacker L, Don A, Rethemeyer J (2017a) ¹⁴CO₂ processing using an improved and robust molecular sieve cartridge. *Nuclear Instruments and Methods in Physics Research Section B: Beam Interactions with Materials and Atoms*, **400**, 65-73.
- Wotte A, Wischhöfer P, Wacker L, Rethemeyer J (2017b) ¹⁴CO₂ analysis of soil gas: Evaluation of sample size limits and sampling devices. *Nuclear Instruments and Methods in Physics Research Section B: Beam Interactions with Materials and Atoms*, **413**, 51-56.
- Zhou W, Zheng Y, Meyers PA, Jull AJT, Xie S (2010) Postglacial climate-change record in biomarker lipid compositions of the Hani peat sequence, Northeastern China. *Earth and Planetary Science Letters*, **294**, 37-46.
- Zimov SA, Davydov SP, Zimova GM, Davydova AI, Schuur EAG, Dutta K, Chapin FS (2006) Permafrost carbon: Stock and decomposability of a globally significant carbon pool. *Geophysical Research Letters*, **33**, L20502.

S1: Bulk geochemical and isotopic analyses of the Yedoma deposit and the Holocene active layer (polygon rim and center) and mean ^{14}C values for the entire thaw layer normalized to TOC.

Site	AMS ID	Depth (cm)	TOC (%) (n=3)	TIC (%)	TN (%) (n=3)	C/N	$\delta^{13}\text{C}$ (‰ VPDB) (n=2)	F ^{14}C ($\pm 1\sigma$)	^{14}C age (yrs BP) ($\pm 1\sigma$)
<i>Yedoma outcrop</i>									
K4	COL4616.1.1	0-3	4.6 \pm 0.2	0.31 \pm 0.28	0.30 \pm 0.02	15.4 \pm 1.5	-28.0 \pm 0.3	0.633 \pm 0.003	3680 \pm 40
	COL4617.1.1	6-11	4.3 \pm 0.3	b.d. ^a	0.28 \pm 0.04	15.3 \pm 3.5	-28.7 \pm 0.1	0.614 \pm 0.003	3920 \pm 40
	COL4618.1.1	14-18	6.8 \pm 0.1	b.d. ^a	0.42 \pm 0.01	16.2 \pm 0.7	-28.9 \pm 1.1	0.962 \pm 0.004	310 \pm 35
	COL4619.1.1	24-28	4.0 \pm 0.3	0.14 \pm 0.62	0.25 \pm 0.04	15.8 \pm 3.6	-27.8 \pm 0.2	0.577 \pm 0.003	4410 \pm 40
	COL4620.1.1	30-34	10.7 \pm 0.1	0.22 \pm 0.38	0.47 \pm 0.01	22.6 \pm 0.8	-26.8 \pm 0.2	1.000 \pm 0.004	>modern
						mean ^b	0.76	2200	
						F $^{14}\text{C}_{\text{OM}}$ ^c	0.61	3970	
K7	COL4621.1.1	0-3	2.1 \pm 0.1	0.30 \pm 0.13	0.18 \pm 0.01	11.6 \pm 0.8	-26.3 \pm 0.1	0.247 \pm 0.002	11250 \pm 60
	COL4622.1.1	4-7	2.4 \pm 0.2	0.05 \pm 0.35	0.18 \pm 0.00	13.3 \pm 1.6	-26.5 \pm 0.4	0.119 \pm 0.001	17150 \pm 90
	COL4623.1.1	10-15	2.2 \pm 0.2	0.21 \pm 0.32	0.17 \pm 0.01	12.6 \pm 1.7	-26.3 \pm 0.3	0.186 \pm 0.002	13500 \pm 70
							mean = F $^{14}\text{C}_{\text{OM}}$ ^b	0.18	13800
KX	COL4624.1.1	0-3	2.3 \pm 0.1	0.17 \pm 0.18	0.20 \pm 0.01	11.3 \pm 1.0	-25.5 \pm 0.4	0.093 \pm 0.001	19050 \pm 110
	COL4625.1.1	4-8	2.0 \pm 0.1	0.16 \pm 0.17	0.18 \pm 0.01	10.9 \pm 1.1	-25.7 \pm 0.5	0.052 \pm 0.001	23800 \pm 170
	COL4626.1.1	10-13	2.0 \pm 0.1	b.d. ^a	0.18 \pm 0.01	11.5 \pm 1.0	-25.7 \pm 0.1	0.028 \pm 0.001	28700 \pm 290
	COL4627.1.1	20-26	1.9 \pm 0.1	0.05 \pm 0.08	0.16 \pm 0.01	11.6 \pm 1.3	-25.5 \pm 0.0	0.029 \pm 0.001	28500 \pm 280
	COL4628.1.1	30-36	1.7 \pm 0.1	0.36 \pm 0.18	0.17 \pm 0.00	10.2 \pm 0.7	-25.7 \pm 0.3	0.028 \pm 0.001	28700 \pm 290
	COL4629.1.1	40-45	1.6 \pm 0.1	0.36 \pm 0.23	0.16 \pm 0.01	9.9 \pm 0.8	-25.7 \pm 0.3	0.021 \pm 0.001	31000 \pm 380
							mean ^b	0.038	26300
						F $^{14}\text{C}_{\text{OM}}$ ^c	0.027	29000	
<i>Active layer</i>									
Centre	organic mat								
	COL1144.1.1	(+6 cm)	17.3		0.61	28.6		1.070 \pm 0.004	>modern
	COL1145.1.1	0-16	8.7		0.41	21.0		0.983 \pm 0.055	140 \pm 45
	COL1146.1.1	16-27	7.9		0.61	13.1		0.952 \pm 0.054	397 \pm 45
COL1147.1.1	27-42	3.4		0.12	28.0		0.605 \pm 0.035	4031 \pm 45	
							mean ^d	0.95	410
Rim	organic mat								
	COL1148.1.1	(+8 cm)	11.5		0.28	41.8		1.155 \pm 0.065	>modern
	COL1149.1.1	0-4	6.3		0.44	14.4		0.935 \pm 0.053	537 \pm 45
	COL1150.1.1	4-6	8.3		0.51	16.3		0.930 \pm 0.052	583 \pm 45
	COL1151.1.1	6-19	3.9		0.22	17.5		0.713 \pm 0.040	2720 \pm 45
							mean ^d	0.98	160

^a b.d. – below detection limit, ^b weighted mean for thawed surface sediment of each site, ^c weighted mean of the thawed sediment without the peat lenses at K4, and without the younger sediments in 0-8 cm at KX, ^d weighted mean of the OM in the active layer, normalized to TOC contents of each depth interval

S2: Lipid biomarker analyses of the Yedoma deposit and the Holocene active layer (polygon rim and center). Abbreviations of lipid biomarkers include CPI – carbon preference index, ACL – average change length, and FA – fatty acids.

Site	AMS ID	Depth (cm)	Sum Alkanes (µg/g TOC) C21-33	C23 (%)	C25 (%)	C27 (%)	C29 (%)	C31 (%)	C33 (%)	CPI	ACL	Sum FA (µg/g TOC) C20-32									
												C20 (%)	C22 (%)	C24 (%)	C26 (%)	C28 (%)	C30 (%)				
<i>Yedoma outcrop</i>																					
K4	COL4616.1.1	0-3	198	6.9	10.6	26.7	16.7	16.3	3.5	6.2	28.3	6525	14.8	25.6	22.8	11.8	7.9	1.8			
	COL4617.1.1	6-11	80	5.3	9.8	26.9	18.3	18.5	4.0	6.4	28.5	6362	14.7	25.4	23.5	11.7	7.8	1.7			
	COL4618.1.1	14-18	54	9.4	14.2	28.3	14.5	12.7	3.4	7.8	28.0	4186	10.8	21.6	26.0	14.1	10.9	2.0			
	COL4619.1.1	24-28	34	10.1	12.1	23.8	14.3	13.2	2.6	5.5	28.1	6560	14.0	24.2	22.6	12.1	8.9	1.9			
	COL4620.1.1	30-34	50	7.2	12.2	27.2	15.8	17.6	4.9	7.2	28.4	1537	19.2	22.6	22.1	10.2	7.4	1.3			
K7	COL4621.1.1	0-3	118	7.3	7.7	15.5	20.1	24.4	8.4	5.4	29.3	2626	11.7	21.2	23.0	14.2	8.9	2.9			
	COL4622.1.1	4-7	68	6.5	6.9	15.5	19.5	25.2	8.9	4.9	29.4	2523	8.2	18.0	22.7	16.7	12.1	3.9			
	COL4623.1.1	10-15	69	6.4	7.4	16.7	20.2	24.6	8.3	5.3	29.3	3316	11.3	22.6	23.4	13.9	8.8	2.4			
	COL4624.1.1	0-3	15	13.8	12.7	23.3	14.3	12.0	3.9	6.1	28.1	1439	7.5	16.3	22.9	19.7	10.3	3.9			
KX	COL4625.1.1	4-8	22	9.2	11.6	18.9	19.3	18.2	5.0	4.6	28.6	182	10.1	15.7	22.2	18.5	12.1	5.1			
	COL4626.1.1	10-13										153	10.7	21.7	22.4	12.7	8.2	2.7			
	COL4627.1.1	20-26	66	9.3	8.3	12.7	18.6	23.1	7.0	4.0	29.2	1304	9.3	18.3	26.2	15.4	8.2	3.2			
	COL4628.1.1	30-36	53	10.7	9.6	14.2	17.7	21.4	6.9	4.6	29.0	1314	8.7	16.1	27.2	17.2	9.5	3.6			
	COL4629.1.1	40-45	37	11.4	9.5	13.9	15.7	17.7	6.1	3.8	28.9	2151	9.8	18.1	22.2	18.0	9.8	3.6			
<i>Active layer</i>																					
Centre	organic mat																				
	COL1144.1.1	(+6 cm)	495	12.1	6.2	28.6	11.9	14.4	8.6	8.3	25.2	2825	18.9	23.2	21.5	10.6	11.9	2.5			
	COL1145.1.1	0-16	421	12.7	12.2	24.3	13.6	11.8	5.8	6.7	24.3	6394	9.1	16.3	29.2	16.2	14.9	3.0			
	COL1146.1.1	16-27	548	10.5	16.0	23.2	14.0	12.2	3.9	5.6	24.7	13572	10.4	17.6	32.9	16.0	10.9	1.5			
COL1147.1.1	27-42	1239	5.3	8.6	26.1	18.4	18.5	4.0	5.2	24.7	31974	13.3	22.6	25.5	14.2	9.8	1.7				
Rim	organic mat																				
	COL1148.1.1	(+8 cm)	102	10.2	16.0	23.8	16.3	9.5	3.0	4.8	25.1	2096	16.5	24.8	24.0	13.9	7.2	2.6			
	COL1149.1.1	0-4	109	9.8	12.1	21.4	14.6	18.4	6.2	5.9	24.0	2576	5.1	14.7	27.7	18.6	13.0	3.8			
	COL1150.1.1	4-6	394	10.4	12.3	25.3	14.6	13.3	4.5	5.9	24.2	6321	6.7	15.7	30.2	16.6	14.9	2.1			
COL1151.1.1	6-19	1250	5.8	9.5	27.5	17.0	18.4	3.8	5.5	24.9	23180	11.2	21.0	27.1	15.0	10.8	1.7				

S3: CO₂ fluxes and carbon isotopic composition of the respired CO₂.

Site	AMS ID	$\delta^{13}\text{C}$ (‰ VPDB) (n=3)	F ¹⁴ C* (± 1σ)	¹⁴ C age* (yrs BP) (± 1σ)	CO ₂ flux (μg CO ₂ m ⁻² s ⁻¹) (± 1σ)	n=	CO ₂ flux (g CO ₂ m ⁻² 120d ⁻¹) (± 1σ)
K4	COL4427.1.0.1b	-20.1 ± 0.3	0.722 ± 0.008	2620 ± 90	49 ± 21	6	139 ± 60
	COL4306.1.0.1a	-19.9 ± 0.1	0.725 ± 0.009	2590 ± 100			
K7	COL4428.1.0.1b	-20.5 ± 0.1	0.566 ± 0.007	4570 ± 100	127 ± 37	3	358 ± 103
	COL4429.1.0.1a	-13.6 ± 0.2	0.484 ± 0.029	5830 ± 480			
KX	COL4307.1.0.1a	-21.1 ± 0.1	0.446 ± 0.013	6490 ± 240	57 ± 5	5	160 ± 13
	COL4308.1.0.1a	-19.2 ± 0.1	0.557 ± 0.011	4700 ± 160			

*corrected for MSC contamination

Discussion

Popular terms like “Pandora's freezer” (Brown, 2013), “sleeping giant” (Mascarelli, 2009), or “permafrost carbon bomb” (Treat & Frolking, 2013) have been used in order to draw the public attention to the potential of the enormous amounts of OC stored in permafrost. Such terms illustrate the risk of these deposits to influence the future magnitude of climate change upon global warming and thawing of permafrost. The purpose of this dissertation is to achieve verified insights on the decomposability of the large amounts of OM stored in Yedoma permafrost deposits. To answer this question, we developed a new method, which makes it possible to study the ^{14}C signature of respired CO_2 in remote areas. This nondestructive method can help to differentiate C sources of different age because the ^{14}C signature of the respired CO_2 reflects the ^{14}C signature of its C source (Trumbore, 2000, Trumbore, 2006). The ^{14}C analysis of CO_2 respired from thawing Yedoma will make it possible to identify if the ancient OC that was frozen for millennia is decomposed and released to the atmosphere. Large volumes of soil gas are needed to obtain sufficient CO_2 for ^{14}C analysis. To collect and concentrate the CO_2 out of these large gas volumes, a new stainless steel MSC was developed and thoroughly tested. This synthesis summarizes and discusses the major outcomes of the method development and improvement in a first step (Paper I and II) and the results of the application concerning the decomposability of Yedoma OM including the consequences for the permafrost C feedback in a next step (Paper III).

Method development and improvement

A new MSC was constructed to collect CO_2 samples for AMS ^{14}C analysis (Paper I). This new device is robust and particularly applicable for field campaigns because it is entirely made of stainless steel. Thus, the new shatter-proof construction improved a previous fragile MSC design from Hardie *et al.* (2005) composed of a glass cartridge and plastic couplings.

Prior application of a new device in the field, it is necessary to thoroughly test the device and the associated methods to obtain reliable results (Hardie *et al.*, 2005, Palonen & Oinonen, 2013). For this reason, we tested different amounts of zeolite, various sampling procedures including the cleaning of the zeolite, the CO_2 adsorption to, and the desorption from the MSC, the direct connection to the AGE system, as well as the potential for cross-contamination and isotopic fractionation effects (Paper I). Additionally, we assessed the lower sample size limits of our new MSC and determined a process blank of the field equipment for collecting gases released from soils or sediments (Paper II).

In the presented papers I and II, the values of the ^{14}C -free standards are given without a blank correction. However, for the following discussion all data are blank corrected, i.e. corrected for the contamination obtained during the AMS measurement itself. This correction makes it possible to compare the data obtained during the development (Paper I) and improvement (Paper II) of the MSC processing, because the samples were analyzed with different devices. On the one hand

samples were directly analyzed as CO₂ with the gas ion source of the MICADAS and others were measured as graphite targets with the 6 MV Tandem AMS. For this reason, the values of the ¹⁴C-free standards compiled in the following discussion are slightly lower in comparison to the data presented in Paper I and II.

Amount of zeolite

Most previous studies used relatively large amounts of more than 1 g of zeolite type 13X for adsorbing sufficient CO₂ for AMS ¹⁴C analysis (Bauer *et al.*, 1992, Bol & Harkness, 1995, Hardie *et al.*, 2005, Palonen & Oinonen, 2013). A critical point with such large amounts of zeolite is, that an enhanced trapping of CO₂ also increases the risk to collect unwanted molecules such as water, which can complicate the desorption process. Hence, the AGE (Ionplus AG, Switzerland) is equipped with a trap containing only a small amount of 200 mg zeolite, which is sufficient to collect at least 1000 µg C (Wacker *et al.*, 2010). To assess if different zeolite amounts influence the trapping of unwanted water molecules or the amount of other exogenous contamination, we tested MSCs filled with 300, 1000, and 3000 mg zeolite. Surprisingly, the zeolite amount did not significantly influence the ¹⁴C blank value (see Fig. 4 of Paper I). We concluded that the ¹⁴C blank was rather attributed the effectiveness of the cleaning procedure than to the amount of zeolite used. However, dependent on the application, cleaning times need to be reduced to be more effective and therefore also a reduced zeolite amount is recommended. A previous study found at that a smaller amount of zeolite seems to minimize contamination issues (Walker *et al.*, 2015). Thus, the zeolite amount inside the MSC was decreased to 500 mg for our MSCs.

Cleaning of the zeolite

Insufficient cleaning of the zeolite can lead to cross-contamination derived from samples previously trapped on the MSC (Palonen & Oinonen, 2013, Walker *et al.*, 2015). Considerable differences were revealed by comparing various cleaning protocols including different durations of heating the MSC. We compared the cleaning of the MSC under vacuum (passive cleaning) with the method where it is flushed with an inert purge gas (e.g. He; active cleaning; *Figure 6*). Additionally, the influence of different heating times and temperatures was investigated. The passive cleaning procedure turned out to be strongly dependent on the duration of the heating time of the zeolite, revealing F¹⁴C values ranging from 0.2993 ± 0.0072 F¹⁴C (15 min at 500°C) to 0.0287 ± 0.0019 F¹⁴C (165 min at 500°C) for ¹⁴C-free CO₂ (see Fig. 5 of Paper I). In contrast, the active cleaning procedure using an inert purge gas is more effective, as much lower ¹⁴C concentrations (0.0024 ± 0.0015 – 0.0113 ± 0.0018 F¹⁴C; 60 min at 500°C) were obtained for ¹⁴C-free CO₂. Further tests illustrated, that the active cleaning procedure entirely removes contamination from CO₂ samples previously loaded onto the MSC. For these tests CO₂ standards of different isotopic compositions were consecutively transferred to and removed from the MSC. The ¹⁴C results indicate no cross-contamination derived from the standards previously trapped (Paper I). A reduced heating time of 30 min (500°C, 40 ml min⁻¹) is also appropriate for a thorough cleaning of the zeolite. This efficiency was shown by the coupling of the MSC with the AGE system, which resulted in a very low modern contamination of less than 1.5 µg C (*Figure 7b*; see chapter ‘Coupling of the MSC with the AGE’). Thus, we recommend an active cleaning procedure of the zeolite as a standard protocol (Table 1; Paper I). However, there is potential to even further

reduce the cleaning time of 30 min down to a few minutes. We infer this from the fact that the cleaning procedure applied for the AGE system requires only a heating of 2 minutes at 450°C (Wacker *et al.*, 2010).

Table 1. Parameters for our optimized MSC procedure. The zeolite cleaning as well as the CO₂ desorption is actively performed under a helium gas flow; the duration of heating varies.

Optimized MSC procedure	
<i>Zeolite cleaning:</i>	<i>CO₂ desorption:</i>
<ul style="list-style-type: none"> • He flow ~40 ml min⁻¹ 5 min ↑500 °C 30 min →500 °C 	<ul style="list-style-type: none"> • He flow ~40 ml min⁻¹ • 3 min ↑150 °C 5 min →150 °C 5 min ↑500 °C 2 min →500 °C

CO₂ adsorption and desorption

Laboratory tests demonstrated that CO₂ standards can be most effectively transferred to the MSC by actively flushing the CO₂ with a stream of He (Paper I). For the application in the field further considerations need to be taken into account. Here, the sample can be transferred to the MSC either passively by diffusion or actively by using a pump-based system. The method of choice finally depends on the type of application and sampling purpose (see chapter ‘Evaluation of the field equipment’). Overall, the chosen method needs to ensure that sufficient CO₂ for ¹⁴C analysis is adsorbed on the zeolite.

Back in the laboratory, the desorption of CO₂ and its transfer to the vacuum rig can be performed either passively under vacuum or actively using a purge gas. We demonstrated that the ¹⁴C results did not differ significantly comparing the two desorption procedures. However, the release and transfer of CO₂ is much faster using a purge gas. After actively cleaning the MSC, both methods yielded ¹⁴C concentrations for ¹⁴C-free CO₂ in the range of 0.0024 ± 0.0015 to 0.0113 ± 0.0018 F¹⁴C, which corresponds to a modern contamination of 3 µg C (Figure 7a; Paper I). However, during the early stages of our method development (Paper I) we had no flow-through CO₂ trap on the vacuum rig, but this trap is necessary to completely collect the desorbed CO₂. To simplify and accelerate the MSC desorption procedure, we extended our multipurpose vacuum rig (Paper II), which is conventionally used for cryogenic distillation of CO₂ samples for ¹⁴C analysis. This extension allows to perform all handling steps on a single vacuum rig and to use the active desorption procedure as the extension includes a flow-through CO₂ trap. Furthermore, the active desorption procedure was modified by decreasing the heating time from ~60 min to 15 min (Table 1). The results obtained with the new method also show a low modern contamination of less than 3 µg C with F¹⁴C values for ¹⁴C-free CO₂ in the range of 0.0000 ± 0.0008 to 0.0082 ± 0.0008 F¹⁴C (Figure 7a; Paper II). With the new method, the CO₂ recovery was significantly increased from ~86% (Paper I) to about 95% (Paper II) and is now in the range of previous studies (Hardie *et al.*, 2005, Garnett & Murray, 2013, Palonen & Oinonen, 2013). Our data are comparable to the data for ¹⁴C-free standards obtained with a passive diffusive zeolite trap showing that it is possible to make reproducible measurements on standard gases with a low modern contamination (Figure 7a; Walker *et al.*, 2015). However, we developed the first MSC, which is unbreakable and thus most suitable for field campaigns.

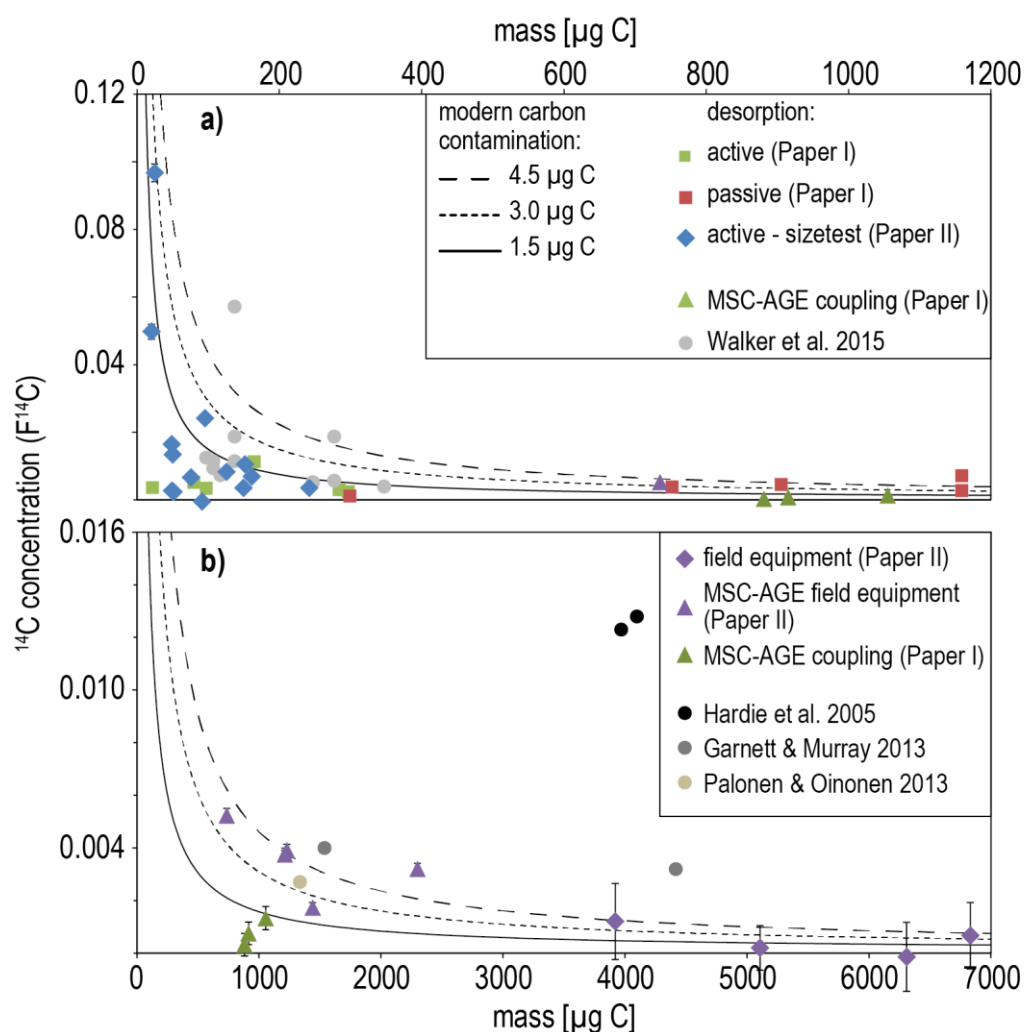


Figure 7. ^{14}C concentration of ^{14}C -free standards of different sizes processed with the molecular sieve cartridge (MSC). a) Different processing methods were compared: active desorption (green squares) and passive (red squares) using the vacuum rig (Paper I), active desorption using the improved vacuum rig (blue diamonds; Paper II), and active desorption to the automatic graphitization equipment (AGE; green triangles; Paper I). The data by Walker *et al.* (2015) are calculated based on their given R-values. b) ^{14}C concentration of ^{14}C -free CO_2 collected with field equipment, i.e. respiration chambers and depth samplers. ^{14}C concentrations were measured with the gas ion source of the MICADAS (purple diamonds) or as graphite targets at CologneAMS (purple triangles; Paper III). For comparison, ^{14}C data of MSCs processed in the laboratory with the MSC-AGE system are given (green triangles). Literature values for a previous MSC design are also given (Hardie *et al.*, 2005, Garnett & Murray, 2013, Palonen & Oinonen, 2013). The curves were calculated with a model of constant contamination and illustrate an exogenous C contamination of a modern C ($F^{14}\text{C} = 1$) source. Where not shown 1- σ uncertainties are within symbol size. Note the different scales of x- and y-axes.

Evaluation of sample size limits of the MSC

Microscale AMS ^{14}C analysis has been already established for sample sizes of less than 10 $\mu\text{g C}$ (Drosg *et al.*, 2007, Santos *et al.*, 2007, Ruff *et al.*, 2010), but $>1000 \mu\text{g C}$ are still typically used for the ^{14}C analysis in MSC studies (Hardie *et al.*, 2005, Garnett & Murray, 2013, Palonen & Oinonen, 2013). So far, only one study exists, which tested the collection of small CO_2 amounts (100–350 $\mu\text{g C}$) on MSCs (Walker *et al.*, 2015). The advantage of sampling smaller CO_2 amounts is a reduction of sampling time and thus minimizing the risk of contamination with exogenous CO_2 , e.g. from the surrounding soil or atmosphere. Additionally, long sampling times can disturb the natural conditions, like CO_2 fluxes and natural CO_2 gradients during the sampling of respired

CO₂ with respiration chambers (Healy *et al.*, 1996, Conen & Smith, 2000). Thus, small mass MSC sampling potentially allows to reduce sampling times and concomitant disturbances.

We processed a size series ranging from 25 to 300 µg C of modern and ¹⁴C-free C standards, which were consecutively loaded onto and desorbed from the zeolite. These laboratory tests showed that reasonable blanks of 0.008 F¹⁴C (~39,000 yrs BP) can be obtained for sample sizes down to 50 µg C (*Figure 7a*). A contamination of less than 2.0 and 3.0 µg C was determined from fossil and modern exogenous C sources, respectively, using the model of constant contamination. Only the ¹⁴C-free CO₂ with C amounts below 100 µg C seems to reflect a slight cross-contamination from the previously trapped sample (Paper II). But it needs to be taken into account that these results were obtained under laboratory conditions. Thus, there might be an additional contribution of exogenous CO₂ during the sampling in the field (see chapter ‘Evaluation of the field equipment’). This contamination might be introduced during the coupling and decoupling of the MSC or from the connected field equipment, such as respiration chambers and depth samplers. The additional contribution of exogenous CO₂ obtained during the field sampling needs to be considered, as well. Assuming a constant contamination, smaller samples will be more affected as the relative contamination increases with decreasing sample size. Thus, if the environmental conditions do not limit the CO₂ amount sampled, we recommend the collection of 1000 µg C. An additional size test involving the field equipment could help to find the lower sample size limit for MSC sampling in the field.

Coupling of the MSC with the AGE

So far, all studies that use a MSC for the collection of CO₂ release the CO₂ trapped on the zeolite first to a vacuum rig and then graphitize it in a second step (Hardie *et al.*, 2005, Garnett & Murray, 2013, Palonen & Oinonen, 2013, Walker *et al.*, 2015). In our study, the released CO₂ was directly transferred to the AGE (Ionplus AG, Switzerland; Wacker *et al.*, 2010) to avoid the additional step of gas purification on a vacuum rig and thus to reduce the risk of sample loss or contamination (Paper I). In the AGE system the CO₂ is automatically transferred to one of the seven reactors, and converted to elemental C (Wacker *et al.*, 2010). This semi-automatic approach and the subsequent AMS ¹⁴C analysis as graphite yields promising low blank values of 0.0008 ± 0.0004 F¹⁴C (Paper I). This corresponds to a very low modern contamination of less than 1.5 µg C (*Figure 7b*). These results were obtained for ¹⁴C-free CO₂ processed in the laboratory. Additionally, a reasonable process blank of 4.5 µg C (*Figure 7b*) was determined for the processing with the MSC-AGE system including the sampling of ¹⁴C-free CO₂ in the field using a respiration chamber (see chapter ‘Evaluation of the field equipment’ for further discussion). Therefore, this semi-automatic approach of coupling the MSC with the AGE is very promising as it can be automated in the future and increase the sample throughput significantly.

Potentials and weaknesses

Despite all the advantages of the direct coupling of the MSC-AGE system, there are two drawbacks: 1) all of the CO₂ released from the MSC is transferred to the AGE so that no splits can be taken for an additional δ¹³C analysis, which can give additional information about the respiration source, and 2) a rather high amount of 1000 µg C is needed for an optimal graphitization with the AGE. The latter turned out to be problematic, as the actually trapped CO₂ amount is often less than the minimal amount of 500 µg C required for a graphitization. Currently,

we are not able to predict the amount of CO₂ collected on the MSC in the field; the collected CO₂ amount varies and is usually less than expected. This discrepancy will need further investigation and might be provoked by a breakthrough of CO₂ through the MSC, i.e. not all of the CO₂ transferred across the zeolite during the sampling process is trapped on the zeolite.

On the vacuum rig the MSCs can be processed with much lower CO₂ amounts of as low as 50 µg C (see chapter ‘Evaluation of sample size limits of the MSC’). Additionally, it is possible to split the samples on the vacuum rig for further analyses (e.g. δ¹³C). Thus, the MSCs are currently processed on our vacuum rig, even if only two MSCs can be processed during an 8-hour work day. In contrast, up to seven MSCs can be treated per day with less user support with the semi-automatic MSC-AGE approach.

Future perspectives

For future projects a more accurate prediction of the amount of CO₂ being sampled on the MSC is mandatory. Therefore, CO₂ concentrations, pump rate, and time need to be monitored properly to estimate the sampled CO₂ amount. Furthermore, a possible sample breakthrough should be evaluated. The parallel δ¹³C and ¹⁴C analysis of CO₂ released from the MSC to the AGE could become possible by developing a system, which allows to transfer a split of the desorbed CO₂ to an IRMS for online δ¹³C analysis. Simultaneously, the main fraction of the desorbed CO₂ is transferred to the AGE for graphitization and subsequent ¹⁴C analysis. This development seems to be realizable on a short term as an IRMS can be already coupled to an AGE (<https://www.ionplus.ch/products/irms/>). Furthermore, online ¹³C and ¹⁴C gas measurements using an EA-IRMS-AMS system were recently established (McIntyre *et al.*, 2017). However, environmental gas samples might complicate the IRMS analysis. During the collection of soil respired CO₂ using a MSC also nitrous oxides (e.g. N₂O) can be trapped on the zeolite type 13X (Godbout *et al.*, 2006). Both gases will be released by heating the zeolite and transferred to the IRMS. N₂O and CO₂ have equal isotopic masses and therefore lead to a discrepancy between measured and true isotopic ratios (Craig & Keeling, 1963, Ehleringer, 1991). We detected those interferences during the IRMS δ¹³C analysis of CO₂ samples collected with our MSC from permafrost in Siberia. We solved the problem by separating CO₂ and N₂O prior IRMS measurement by using a gas chromatography (GC)-IRMS. Thus, for an automated ¹³C and ¹⁴C analysis the development of a MSC-AGE-GC-IRMS system is needed.

Evaluation of the field equipment

To determine the analytical background of our CO₂ sampling equipment, including the respiration chamber and depth sampler, we collected naturally ¹⁴C-free CO₂ emitted from a gas vent in the Eifel volcanic field using both equipment sets. Any contamination introduced during sampling, transport of the MSC, and desorption in the laboratory, will result in enriched ¹⁴C concentrations compared to the analytical background of the ¹⁴C analysis alone. The entire process blank for CO₂ collected with the respiration chamber was not only obtained for the processing of the MSC on the vacuum rig, but also for the coupling of the MSC with the AGE. The CO₂ collected with the passive depths samplers was only processed on the vacuum rig.

All measurements reveal very promising low process blank values for the entire sampling and purification procedure at the vacuum rig of 0.0006 ± 0.0014 F¹⁴C and 0.0002 ± 0.0013 F¹⁴C using the respiration chambers and depth samplers, respectively. The ¹⁴C concentration of ¹⁴C-free field

samples graphitized with the AGE is slightly enriched ($0.0036 \pm 0.0011 \text{ F}^{14}\text{C}$; Paper II), but the data for both treatments, vacuum rig vs. MSC-AGE system, show a similar modern contamination of about 3 and 4.5 $\mu\text{g C}$, respectively (*Figure 7b*). Less contamination of 1.5 $\mu\text{g C}$ was introduced by adsorbing ^{14}C -free CO_2 on a MSC and its desorption from the MSC directly to the AGE under laboratory conditions (*Figure 7b*; see ‘Coupling of the MSC with the AGE’). A contamination of $\sim 3 \mu\text{g}$ modern C is introduced during the whole sampling process including the coupling and decoupling of the MSC and is therefore at the moment the limitation of the entire CO_2 sampling and purification procedure. However, the contamination obtained during the sampling with the stainless steel MSC is lower compared to previous studies, which used the original MSC design made up of glass tubes and plastic couplings (*Figure 7b*; Garnett & Murray, 2013, Hardie *et al.*, 2005). Overall the results show that no significant atmospheric contamination is introduced during the entire sampling procedure for large sample sizes ($>500 \mu\text{g C}$; *Figure 7*). Consequently, the MSC can be used in combination with our respiration chamber or depth sampler to collect respired CO_2 for ^{14}C analysis from different environments. The results will help to understand the changes in respiration caused by the present global warming.

Decomposability of Yedoma determined by $^{14}\text{CO}_2$ analysis

The decomposability of Yedoma OM was evaluated by determining CO_2 fluxes as well as by quantifying the proportion of ancient Yedoma derived OC that is respired (Paper III). Therefore, ^{14}C analyses of in-situ respired CO_2 were compared with the ^{14}C content of the bulk sedimentary OM and its chemical composition at an outcrop of Pleistocene Yedoma deposits on Kurungnakh Island in the Lena River Delta, northeast Siberia. The outcrop along the river shoreline is exposed by thermal erosion and thus has great potential to provide insights into how these deposits will react towards global warming and thawing in the future. The location is characterized by the relocation of sediment, i.e. mixing of Pleistocene sediments with the overlying Holocene OM, as well as by the growth of new vegetation on the previously bare sediment. To study the OM degradability and its stimulation by the incorporation of more easily degradable substrates (known as priming effect; Bingeman *et al.*, 1953, Fontaine *et al.*, 2003, Kuzyakov & Bol, 2006), three sampling sites (K4, K7, and KX) were compared that differ in their depositional age and the admixture of younger OM. Using $^{14}\text{CO}_2$ analysis to trace the degradation of ancient vs. young OM directly in field, has not been performed on Yedoma deposits before. The sampling of respired CO_2 for subsequent ^{14}C analysis was too challenging in these remote locations until the development (Hardie *et al.*, 2005, Garnett & Murray, 2013) and the above described improvement (see ‘Method development and improvement’) of the MSC sampling approach. During the progress of this dissertation, the MSC design and method was successfully improved to enable CO_2 sampling in remote areas for subsequent ^{14}C analysis. This new and robust MSC can now be used to investigate the OM decomposition in permafrost and thus will help unravel the permafrost C feedback.

Composition of OM in thawing Yedoma deposits

Sediment samples at each site were collected to obtain the underlying bulk OM characteristics. This characterization is important because the decomposition of OM in permafrost depends on the

chemical composition of the source material, i.e. vegetation type (Jenkins & Adams, 2010) and their degree of degradation (Schädel *et al.*, 2014, Treat *et al.*, 2014, Chen *et al.*, 2016). Different proxies were used to assess the degradability and stage of degradation of the OM in the thawing Yedoma deposits. High TOC and C/N and low $\delta^{13}\text{C}$ are supposed to reflect the least degraded OM (Nadelhoffer & Fry, 1988, Melillo *et al.*, 1989, Ågren *et al.*, 1996, Kuhry & Vitt, 1996) and thus, these proxies are widely applied to describe the vulnerability of permafrost to microbial decomposition (e.g. Schädel *et al.*, 2014, Gentsch *et al.*, 2015, Strauss *et al.*, 2015, Weiss *et al.*, 2016).

Site K4 is located between thermokarst mounds on allochthonous material with a Holocene sedimentary bulk age of 4000 yrs BP. This site is characterized by a considerable admixture of younger OM, which becomes obvious by two intercalated peat lenses that originate from the active layer. An affiliation of the peat lenses to the active layer deposits is supported by comparable ^{14}C signatures and geochemical compositions. Besides the peat lenses, the surrounding sediment at K4 contains less degraded OM, characterized by higher TOC and C/N and lower $\delta^{13}\text{C}$ values in comparison to the two other sites (see Fig. 3 of Paper III).

Sites K7 and KX are located on thermokarst mounds and thus represent thawing Yedoma deposits. Based on their average bulk ^{14}C ages of 13,600 yrs BP at K7 and 26,300 yrs BP at KX, these deposits can be correlated with the upper Yedoma unit (Unit IV in Wetterich *et al.*, 2008). The TOC, C/N and $\delta^{13}\text{C}$ values of the thawed sediments are in the range of previous analyses of the Yedoma deposits on Kurungnakh Island (Wetterich *et al.*, 2008, Knoblauch *et al.*, 2013) and indicate a higher degradation stage of the OM than those at K4. Both thermokarst sites seem to be little influenced by younger OM accumulated onto their surface layer. This influence is suggested by younger bulk ^{14}C ages in the upper part of the sediment profiles (see Fig. 3 of Paper III). A difference between both sites is the extent of the plant cover. Whereas some fresh vegetation started growing on the bare sediment at K7, only very sparse vegetation was found on the surface at KX (see Fig. 2 of Paper III). Therefore, these three sites reflect different characteristics of thawing deep permafrost including typical relocation processes and the interplay with newly grown vegetation within the dynamic environment of a thermal erosional site.

Degradability of OM in thawing Yedoma deposits

Based on several laboratory incubation experiments (see Schädel *et al.*, 2014), we expected the highest CO_2 flux at the site with the highest C/N ratio and thus at the site with the least degraded OM, i.e. K4. However, we revealed CO_2 fluxes of about 50, 130, and 60 $\mu\text{g CO}_2 \text{ m}^{-2} \text{ s}^{-1}$ for sites K4, K7, and KX, respectively. Thus, we determined similar CO_2 fluxes at the Holocene site K4 and at the Pleistocene thermokarst mound at KX. These results confirm the data from a previous incubation study, which showed similar respiration rates for Holocene and Pleistocene permafrost deposits of the same Yedoma sequence (Knoblauch *et al.*, 2013). At K4, a maximal proportion of ancient OC of 70% in the respired CO_2 was calculated using an isotopic mass balance calculation with the ^{14}C contents of the respired CO_2 and of the underlying bulk OM (see Paper III for more details).

Previous studies showed that increased temperatures can intensify respiration (Dutta *et al.*, 2006, Schädel *et al.*, 2014, Treat *et al.*, 2015, Hicks Pries *et al.*, 2016). Thus, the high CO_2 fluxes measured at the thermokarst mound K7 might be affected by higher temperatures (about 5°C)

during the day of measurement. Despite the more intense plant cover at K7, CO₂ contributions from root respiration can be excluded because the ¹⁴CO₂ concentration is relatively low. Instead, a contribution from roots would lead to higher ¹⁴CO₂ concentrations as the ¹⁴C content of root respired CO₂ is similar to that of the atmosphere (Trumbore, 2000). Although the ¹⁴C content of the underlying bulk OM is higher at K7 than at KX, the respired CO₂ at both thermokarst mounds has a similar ¹⁴C content. Thus, the difference in the ¹⁴C content between the bulk OM and the respired CO₂ is lower at K7 than at KX. This difference is expressed in the proportion of ancient OC in the respired CO₂, which is about 60% at K7 and about 50% at KX according to the mass balance calculation.

These results demonstrate that the admixture of less decomposed, C-rich OM (K4) stimulates the degradation of more strongly transformed OM in the field having the strongest priming effect and resulting in the largest proportion of ancient sedimentary OM that is respired. This positive priming was shown before during incubation experiments in which permafrost soils were mixed with poorly decomposed OM from the active layer or with plant remnants (Wild *et al.*, 2014, Wild *et al.*, 2016, Walz *et al.*, 2017). Additionally, also roots and their exudates of the sparse plant cover at site K7 seem to fuel the decomposition of ancient OM (apparent priming; Kuzyakov, 2002), even if less intense.

By applying the calculated fractions of ancient OM being respired and by assuming constant CO₂ fluxes over the growing season, we assessed the potential release of ancient OC from the thawing Yedoma deposits over one year. Accordingly, maximal amounts of ancient OC of 85, 210, and 110 g C m⁻² yr⁻¹ could be lost at the sites K4, K7, and KX, respectively. Lower annual respiration rates of 20–80 g C m⁻² yr⁻¹ were obtained for the microbial mineralization of active layer soils in different Holocene tundra landscapes (Schuur *et al.*, 2009, Biasi *et al.*, 2014). This may indicate that mineral permafrost soils (e.g. Pleistocene Yedoma deposit) are more vulnerable to OM decomposition compared to C-rich organic soils (e.g. active layer soils of the Holocene tundra; Schneider von Deimling *et al.*, 2015). In consequence, higher proportions of yet frozen OC of the Yedoma region might be respired upon thawing of these deposits potentially on short time scales. However, whether and to what extent the decomposition continuous over longer time scales is questionable, since laboratory incubations of permafrost OM show that decomposition rates are decreasing after the labile OM fraction has been decomposed (Schädel *et al.*, 2014; Knoblauch *et al.*, 2018).

The ¹⁴C analyses of the in-situ respired CO₂ indicate that up to 6500 yrs BP old CO₂ is released from the Yedoma deposits to the atmosphere. Only one other study exists, which showed the degradability of the OM in thawing Yedoma from the Kolyma River using the ¹⁴C signature of respired CO₂ (Dutta *et al.*, 2006). Their Yedoma sediments released up to 24,000 yrs BP old CO₂ in laboratory incubations. The comparison of both results, our field study and the incubation experiment, shows that field studies are necessary to consider all environmental conditions and that laboratory conditions alone might not deliver the results obtained in the environment. In-situ studies exist so far for analyzing the ¹⁴C concentration of CO₂ respired from the active layer on top of permafrost deposits, but not yet for deep permafrost (Yedoma) deposits. Whereas surface respired CO₂ is mainly ~decadal old, (Schuur *et al.*, 2009, Czimeczik & Welker, 2010, Nowinski *et al.*, 2010, Natali *et al.*, 2011, Hicks Pries *et al.*, 2013, Biasi *et al.*, 2014, Lupascu *et al.*, 2014, Hicks Pries *et al.*, 2015, Hicks Pries *et al.*, 2016) the CO₂ respired within depth can be up to about 4000 yrs BP old (Schuur *et al.*, 2009, Nowinski *et al.*, 2010). Thus, the release of up to 6500 yrs BP

old CO₂ from the surface of thawing Yedoma deposits is remarkable as the CO₂ is directly released to the atmosphere and becomes part of the active C cycle, i.e. increasing the permafrost C feedback.

Summary

This thesis provides a new and robust sampling device for the collection of CO₂ released from soils or sediments for subsequent AMS ¹⁴C analysis as a tool to investigate the decomposability of organic matter stored in permafrost. The achievements of this thesis are built on (i) the construction of the MSC and accompanying ¹⁴CO₂ method development, and (ii) the application of the MSC involving the sampling for ¹⁴CO₂ analyses to trace the degradation of ancient vs. young organic matter sources in permafrost. The most significant findings related to these two main objectives of this thesis are given below:

Method development and improvement

- A new MSC was constructed, which is entirely made of stainless steel and thus particularly useful for field applications under extreme conditions in remote areas.
- For the processing of the MSC in the laboratory, the exogenous carbon contamination was quantified to be less than 3.0 and 2.0 μg C for modern and fossil sources, respectively.
- A slightly higher modern carbon contamination of maximum 4.5 μg C was obtained for the entire CO₂ sampling procedure in the field using respiration chambers as well as depths samplers and including the processing of the MSC in the laboratory. This minor increase in contamination shows that no significant atmospheric contamination was introduced during the sampling in the field.
- The low contributions of exogenous carbon are insignificant for processed CO₂ samples of more than 500 μg.
- The new MSC makes it possible to collect CO₂ samples of as small as 50 μg C, when their data are corrected for exogenous carbon contamination.
- The lowest modern carbon contamination of less than 1.5 μg C was obtained for the direct CO₂ transfer from the MSC to the automatic graphitization system AGE under laboratory conditions. This semi-automatic approach allows a higher sample throughput and is thus a promising approach for large CO₂ samples (>1000 μg C).
- The exogenous carbon contamination obtained during the whole MSC sampling and purification process should be regularly examined by using standards of known ¹⁴C concentration.

This methodological development gave the basis for the second part of this thesis: the application of the MSC and sampling of CO₂ for subsequent ¹⁴C analysis in the permafrost.

Decomposability of Yedoma deposits

- The respired CO₂ is younger (2600–6500 yrs BP) than the bulk sediment (4000–31,000 yrs BP).
- Decomposition and respiration of ancient organic matter is promoted by the input of fresher, carbon-rich substrates leading to the release of CO₂ consisting of up to 70% ancient organic carbon.
- Ancient organic carbon stored in Pleistocene Yedoma deposits is highly vulnerable to microbial decomposition.
- The release of large amounts of ancient carbon from thawing Yedoma to the atmosphere reveal the potential contribution of this carbon pool to rising atmospheric CO₂ levels and thus the potential to increase the permafrost carbon feedback.

References

- Ågren GI, Bosatta E, Balesdent J (1996) Isotope discrimination during decomposition of organic matter: A theoretical analysis. *Soil Science Society of America Journal*, **60**, 1121-1126.
- Antonov VS (1967) The mouth area of the Lena (the Hydrogeographic Review), *Gidrometeorizdat*, Leningrad, 107 pp.
- Bauer JE, Williams PM, Druffel ERM (1992) Recovery of submilligram quantities of carbon dioxide from gas streams by molecular sieve for subsequent determination of isotopic (^{13}C and ^{14}C) natural abundances. *Analytical Chemistry*, **64**, 824-827.
- Biasi C, Jokinen S, Marushchak M, Hämäläinen K, Trubnikova T, Oinonen M, Martikainen P (2014) Microbial respiration in arctic upland and peat soils as a source of atmospheric carbon dioxide. *Ecosystems*, **17**, 112-126.
- Bingeman CW, Varner JE, Martin WP (1953) The effect of the addition of organic materials on the decomposition of an organic soil. *Soil Science Society of America Journal*, **17**, 34-38.
- Boike J, Kattenstroth B, Abramova K, Bornemann N, Chetverova A, Fedorova I, Fröb K, Grigoriev M, Grüber M, Kutzbach L, Langer M, Minke M, Muster S, Piel K, Pfeiffer EM, Stoof G, Westermann S, Wischniewski K, Wille C, Hubberten HW (2013) Baseline characteristics of climate, permafrost and land cover from a new permafrost observatory in the Lena River Delta, Siberia (1998-2011). *Biogeosciences*, **10**, 2105-2128.
- Bol RA, Harkness DD (1995) The use of zeolite molecular sieves for trapping low concentrations of CO_2 from environmental atmospheres. *Radiocarbon*, **37**, 643-647.
- Brown A (2013) Pandora's freezer? *Nature Climate Change*, **3**, 442.
- Brown J, Ferrians OJ, Heginbottom JA, Melnikov ES (2002) Circum-Arctic map of permafrost and ground-ice conditions, Version 2, Boulder, Colorado, USA, NSIDC: National Snow and Ice Data Center.
- Chen L, Liang J, Qin S, Liu L, Fang K, Xu Y, Ding J, Li F, Luo Y, Yang Y (2016) Determinants of carbon release from the active layer and permafrost deposits on the Tibetan Plateau. *Nature Communications*, **7**, 13046.
- Ciais P, Sabine C, Bala G, Bopp L, Brovkin V, Canadell J, Chhabra A, Defries R, Galloway J, Heimann M, Jones C, Le Quéré C, Myneni RB, Piao S, Thornton P (2013) Carbon and other biogeochemical cycles. In: *Climate change 2013: The physical science basis. Contribution of Working Group I to the Fifth Assessment Report of the Intergovernmental Panel on Climate Change*. (eds Stocker TF, Qin D, Plattner G-K, Tignor M, Allen SK, Boschung J, Nauels A, Xia Y, Bex V, Midgley PM). Cambridge, UK and New York, USA, Cambridge University Press, 465-570.
- Conen F, Smith KA (2000) An explanation of linear increases in gas concentration under closed chambers used to measure gas exchange between soil and the atmosphere. *European Journal of Soil Science*, **51**, 111-117.
- Craig H, Keeling CD (1963) The effects of atmospheric NO_2 on the measured isotopic composition of atmospheric CO_2 . *Geochimica et Cosmochimica Acta*, **27**, 549-551.
- Czimczik CI, Welker JM (2010) Radiocarbon content of CO_2 respired from high arctic tundra in Northwest Greenland. *Arctic Antarctic and Alpine Research*, **42**, 342-350.
- Dewald A, Heinze S, Jolie J, Zilges A, Dunai T, Rethemeyer J, Melles M, Staubwasser M, Kuczewski B, Richter J, Radtke U, Von Blanckenburg F, Klein M (2013) CologneAMS, a dedicated center for accelerator mass spectrometry in Germany. *Nuclear Instruments and Methods in Physics Research Section B: Beam Interactions with Materials and Atoms*, **294**, 18-23.
- Drosg R, Kutschera W, Scholz K, Steier P, Wagenbach D, Wild EM (2007) Treatment of small samples of particulate organic carbon (POC) for radiocarbon dating of ice. *Nuclear Instruments and Methods in Physics Research Section B: Beam Interactions with Materials and Atoms*, **259**, 340-344.
- Dutta K, Schuur EAG, Neff JC, Zimov SA (2006) Potential carbon release from permafrost soils of Northeastern Siberia. *Global Change Biology*, **12**, 2336-2351.
- Ehleringer JR (1991) $^{13}\text{C}/^{12}\text{C}$ fractionation and its utility in terrestrial plant studies. In: *Carbon isotope techniques*. (eds Coleman DC, Fry B). Academic Press, In. New York, 187-200.

- Elberling B, Michelsen A, Schadel C, Schuur EAG, Christiansen HH, Berg L, Tamstorf MP, Sigsgaard C (2013) Long-term CO₂ production following permafrost thaw. *Nature Climate Change*, **3**, 890-894.
- Fahrni SM, Wacker L, Synal HA, Szidat S (2013) Improving a gas ion source for ¹⁴C AMS. *Nuclear Instruments and Methods in Physics Research Section B: Beam Interactions with Materials and Atoms*, **294**, 320-327.
- Flanigen EM (1991) Zeolites and molecular sieves an historical perspective. In: *Studies in surface science and catalysis*. (eds Van Bekkum H, Flanigen EM, Jansen JC). New York, Elsevier, **58**, 13-34.
- Fontaine S, Mariotti A, Abbadie L (2003) The priming effect of organic matter: a question of microbial competition? *Soil Biology and Biochemistry*, **35**, 837-843.
- French HM (2017) Thermokarst processes and landforms. In: *The Periglacial Environment*. (ed French HM). Chichester, UK, John Wiley & Sons, Ltd, 169-192.
- Garnett MH, Murray C (2013) Processing of CO₂ samples collected using zeolite molecular sieve for ¹⁴C analysis at the NERC Radiocarbon Facility (East Kilbride, UK). *Radiocarbon*, **55**, 410-415.
- Garnett MH, Hartley IP, Hopkins DW, Sornmerkorn M, Wookey PA (2009) A passive sampling method for radiocarbon analysis of soil respiration using molecular sieve. *Soil Biology and Biochemistry*, **41**, 1450-1456.
- Gentsch N, Mikutta R, Alves RJE, Barta J, Čapek P, Gittel A, Hugelius G, Kuhry P, Lashchinskiy N, Palmtag J, Richter A, Šantrůčková H, Schnecker J, Shibistova O, Urich T, Wild B, Guggenberger G (2015) Storage and transformation of organic matter fractions in cryoturbated permafrost soils across the Siberian Arctic. *Biogeosciences*, **12**, 4525-4542.
- Godbout S, Phillips VR, Sneath RW (2006) Passive flux samplers to measure nitrous oxide and methane emissions from agricultural sources, Part 1: Adsorbent selection. *Biosystems Engineering*, **94**, 587-596.
- Godwin H (1962) Half-life of radiocarbon. *Nature*, **195**, 984-984.
- Grigoriev MN (1993) Cryomorphogenesis in the Lena Delta. Permafrost Institute Press, Yakutsk, 176 pp. (in Russian)
- Grigoriev NF (1960) The temperature of permafrost in the Lena delta basin—deposit conditions and properties of the permafrost in Yakutia. *Yakutsk*, **2**, 97-101.
- Grosse G, Harden J, Turetsky M, McGuire AD, Camill P, Tarnocai C, Frohling S, Schuur EAG, Jorgenson T, Marchenko S, Romanovsky V, Wickland KP, French N, Waldrop M, Bourgeau-Chavez L, Striegl RG (2011a) Vulnerability of high-latitude soil organic carbon in North America to disturbance. *Journal of Geophysical Research: Biogeosciences*, **116**, G00K06.
- Grosse G, Romanovsky V, Jorgenson T, Anthony KW, Brown J, Overduin PP (2011b) Vulnerability and Feedbacks of Permafrost to Climate Change. *Eos, Transactions American Geophysical Union*, **92**, 73-74.
- Grosse G, Robinson JE, Bryant R, Taylor MD, Harper W, Demasi A, Kyker-Snowman E, Veremeeva A, Schirrmeister L, Harden J (2013) Distribution of late Pleistocene ice-rich syngenetic permafrost of the Yedoma Suite in east and central Siberia, Russia. *US Geological Survey Open File Report*, **2013**, 1-37.
- Günther F, Overduin PP, Sandakov AV, Grosse G, Grigoriev MN (2013) Short- and long-term thermo-erosion of ice-rich permafrost coasts in the Laptev Sea region. *Biogeosciences*, **10**, 4297-4318.
- Harden JW, Mark RK, Sundquist ET, Stallard RF (1992) Dynamics of soil carbon during deglaciation of the laurentide ice sheet. *Science*, **258**, 1921-1924.
- Hardie SML, Garnett MH, Fallick AE, Rowland AP, Ostle NJ (2005) Carbon dioxide capture using a zeolite molecular sieve sampling system for isotopic studies (¹³C and ¹⁴C) of respiration. *Radiocarbon*, **47**, 441-451.
- Healy RW, Striegl RG, Russell TF, Hutchinson GL, Livingston GP (1996) Numerical evaluation of static-chamber measurements of soil—atmosphere gas exchange: Identification of physical processes. *Soil Science Society of America Journal*, **60**, 740-747.
- Hicks Pries CE, Schuur EAG, Crummer KG (2013) Thawing permafrost increases old soil and autotrophic respiration in tundra: Partitioning ecosystem respiration using δ¹³C and Δ¹⁴C. *Global Change Biology*, **19**, 649-661.
- Hicks Pries CE, Van Logtestijn RSP, Schuur EAG, Natali SM, Cornelissen JHC, Aerts R, Dorrepaal E (2015) Decadal warming causes a consistent and persistent shift from heterotrophic to autotrophic respiration in contrasting permafrost ecosystems. *Global Change Biology*, **21**, 4508-4519.
- Hicks Pries CE, Schuur EAG, Natali SM, Crummer KG (2016) Old soil carbon losses increase with ecosystem respiration in experimentally thawed tundra. *Nature Climate Change*, **6**, 214-218.

- Hugelius G, Strauss J, Zubrzycki S, Harden JW, Schuur EAG, Ping CL, Schirmermeister L, Grosse G, Michaelson GJ, Koven CD, O'Donnell JA, Elberling B, Mishra U, Camill P, Yu Z, Palmtag J, Kuhry P (2014) Estimated stocks of circumpolar permafrost carbon with quantified uncertainty ranges and identified data gaps. *Biogeosciences*, **11**, 6573-6593.
- Jenkins M, Adams MA (2010) Vegetation type determines heterotrophic respiration in subalpine Australian ecosystems. *Global Change Biology*, **16**, 209-219.
- Jorgenson MT, Shur YL, Pullman ER (2006) Abrupt increase in permafrost degradation in Arctic Alaska. *Geophysical Research Letters*, **33**, 4.
- Kanevskiy M, Shur Y, Fortier D, Jorgenson MT, Stephani E (2011) Cryostratigraphy of late Pleistocene syngenetic permafrost (yedoma) in northern Alaska, Itkillik River exposure. *Quaternary Research*, **75**, 584-596.
- Kanevskiy M, Shur Y, Strauss J, Jorgenson T, Fortier D, Stephani E, Vasiliev A (2016) Patterns and rates of riverbank erosion involving ice-rich permafrost (yedoma) in northern Alaska. *Geomorphology*, **253**, 370-384.
- Knoblauch C, Beer C, Sosnin A, Wagner D, Pfeiffer E-M (2013) Predicting long-term carbon mineralization and trace gas production from thawing permafrost of Northeast Siberia. *Global Change Biology*, **19**, 1160-1172.
- Kokelj SV, Lacelle D, Lantz TC, Tunnicliffe J, Malone L, Clark ID, Chin KS (2013) Thawing of massive ground ice in mega slumps drives increases in stream sediment and solute flux across a range of watershed scales. *Journal of Geophysical Research: Earth Surface*, **118**, 681-692.
- Koven CD, Lawrence DM, Riley WJ (2015) Permafrost carbon-climate feedback is sensitive to deep soil carbon decomposability but not deep soil nitrogen dynamics. *Proceedings of the National Academy of Sciences*, **112**, 3752-3757.
- Kuhry P, Vitt DH (1996) Fossil carbon/nitrogen ratios as a measure of peat decomposition. *Ecology*, **77**, 271-275.
- Kuzyakov Y (2002) Review: Factors affecting rhizosphere priming effects. *Journal of Plant Nutrition and Soil Science*, **165**, 382-396.
- Kuzyakov Y, Bol R (2006) Sources and mechanisms of priming effect induced in two grassland soils amended with slurry and sugar. *Soil Biology and Biochemistry*, **38**, 747-758.
- Lee H, Schuur EAG, Inglett KS, Lavoie M, Chanton JP (2012) The rate of permafrost carbon release under aerobic and anaerobic conditions and its potential effects on climate. *Global Change Biology*, **18**, 515-527.
- Libby WF (1946) Atmospheric helium three and radiocarbon from cosmic radiation. *Physical Review*, **69**, 671-672.
- Libby WF (1952) *Radiocarbon Dating*, University of Chicago Press, 124 pp.
- Liebl J, Ortiz RA, Golser R, Handle F, Kutschera W, Steier P, Wild EM (2010) Studies on the preparation of small ^{14}C samples with an RGA and ^{13}C -enriched material. *Radiocarbon*, **52**, 1394-1404.
- Lupascu M, Welker JM, Xu X, Czimczik CI (2014) Rates and radiocarbon content of summer ecosystem respiration in response to long-term deeper snow in the High Arctic of NW Greenland. *Journal of Geophysical Research: Biogeosciences*, **119**, 1180-1194.
- Mascarelli A (2009) A sleeping giant? *Nature Reports Climate Change*, 46.
- McGuire AD, Anderson LG, Christensen TR, Dallimore S, Guo L, Hayes DJ, Heimann M, Lorenson TD, Macdonald RW, Roulet N (2009) Sensitivity of the carbon cycle in the Arctic to climate change. *Ecological Monographs*, **79**, 523-555.
- McIntyre CP, McNichol AP, Roberts ML, Seewald JS, Von Reden KF, Jenkins WJ (2013) Improved precision of ^{14}C measurements for CH_4 and CO_2 using GC and continuous-flow AMS achieved by summation of repeated injections. *Radiocarbon*, **55**, 677-685.
- McIntyre CP, Wacker L, Haghypour N, Blattmann TM, Fahrni S, Usman M, Eglinton TI, Synal H-A (2017) Online ^{13}C and ^{14}C gas measurements by EA-IRMS-AMS at ETH Zürich. *Radiocarbon*, **59**, 893-903.
- Melillo JM, Aber JD, Linkins AE, Ricca A, Fry B, Nadelhoffer KJ (1989) Carbon and nitrogen dynamics along the decay continuum: Plant litter to soil organic matter. *Plant and Soil*, **115**, 189-198.
- Morgenstern A, Ulrich M, Günther F, Roessler S, Fedorova IV, Rudaya NA, Wetterich S, Boike J, Schirmermeister L (2013) Evolution of thermokarst in East Siberian ice-rich permafrost: A case study. *Geomorphology*, **201**, 363-379.
- Muller SW (1947) Permafrost or permanently frozen ground and related engineering problems. J.W. Edwards Press, 231 pp.

- Nadelhoffer KJ, Fry B (1988) Controls on natural ^{15}N and ^{13}C abundances in forest soil organic matter. *Soil Science Society of America Journal*, **52**, 1633-1640.
- Natali SM, Schuur EAG, Trucco C, Pries CEH, Crummer KG, Lopez AFB (2011) Effects of experimental warming of air, soil and permafrost on carbon balance in Alaskan tundra. *Global Change Biology*, **17**, 1394-1407.
- Nowinski NS, Taneva L, Trumbore SE, Welker JM (2010) Decomposition of old organic matter as a result of deeper active layers in a snow depth manipulation experiment. *Oecologia*, **163**, 785-792.
- Overland JE, Hanna E, Hanssen-Bauer I, Kim S-J, Walsh JE, Wang M, Bhatt US, Thoman RL (2017) Surface air temperature. In: *State of the Climate in 2016*. (eds Blunden J, Arndt DS). Bulletin of the American Meteorological Society, S130-S131.
- Palonen V, Oinonen M (2013) Molecular sieves in $^{14}\text{CO}_2$ sampling and handling. *Radiocarbon*, **55**, 416-420.
- Poincaré H (1905) *Science nad Hyothesis*, London, The Walter Scott Publishing.
- Reimer PJ, Brown TA, Reimer RW (2004) Discussion: Reporting and Calibration of Post-Bomb ^{14}C Data. *Radiocarbon*, **46**, 1299-1304.
- Reimer PJ, Bard E, Bayliss A, Beck JW, Blackwell PG, Ramsey CB, Buck CE, Cheng H, Edwards RL, Friedrich M, Grootes PM, Guilderson TP, Haflidason H, Hajdas I, Hatté C, Heaton TJ, Hoffmann DL, Hogg AG, Hughen KA, Kaiser KF, Kromer B, Manning SW, Niu M, Reimer RW, Richards DA, Scott EM, Southon JR, Staff RA, Turney CSM, Van Der Plicht J (2013) IntCal13 and Marine13 Radiocarbon Age Calibration Curves 0–50,000 Years cal BP. *Radiocarbon*, **55**, 1869-1887.
- Romanovsky N (1993) *Osnovy Kriogeneza Litosfery (Fundamentals of Lithosphere Cryogenesis)*. Izdatelsky dom of Moscow State University, Moscow, 336 pp. (in Russian).
- Romanovsky VE, Drozdov DS, Oberman NG, Malkova GV, Kholodov AL, Marchenko SS, Moskalenko NG, Sergeev DO, Ukraintseva NG, Abramov AA, Gilichinsky DA, Vasiliev AA (2010) Thermal state of permafrost in Russia. *Permafrost and Periglacial Processes*, **21**, 136-155.
- Ruff M, Wacker L, Gäggeler HW, Suter M, Synal H-A, Szidat S (2007) A gas ion source for radiocarbon measurements at 200 kV. *Radiocarbon*, **49**, 307-314.
- Ruff M, Szidat S, Gäggeler HW, Suter M, Synal HA, Wacker L (2010) Gaseous radiocarbon measurements of small samples. *Nuclear Instruments and Methods in Physics Research Section B: Beam Interactions with Materials and Atoms*, **268**, 790-794.
- Santos GM, Southon JR, Griffin S, Beupre SR, Druffel ERM (2007) Ultra small-mass AMS ^{14}C sample preparation and analyses at KCCAMS/UCI Facility. *Nuclear Instruments and Methods in Physics Research Section B: Beam Interactions with Materials and Atoms*, **259**, 293-302.
- Schädel C, Schuur EAG, Bracho R, Elberling B, Knoblauch C, Lee H, Luo Y, Shaver GR, Turetsky MR (2014) Circumpolar assessment of permafrost C quality and its vulnerability over time using long-term incubation data. *Global Change Biology*, **20**, 641-652.
- Schaefer K, Lantuit H, Romanovsky VE, Schuur EAG, Witt R (2014) The impact of the permafrost carbon feedback on global climate. *Environmental Research Letters*, **9**, 085003.
- Schirrmeyer L, Siegert C, Kuznetsova T, Kuzmina S, Andreev A, Kienast F, Meyer H, Bobrov A (2002) Paleoenvironmental and paleoclimatic records from permafrost deposits in the Arctic region of Northern Siberia. *Quaternary International*, **89**, 97-118.
- Schirrmeyer L, Kunitsky V, Grosse G, Wetterich S, Meyer H, Schwamborn G, Babiy O, Derevyagin A, Siegert C (2011) Sedimentary characteristics and origin of the Late Pleistocene Ice Complex on north-east Siberian Arctic coastal lowlands and islands – A review. *Quaternary International*, **241**, 3-25.
- Schirrmeyer L, Froese D, Tumskey V, Grosse G, Wetterich S (2013) Yedoma: Late Pleistocene ice-rich syngenetic permafrost of Beringia. In: *Encyclopedia of Quaternary Science. 2nd edition*. (eds Elias S, Mock C, Murton J) Amsterdam, Elsevier, **3**, 542-552.
- Schneider Von Deimling T, Grosse G, Strauss J, Schirrmeyer L, Morgenstern A, Schaphoff S, Meinshausen M, Boike J (2015) Observation-based modelling of permafrost carbon fluxes with accounting for deep carbon deposits and thermokarst activity. *Biogeosciences*, **12**, 3469-3488.
- Schuur EAG, Trumbore SE (2006) Partitioning sources of soil respiration in boreal black spruce forest using radiocarbon. *Global Change Biology*, **12**, 165-176.
- Schuur EAG, Bockheim J, Canadell JG, Euskirchen E, Field CB, Goryachkin SV, Hagemann S, Kuhry P, Laflour PM, Lee H, Mazhitova G, Nelson FE, Rinke A, Romanovsky VE, Shiklomanov N,

- Tarnocai C, Venevsky S, Vogel JG, Zimov SA (2008) Vulnerability of permafrost carbon to climate change: Implications for the global carbon cycle. *BioScience*, **58**, 701-714.
- Schuur EAG, Vogel JG, Crummer KG, Lee H, Sickman JO, Osterkamp TE (2009) The effect of permafrost thaw on old carbon release and net carbon exchange from tundra. *Nature*, **459**, 556-559.
- Schuur EAG, Abbott BW, Bowden WB, Brovkin V, Camill P, Canadell JG, Chanton JP, Chapin FS, Christensen TR, Ciais P, Crosby BT, Czimczik CI, Grosse G, Harden J, Hayes DJ, Hugelius G, Jastrow JD, Jones JB, Kleinen T, Koven CD, Krinner G, Kuhry P, Lawrence DM, McGuire AD, Natali SM, O'donnell JA, Ping CL, Riley WJ, Rinke A, Romanovsky VE, Sannel ABK, Schädel C, Schaefer K, Sky J, Subin ZM, Tarnocai C, Turetsky MR, Waldrop MP, Walter Anthony KM, Wickland KP, Wilson CJ, Zimov SA (2013) Expert assessment of vulnerability of permafrost carbon to climate change. *Climatic Change*, **119**, 359-374.
- Schuur EAG, McGuire AD, Schadel C, Grosse G, Harden JW, Hayes DJ, Hugelius G, Koven CD, Kuhry P, Lawrence DM, Natali SM, Olefeldt D, Romanovsky VE, Schaefer K, Turetsky MR, Treat CC, Vonk JE (2015) Climate change and the permafrost carbon feedback. *Nature*, **520**, 171-179.
- Schwamborn G, Rachold V, Grigoriev MN (2002) Late Quaternary sedimentation history of the Lena Delta. *Quaternary International*, **89**, 119-134.
- Serreze MC, Barry RG (2011) Processes and impacts of Arctic amplification: A research synthesis. *Global and Planetary Change*, **77**, 85-96.
- Smith LC, MacDonald GM, Velichko AA, Beilman DW, Borisova OK, Frey KE, Kremenetski KV, Sheng Y (2004) Siberian Peatlands a Net Carbon Sink and Global Methane Source Since the Early Holocene. *Science*, **303**, 353-356.
- Smith SL, Romanovsky VE, Lewkowicz AG, Burn CR, Allard M, Clow GD, Yoshikawa K, Throop J (2010) Thermal state of permafrost in North America: a contribution to the international polar year. *Permafrost and Periglacial Processes*, **21**, 117-135.
- Stapel JG, Schirrmeister L, Overduin PP, Wetterich S, Strauss J, Horsfield B, Mangelsdorf K (2016) Microbial lipid signatures and substrate potential of organic matter in permafrost deposits: Implications for future greenhouse gas production. *Journal of Geophysical Research: Biogeosciences*, **121**, 2652-2666.
- Stettner S, Beamish LA, Bartsch A, Heim B, Grosse G, Roth A, Lantuit H (2018) Monitoring Inter- and Intra-Seasonal Dynamics of Rapidly Degrading Ice-Rich Permafrost Riverbanks in the Lena Delta with TerraSAR-X Time Series. *Remote Sensing*, **10**.
- Strauss J, Schirrmeister L, Grosse G, Wetterich S, Ulrich M, Herzsuh U, Hubberten H-W (2013) The deep permafrost carbon pool of the Yedoma region in Siberia and Alaska. *Geophysical Research Letters*, **40**, 6165-6170.
- Strauss J, Schirrmeister L, Mangelsdorf K, Eichhorn L, Wetterich S, Herzsuh U (2015) Organic-matter quality of deep permafrost carbon – a study from Arctic Siberia. *Biogeosciences*, **12**, 2227-2245.
- Strauss J, Schirrmeister L, Grosse G, Fortier D, Hugelius G, Knoblauch C, Romanovsky V, Schädel C, Schneider Von Deimling T, Schuur EAG, Shmelev D, Ulrich M, Veremeeva A (2017) Deep Yedoma permafrost: A synthesis of depositional characteristics and carbon vulnerability. *Earth-Science Reviews*, **172**, 75-86.
- Stuiver M, Polach HA (1977) Reporting of ¹⁴C data - discussion. *Radiocarbon*, **19**, 355-363.
- Synal HA, Stocker M, Suter M (2007) MICADAS: A new compact radiocarbon AMS system. *Nuclear Instruments and Methods in Physics Research Section B: Beam Interactions with Materials and Atoms*, **259**, 7-13.
- Treat CC, Frolking S (2013) A permafrost carbon bomb? *Nature Climate Change*, **3**, 865.
- Treat CC, Wollheim WM, Varner RK, Grandy AS, Talbot J, Frolking S (2014) Temperature and peat type control CO₂ and CH₄ production in Alaskan permafrost peats. *Global Change Biology*, **20**, 2674-2686.
- Treat CC, Natali SM, Ernakovich J, Iversen CM, Lupascu M, McGuire AD, Norby RJ, Roy Chowdhury T, Richter A, Šantrůčková H, Schädel C, Schuur EAG, Sloan VL, Turetsky MR, Waldrop MP (2015) A pan-Arctic synthesis of CH₄ and CO₂ production from anoxic soil incubations. *Global Change Biology*, **21**, 2787-2803.
- Trumbore SE (2000) Age of soil organic matter and soil respiration: Radiocarbon constraints on belowground C dynamics. *Ecological Applications*, **10**, 399-411.
- Trumbore SE (2006) Carbon respired by terrestrial ecosystems – recent progress and challenges. *Global Change Biology*, **12**, 141-153.

- Voigt C, Lamprecht RE, Marushchak ME, Lind SE, Novakovskiy A, Aurela M, Martikainen PJ, Biasi C (2016) Warming of subarctic tundra increases emissions of all three important greenhouse gases – carbon dioxide, methane, and nitrous oxide. *Global Change Biology*, **23**, 3121-3138.
- Wacker L, Nemeč M, Bourquin J (2010) A revolutionary graphitisation system: Fully automated, compact and simple. *Nuclear Instruments and Methods in Physics Research Section B: Beam Interactions with Materials and Atoms*, **268**, 931-934.
- Walker HJ (1998) Arctic Deltas. *Journal of Coastal Research*, **14**, 719-738.
- Walker JC, Xu X, Fahrni SM, Lupascu M, Czimczik CI (2015) Developing a passive trap for diffusive atmospheric $^{14}\text{CO}_2$ sampling. *Nuclear Instruments and Methods in Physics Research Section B: Beam Interactions with Materials and Atoms*, **361**, 632-637.
- Walter Anthony KM, Zimov SA, Grosse G, Jones MC, Anthony PM, Chapin FS, Finlay JC, Mack MC, Davydov S, Frenzel P, Frolking S (2014) A shift of thermokarst lakes from carbon sources to sinks during the Holocene epoch. *Nature*, **511**, 452-456.
- Walz J, Knoblauch C, Böhme L, Pfeiffer E-M (2017) Regulation of soil organic matter decomposition in permafrost-affected Siberian tundra soils - Impact of oxygen availability, freezing and thawing, temperature, and labile organic matter. *Soil Biology and Biochemistry*, **110**, 34-43.
- Washburn AL (1980) Permafrost features as evidence of climatic change. *Earth-Science Reviews*, **15**, 327-402.
- Weiss N, Blok D, Elberling B, Hugelius G, Jørgensen CJ, Siewert MB, Kuhry P (2016) Thermokarst dynamics and soil organic matter characteristics controlling initial carbon release from permafrost soils in the Siberian Yedoma region. *Sedimentary Geology*, **340**, 38-48.
- Wetterich S, Kuzmina S, Andreev AA, Kienast F, Meyer H, Schirrmeister L, Kuznetsova T, Sierralta M (2008) Palaeoenvironmental dynamics inferred from late Quaternary permafrost deposits on Kurungnakh Island, Lena Delta, Northeast Siberia, Russia. *Quaternary Science Reviews*, **27**, 1523-1540.
- Wild B, Schneckner J, Alves RJE, Barsukov P, Bárta J, Čapek P, Gentsch N, Gittel A, Guggenberger G, Lashchinskiy N, Mikutta R, Rusalimova O, Šantrůčková H, Shibistova O, Urich T, Watzka M, Zrazhevskaya G, Richter A (2014) Input of easily available organic C and N stimulates microbial decomposition of soil organic matter in arctic permafrost soil. *Soil Biology and Biochemistry*, **75**, 143-151.
- Wild B, Gentsch N, Čapek P, Diáková K, Alves RJE, Bárta J, Gittel A, Hugelius G, Knoltsch A, Kuhry P, Lashchinskiy N, Mikutta R, Palmtag J, Schleper C, Schneckner J, Shibistova O, Takriti M, Torsvik VL, Urich T, Watzka M, Šantrůčková H, Guggenberger G, Richter A (2016) Plant-derived compounds stimulate the decomposition of organic matter in arctic permafrost soils. *Scientific Reports*, **6**, srep25607.
- Zhang T, Barry RG, Knowles K, Heginbottom JA, Brown J (2008) Statistics and characteristics of permafrost and ground-ice distribution in the Northern Hemisphere. *Polar Geography*, **31**, 47-68.
- Zimov SA, Davydov SP, Zimova GM, Davydova AI, Schuur EAG, Dutta K, Chapin FS (2006) Permafrost carbon: Stock and decomposability of a globally significant carbon pool. *Geophysical Research Letters*, **33**, L20502.

Acknowledgements

First of all, I would like to thank my supervisor, Prof. Janet Rethemeyer. In the beginning of my thesis, she gave me the freedom to test different methods and in the end I received the support I needed to finish the last manuscript. Janet, thank you that you gave me the opportunity to take part in three expeditions to the Arctic.

I am also grateful to Prof. Martin Melles for being my second supervisor and to Prof. Frank Schäbitz for taking the chair of my examination committee.

There are many people at the institute, whom I would like to thank for their help and friendship during the past years, for creating this special environment, in which I enjoyed working most of the time. Thanks to Doro, Andrea, Merle, Lana, Ulrike, Dani, Bianca, Gabriel, Ninja, Sandra, Matthias, Stephan, Silke, ... and many more. A big thank you goes to my two boys, Philipp and Jan. They let me work under sun power, while they had to put their sunglasses on. That was really generous.

I especially want to acknowledge our student helpers: Vera, Reaz, Jan, Ilona, Olga, Elisabeth, Jannik, Thorsten (I hope, I did not forget anyone). You kept me working in the AGE-room, because you supplied me with dry-ice, liquid nitrogen and cleaned glass tubes. You helped me in whatever I asked you for, thanks a lot. Please keep in mind, that without your work this working group would not exist. I especially need to highlight the great support by Ilona and Reaz. Ilona, you were a great assistance during the preparation of the Lena and Svalbard expeditions, and Reaz thank you for doing all the lipid extraction in the lab. It was a pleasure for me to work with all of you guys.

During my time as a PhD student I had the opportunity to take part in three expeditions to the Arctic. I enjoyed the time in the Lena Delta in 2016 and 2017 and loved our short trip to Ny Ålesund. These are all very special places and I want to thank all the people, who made these places so special to me. Waldemar and Molo thanks for your logistic and technical support, the boat-taxi to Kurungnakh and the lovely Banya-nights on Samoylov. Sveta, you helped me more than once to get our MSCs from Yakutsk to Tiksi. Thus, this thesis would not have been possible without you. Regina, Fjordor, Natascha, Katja, Oleg, Ina, Slava, Olga, Lena, Lasse, Svenja, Rune, the Swiss-students – it was a great time with you during the meals, Durak-sessions, banya-nights, never-ending bonfire days, and in the field. Thank you!

I want to acknowledge my co-authors Christian Knoblauch and Lukas Wacker for their helpful discussions on the phone. I am also very thankful to all my proof-readers Andrea, Mats, Merle, Thomas, and Anne Wegener. You gave great suggestions, which improved this thesis.

At the very end of my PhD I found my companion in misery, Sandra. It was very motivating to have someone else, who still had lots to do and wanted to finish on the same day. Now our defense will be on the same day, I hope.

Patricia, I am sorry, that I finally had to stay that long in your flat, but I am very, very grateful that you gave me, der Mietmade, a little home at the end of my PhD thesis. You gave me the opportunity to fully concentrate on my thesis because I did not had to search for a new flat or to sleep under a bridge.

I hope that all my friends from school and Münster forgive me that I did not had much time for you during the last months of my PhD. I hope to see you soon again, wherever you are: Johanna, Melanie, Hannah, Janina & David, Kristin & Lars, Elsa, Joana,...

Of course I also want thank my family, especially my parents. It is always great to have a place that you can call your home and it is also great that this place is not perfect. Thus, gardening at home is always great to relax mentally and to exhaust yourself physically. At the end of the day you always see the results of your work, which is not the case for every day during your PhD.

Last but not least thank you, Thomas, for your support during the whole PhD period!

Contribution to Papers

I, Anja Wotte, contributed to the papers included in this thesis through the following:

- *Paper I: Wotte, A., Wordell-Dietrich, P., Wacker, L., Don, A., Rethemeyer, J. (2017) $^{14}\text{CO}_2$ processing using an improved and robust molecular sieve cartridge. Nuclear Instruments and Methods in Physics Research Section B: Beam Interactions with Materials and Atoms 400, 65–73.*

The experimental set-up was designed by myself. I developed and modified the methodology considering preliminary data. I carried out all laboratory tests. The interpretation of the data and the writing of the manuscript was done with myself in the leading role.

Overall contribution of A. Wotte: 90%

- *Paper II: Wotte, A., Wischhöfer, P., Wacker, L., Rethemeyer, J. (2017) $^{14}\text{CO}_2$ analysis of soil gas: Evaluation of sample size limits and sampling devices, Nuclear Instruments and Methods in Physics Research Section B: Beam Interactions with Materials and Atoms, 413, 51–56.*

I designed this project, developed and improved the experimental set-up and methodology. Together with P. Wischhöfer, I performed the laboratory tests. The interpretation of the results and the writing of the manuscript was in close collaboration with P. Wischhöfer.

Overall contribution of A. Wotte: 70%

- *Paper III: Wotte, A., Rethemeyer, J., Wischhöfer, P., Jaeschke, A., Knoblauch, C. Radiocarbon analyses of respired CO_2 reveal the release of large amounts of ancient carbon from thawing deep permafrost deposits. Submitted to Global Change Biology.*

The sampling campaign in the Siberian Arctic was planned and executed by myself. I carried out the laboratory analyses of the CO_2 samples and coordinated the other analyses. I had the leading role in the interpretation of the data and the writing of the manuscript.

Overall contribution of A. Wotte: 80%

Erklärung

Ich versichere, dass ich die von mir vorgelegte Dissertation selbständig angefertigt, die benutzten Quellen und Hilfsmittel vollständig angegeben und die Stellen der Arbeit – einschließlich Tabellen, Karten und Abbildungen –, die anderen Werken im Wortlaut oder dem Sinn nach entnommen sind, in jedem Einzelfall als Entlehnung kenntlich gemacht habe; dass diese Dissertation noch keiner anderen Fakultät oder Universität zur Prüfung vorgelegen hat; dass sie – abgesehen von unten angegebenen Teilpublikationen – noch nicht veröffentlicht worden ist, sowie, dass ich eine solche Veröffentlichung vor Abschluss des Promotionsverfahrens nicht vornehmen werde. Die Bestimmungen der Promotionsordnung sind mir bekannt. Die von mir vorgelegte Dissertation ist von Prof. Janet Rethemeyer betreut worden.

Nachfolgend genannte Teilpublikationen liegen vor:

1. Wotte, A., Wordell-Dietrich, P., Wacker, L., Don, A., Rethemeyer, J. (2017) $^{14}\text{CO}_2$ processing using an improved and robust molecular sieve cartridge. Nuclear Instruments and Methods in Physics Research Section B: Beam Interactions with Materials and Atoms 400, 65-73.
2. Wotte, A., Wischhöfer, P., Wacker, L., Rethemeyer, J. (2017) $^{14}\text{CO}_2$ analysis of soil gas: Evaluation of sample size limits and sampling devices, Nuclear Instruments and Methods in Physics Research Section B: Beam Interactions with Materials and Atoms, 413, 51-56.
3. Wotte, A., Rethemeyer, J., Wischhöfer, P., Jaeschke, A., Knoblauch, C. Radiocarbon analyses of respired CO_2 reveal the release of large amounts of ancient carbon from thawing deep permafrost deposits. Unter Begutachtung bei Global Change Biology.

Köln, 23. April 2018

Anja Wotte